ISSN 2414-6056

DEW-DROP

A Scientific Journal of Meteorology and Geo-Physics

Bangladesh Meteorological Department

March 2016

Volume 2 ▪ Number 1

ISSN 2414-6056

DEW-DROP

A Scientific Journal of Meteorology and Geo-Physics

Bangladesh Meteorological Department

March 2016

Volume 2 ■ Number 1

EDITORIAL BOARD

Published By:
Bangladesh Meteorological Department
Agargaon, Dhaka-1207, Bangladesh
E-mail: info@bmd.gov.bd, swc@bmd.gov.bd

A case study of very Severe Cyclonic Storm Hudhud using WRF ARW

Kh. Hafizur Rahman*, Shamsuddin Ahmed, Md. Sanaul Hoque Mondal, S.M. Quamrul Hassan and Md. Bazlur Rashid

Storm Warning Centre (SWC), Bangladesh Meteorological Department
**Author for correspondence: rs77_hafizbmd@yahoo.com*

Abstract: Tropical cyclones are the most deadly natural disasters in the world. They have significant socio-economic impact on the countries affected by tropical cyclone.Proper prediction with sufficient lead time of these systems can save millions of lives and properties. In this study, the numerical simulations of tropical cyclone Hudhud is carried out with a view to examine the movements and structures along with various parameters. For this purpose, the tropical cyclone Hudhud has been simulated by the advanced Weather Research and Forecasting (WRF) model with a single domain. Model simulated fields are compared with corresponding analysis or observed data. The intensity of simulated cyclone is compared with best track estimates provided by RSMC, New Delhi. The model simulated rainfall iscompared with the TRMM derivedrainfall data. The various fields along with horizontal and vertical structure of the system are well captured by the model.

Key words: Tropical Cyclone, TRMM, NWP.

1. Introduction

Tropical cyclones are the natural hazard with the greatest potential for economic damages and loss of human lives. Among the other natural disasters, tropical cyclones are the most destructive and indeed, as an agent of death and destruction on a scale at least as massive as that of earthquakes. Death and destruction take place directly from the intense winds of tropical cyclone blowing over a large area of watersurface, which causes high storm surge and inundates coastal region.Tropical cyclones over the Bay of Bengal (BOB) are the most destructive in the world. The shallow water of the Bay of Bengal, the low flat coastal terrain and the concentrating shape of the coastline can lead to devastating surges causing loss of lives and properties. In order to save lives and reduce economic damage, it is very important to extend the lead time in the prediction of tropical cyclone. In this respect, Numerical Weather Prediction (NWP) model can play a very significant role.

Cyclones are greatly influenced by the underlying ocean surface over which they form. As long as cyclone remains over warm water, it can gain the energy enormously. Warm and highly humid equatorial and maritime tropical air spirals inward towards the centre of the low pressure to replace the heated and rapidly ascending air. Ascending air releases heat into the atmosphere in the vicinity of colder upper air and are condensed into cloud. Tropical cyclones are characterized by awarm core vortexin the troposphere. The greatest temperature anomaly generally occurs in the upper troposphere around 250hPa. It is this unique warm-core structure within a tropical cyclone that produces very strong winds near the surface and causes damage to coastal regions and islands through extreme wind driven storm surge, wave action and torrential rains [1].

Numerical Weather Prediction (NWP) is one of the best tools for the near real time prediction of various atmospheric phenomena. It is a complex system represented by interaction of atmosphere and oceans with non-linear dynamics and physics. The use of NWP model for tropical cyclone studies started in the early 1960's and there have been a significant improvement in numerical weather prediction in last three decades. Much of this up gradation is due to computational resources, developments in numerical techniques, improved modelling of physical processes and improvements in observing systems, data assimilation and initialization. One such system in present use is Weather Research and Forecasting (WRF) with Advanced Research WRF (ARW) core & Non-hydrostatic Mesoscale Model (NMM) core, which are designed to be flexible, state-of-the art atmospheric simulation system.

2. Brief history of Hudhud

The Very Severe Cyclonic Storm 'HUDHUD' developed from alow pressure area which lay over Tenasserim coast and adjoining North Andaman Sea in the morning of 06 October, 2014. It concentrated into a Depression in the morning of the 07 October over the North Andaman Sea. Moving west-northwestwards it intensified into

a Cyclonic Storm (CS) in the morning of 08 October and crossed Andaman Islands between 0300UTC and 0400UTC of 08 October. It then emerged into Southeast Bay of Bengal and continued to move west-northwestwards. It intensified into a Severe Cyclonic Storm (SCS) in the morning of 09 October and further into a Very Severe Cyclonic Storm (VSCS) in the afternoon of 10 October,2014. It continued to intensify while moving north-westwards and reached maximum intensity in the early morning of 12October,2014 with a maximum sustained wind speed (MSW) of 180 kmph over the West Central Bay of Bengal off Andhra Pradesh coast. It crossed north Andhra Pradesh coast over Visakhapatnam (VSK) between 0630UTC and 0730UTC of 12 October with the same wind speed [2]. After landfall, it continued to move northwestwards for some time and weakened gradually into SCS in the evening and further into a CS in the same midnight. It then, weakened further into a Deep Depression in the early morning of 13th and weakened into a depression in the evening of 13October. Thereafter, it moved nearly northward and weakened into a well-marked low pressure area over East Uttar Pradesh and neighbourhood in the evening of 14October 2014.

According to IMD report the salient features of the system are as follows:

i. At the time of landfall on 12th Oct, the estimated maximum sustained surface wind speed in association with the cyclone was about 100 Knots.

ii. The estimated central pressure was 950hPa with a pressure drop of 54hPa at the centre compared to surroundings.

iii. It caused very heavy to extremely heavy rainfall over North Andhra Pradesh and South Odisha and strong gale winds leading to large scale structural damage over North Andhra Pradesh and adjoining districts of South Odisha and storm surge over North Andhra Pradesh coast.

iv. Maximum 24 hour cumulative rainfall of 38 cm ending at 0830 hrs IST of 13October was reported from Gantyada (dist Vizianagaram) in Andhra Pradesh. Maximum of storm surge of 1.4 meters above the astronomical tide has been reported by the tide gauge at Visakhapatnam.

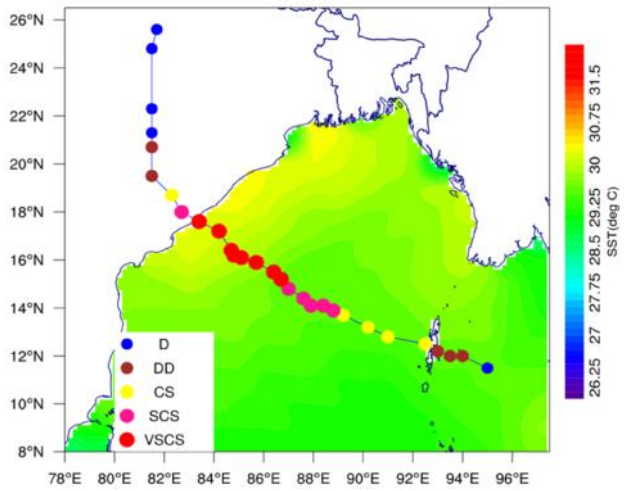

Fig-1: Observed track of very severe cyclonic storm Hudhud, background colours represent the sea surface temperature (SST).

3. Description of the model

The non-hydrostatic compressible WRF model was developed by national Centre for Atmospheric Research (NCAR). It has features like a fully compressible, Eulerian non-hydrostatic control equation set, a terrain following, hydrostatic pressure vertical coordinate system with the constant pressure surface at the top level of the model. The staggered grid, like Arakawa-C grid, used in the model and a third order Runge-Kutta time integration scheme used for both horizontal and vertical directions. The WRF model incorporates several processeslike MP, CP, PBL, surface layer, land surface, long wave & short wave radiations with multiple options for each process [3, 4]. In the present study, WRF-ARW model was used to simulate the very severe cyclone Hudhud. The horizontal resolution used is 20 km with 29 vertical levels. The input details of the model are given in table 1.

Table-1: Brief description of WRF model configuration

Model	WRF V3.5.1
Max_domain	1
Start_date	2014-10-08_00
End_date	2014-10-13_00
Map Projection	Mercator
Resolution	20 Km
Time step	120s
Central point of the domain	17.5°N, 87.5°E
No. Of grid points	112 (WE), 112 (NS)
Run time	120hrs
No. Of Vertical levels	29Sigma Levels
Horizontal Grid	Arakawa C Grid
Time Integration	Runge-Kutta second and third order time
Radiation Scheme	Dudhia's short wave/RRTM long wave
PBL Scheme	YSU scheme
Convection	Kain-Fritsch(new Eta) scheme
Micro Physics	WSM3-class simple ice scheme

4. Data used

The United States Geological Survey (USGS) 10`resolution terrain topographical data have been used in the WRF preprocessing system (WPS) [5]. The 1° resolution FNL data from the National Center for Environmental Prediction (NCEP) have been used as initial and boundary conditions. Simulation was initiated on 08 October 2014, 00 UTC with lateral boundary conditions and was carried out up to 13 October 2014, 00 UTC. The lateral boundary conditions are available at 3hours intervals. RSMC (Regional Specialized Meteorological Centre), New Delhi observed/estimated data as well as TRMM 3B42V7 data have been used to compare the model simulated various fields.

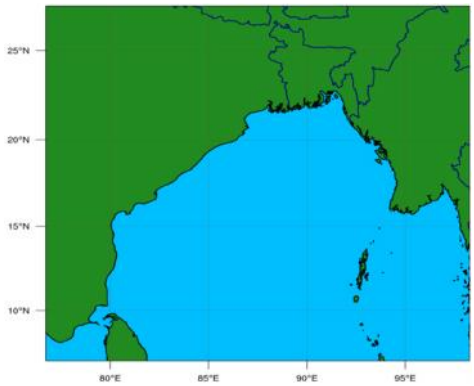

Fig-2: Model domain employed in the present study, 08October 2014, 00UTC. The resolution of the domain is 20 km

5. Results & discussion

Simulation of Minimum Central Pressure (MCP) is presented by grey line whereas black line represents RSMC estimated Minimum Central Pressure (MCP) in fig-5.1. Initially model simulated and estimated MCP is very close and it is up to 36hrs. After that variation in MCPs are very large and again last 24hrs MCPs are very close. Model simulates sharp fall in MCP and lowest MCP is 938hPa at 00UTC, 11 October. On the other hand RSMC

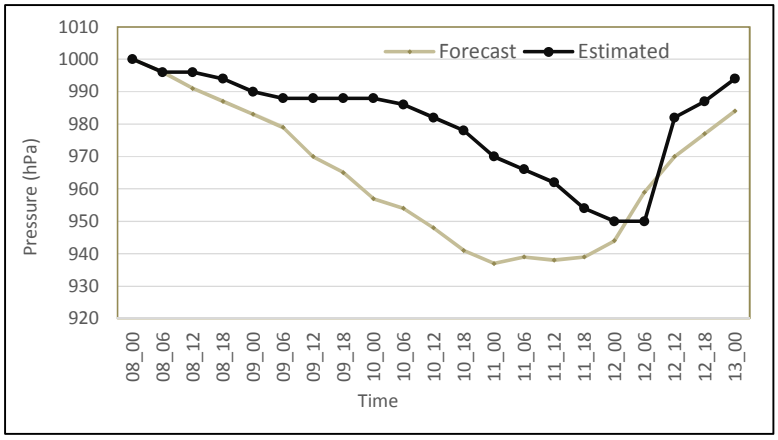

Fig-5.1: Comparison of model simulated minimum central pressure with observation.

estimated lowest MCP was 950hPa at 00UTC, 12 October. Therefore model has predicted the intensification of the system 24hours in advance but overestimated in pressure falling by 12hPa. Also model shows the system retains its peak intensity up to 18hrs whereas observation shows only 06hrs. On 12 October 06UTC to 12UTC observation depicts very sharp rise in pressure and the value is 32hPa in 06hrs. But model unable to capture the phenomena.

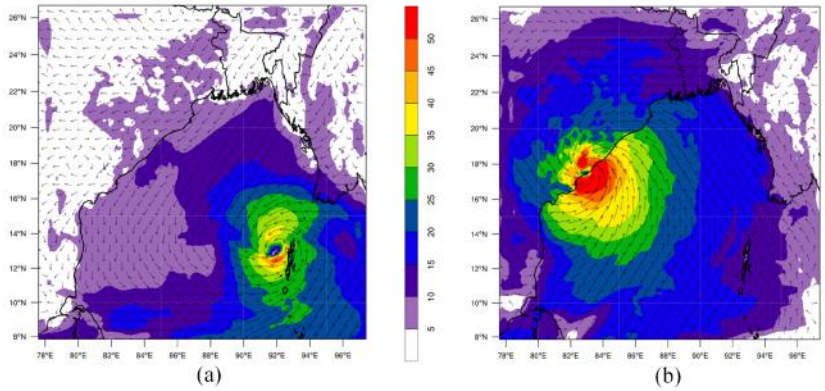

Fig-5.2: Simulation of surface wind field (speed in m/s) on (a) 06UTC, 08October; (b) 06UTC, 12 October.

Simulation of surface wind field is shown in (fig-5.2a,b). It is clearly seen that well organised centre of the system with relatively stronger wind speed in the southeast and northern sector (fig-5.2a) at cyclonic storm stage. On 06UTC, 12 October 2014, during the time of landfall variationin wind speed is increased in the north-eastern sector whereas the core wind remained symmetric around the centre (fig-5.2b). During the time of landfall model simulated strong wind of order more than 100kts which is good in agreement with the observation. Also from the figure, it can easily be concluded that the west-northwesterly movement of the system.

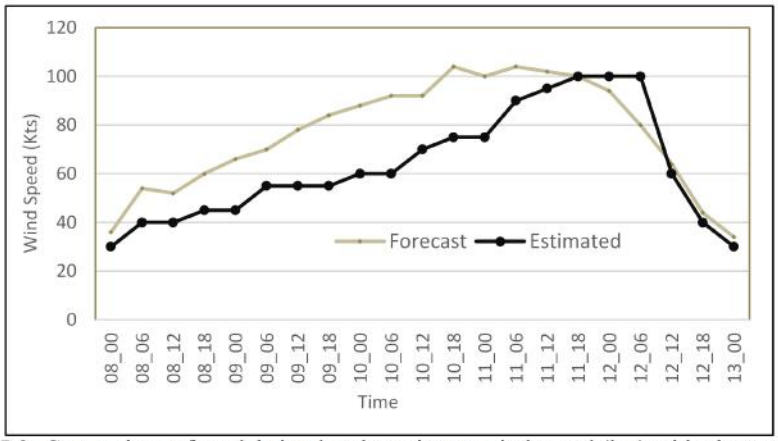

Fig-5.3: Comparison of model simulated maximum wind speed (kts) with observation.

Simulation of Maximum Wind Speed (MWS) is presented by grey line whereas black line represents estimated Maximum Wind Speed (MWS) (fig-5.3). It is clearly seen that model simulated MWS overestimate compared with RSMC estimated MWS up to 90hrs. During decaying stage estimated and simulated MWS are very good in agreement. This is because of there is a less variation in wind speed during decaying stage. There is a sharp change in wind speed during decaying stage which model unable to capture. Again model simulated highest MWS is found 24hrs in advance than RSMC estimated and retain its intensity up to 24hrs. However simulated highest MWS value is very close to that of RSMC estimation.

Simulation of 500hPa wind field is presented in fig. (5.3a,b). On 08 October, 06UTC the horizontal structure of the wind at 500hPa level (fig-5.3a) depicted an organized centre with stronger wind to the northeast sector of the system. A feeble trough to the northwest of the system associated with a ridge to the west of the system roughly ran along 80°E and to the north of 15°N. Another ridge is located to the north of the system. On 12 October, 06UTC (fig-5.3b), clearly indicate that the centre of the system moved west-northwestwards with stronger wind to the eastern and northern sector of the system. An anti cyclonic circulation exists to the east northeast of the system near (lat. 20°N, lon.96°E). These troughs and ridges are favourable for further intensification and controlling the direction of movement which is simulated precisely by the model.

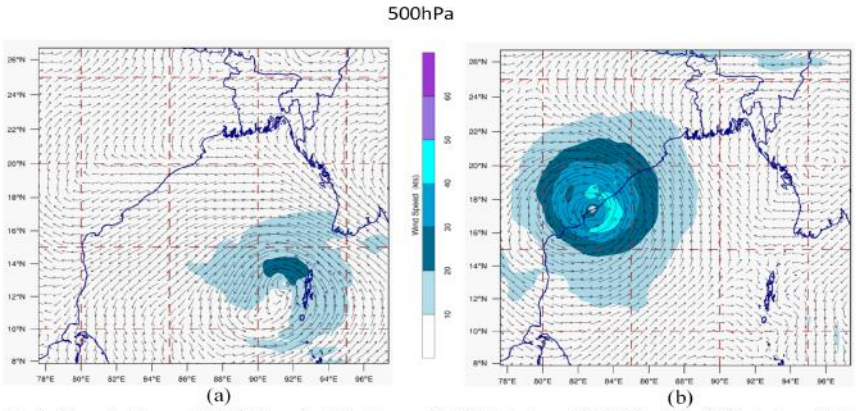

Fig-5.4: Simulation of 500hPa wind field on (a) 08October, 06UTC; (b) 12October, 06UTC.

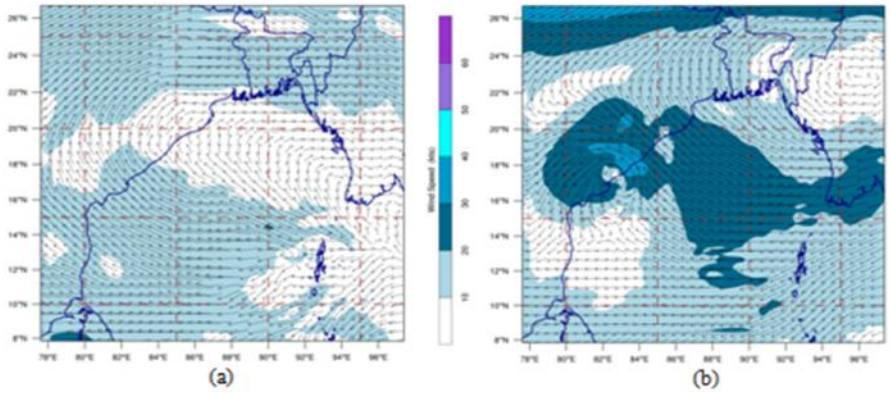

Fig-5.5: Simulation of 200hPa wind field on (a) 08October, 06UTC; (b) 12October, 06UTC.

Simulation of 200hPa wind field is presented in fig.(5.4a,b). On 08 October 06UTC, horizontal structure of the wind at 200ha (fig-5.4a) depicted an organized centre of anti cyclonic circulation of the system at cyclonic storm stage. A feeble trough to the northwest of the system associated with a ridge roughly ran along 80°E and to the north of 15°N. Another ridge is located to the northeast of the system. As the system intensified into a very severe cyclonic storm, the cyclonic circulation in association with the system extended vertically up to 200hPa during in the mature stage (fig-5.4b). The anticyclonic circulation located to the east northeast of the system centre. Another ridge located to the northwest of the system roughly runs along 78°E to the north of 20°N. The anti cyclonic circulation over east-northeastern and northwestern side of the system maintained west-northwesterly movement of the system. Finally, the system crossed Andhra Pradesh coast over Visakhapatnam (near lat.17.7°N and long.83.3°E) between 0630-0730 UTC.

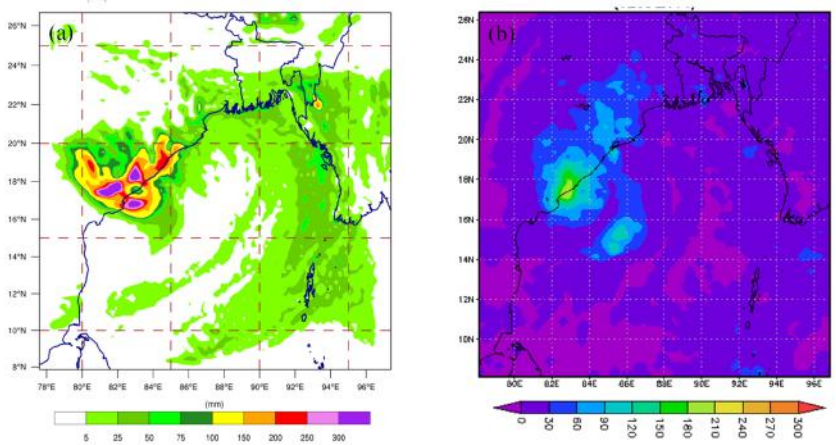

Fig-5.6: Comparison of model simulated 24hours total rainfall and TRMM daily accumulated rainfall on 12 October, 2014.

The spatial distribution of model simulated 24hrs total rainfall on 13 October, 00UTC (during the time of landfall) depicts a huge total of rainfall with three distinct coremore than 300mm of rain (fig-5.5a), whereas corresponding TRMM observation has well captured the spatial distribution of rainfall with fewer amounts (fig-5.5b). Also model simulated a good amount of rainfall over east central Bay and adjoining south east Bay but TRMM shows relatively less amount of rainfall. According to IMD's report, few stations of Andhra Pradesh have reported more than 300mm of rain (viz. Srungavarapukota 340mm, Gantyada 380mm) which is well in agreement with model simulation. Thus spatially and quantitatively model has simulated good rainfall, whereas quantitatively TRMM underestimate the amount of rainfall compared to model and observation.

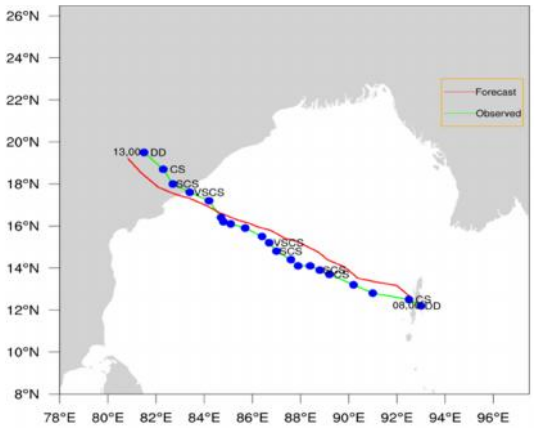

Fig-5.7: Comparison of model simulated track with observation

Simulated track is presented by red line and green line represents observed track (fig-5.7). It is clearly seen that model simulated track is well in agreement compared to observe track. Initially simulated and observed track is very close and again before landfall both tracks are very close to each other. After landfall variation between both tracks is increased, because there is a rapid change in intensity of a tropical cyclone after landfall. However model simulated track is a very good guidance to the forecasters.

6. Conclusion

WRF model is used to simulate various parameters such as SLP, maximum wind speed, rainfall and horizontal structure of cyclone Hudhud. Simulated fields are compared with the available observations and RSMC estimations. Comparison of simulated and estimated minimum central pressure shows that there is a good in agreement for the first 24hrs and last 24hrs of the simulation period, but there is a large variation in the middle (72hrs) of the simulation period. Comparison of simulated and estimated maximum wind speed indicates that for the last 30hrs of the simulation period result is quite reasonable, but for the first 90hrs of the simulation period result is less reasonable. Simulation of gale wind is well in agreement with the estimation though there is temporal variation of 24hrs. Model simulates the intensification of the system 24hours in advance but over estimates in pressure falling by 12hPa. Spatially and quantitatively model simulated rainfall is well matched with the observation. Model simulated track is very good in agreement with observation though there are some temporal and spatial biases. However, model has simulated various parameters as well as vertical and horizontal structure of the system is very well. This is because of improved initial conditions in the FNL data for the simulation of cyclone Hudhud.

Acknowledgement

Authors are very grateful to NCEP and NCAR for providing FNL data. The precipitation data provided by TRMM is highly recognized. Especial credit goes to WRF model developers for the study. Authors alsolike to thankstheir colleagues for precious suggestion during the study.

References:

1. Henderson-Sellers, A., H. Zhang, G. Berz, K. Emanuel, W. Gray, C. Landsea, G. Holland, J. Lighthill, S. L. Shieh, P. Webster and K. McGuffie, 1998, "Tropical cyclones and global climate change: A post-IPCC assessment", Bulletin of the American Meteorological Society, 79, 19–38.
2. Very Severe Cyclonic Storm, HUDHUD: A Preliminary Report, Cyclone Warning Division, IMD (RSMC).
3. Skamarock W C, Klemp J B, Gill D O, Barker D M, Duda M G, Huang X, Wang W & Powers J G, A description of the advanced research WRF version 3, NCAR Technical Note TN-475+STR, (NCAR, Boulder, USA),2008.
4. M Venkatarami Reddy, S B Surendra Prasad, U V Murali Krishna& K Krishna Reddy, Effect of cumulus and microphysical parameterizations the JAL cyclone prediction, Indian Journal of Radio & Space Physics, Vol.43, February 2014,pp103-104.
5. R Chandrasekar and C Balaji, Sensitivity of tropical cyclone Jalsimulationsto physics parameterizations, *J. Earth Syst. Sci.* 121, No. 4, August 2012, pp. 923–946.

Feasibility of Fog Forecasting over Bangladesh using WRF Model and a Comparison with ECMWF model products

Md. Omar Faruq[1*], Shamsuddin Ahmed[1], S.M. Quamrul Hassan[1], M. A. K. Mallik[1], Md. A.E. Akhter[2], Md. S. Alam[1], Md. A. Hossain[1] and S.M. M. Huque[1]

[1]Bangladesh Meteorological Department, Agargaon, Dhaka -1207, Bangladesh
[2]Department of Physics, Khulna University of Engineering & Technology, Bangladesh
[*]corresponding author e-mail: omarfaruq_78@yahoo.com

Abstract: An attempt has been made to forecast fog over Bangladesh using Weather Research and Forecasting (WRF) model. Thirteen micro-physics schemes are used in this study to evaluate the simulation of fog episode. An empirical relation is made of in-situ visibility with temperature and dew point temperature of Hazrat Shahjalal International Airport (VGHS), Dhaka, Bangladesh of winter seasons (January-February-December) during 2012-2015. This empirical relation is used in the model for the visibility forecasting over Bangladesh. The model predicted visibility is capable to internment the commencement and dissipated of fog event. Moreover, dissipated of fog is very steep in model prediction as compared to in-situ. No major impact of visibility is discernable on different micro-physics of the model. The results indicate that the WRF model is capable to predict the visibility, temperature and relative humidity reasonably well over Bangladesh in 24-h advance with comparison than that of European Centre for Medium range Weather Forecast (ECMWF) Model output.

Keywords: WRF, ECMWF & visibility.

1. INTRODUCTION

Fog consists of water droplets and/or ice crystals that are suspended close to the Earth's surface [1] i.e. it is a low-level stratus cloud [2]. Fog formation is directly related to thermodynamical, dynamical, radiative, aerosol and microphysical processes and to surface conditions [3]. The physical mechanism of the formation of fog can be reduced to the three primary processes- cooling, moistening and vertical mixing of air parcels with different temperature and humidity [4]. The necessary conditions for fog formation are high relative humidity (more than 85%), light winds, surface cool water droplets and lower level temperature inversion [5]. The Fog Phenomenon is associated with the comprehensive physical processes such as cloud microphysics, radiative transfer, horizontal and vertical diffusions in the planetary boundary layer (PBL) that are forced by the prevailing synoptic background as well as mesoscale disturbances [6-7]. The prediction of fog using Numerical Weather Prediction (NWP) models is important because satellite observations cannot be used accurately during night time and when ice and/or snow cover(s) the earth's surface. Surface observations over the land are also insufficient to determine the true extent of fog [8]. Numerical modeling of radiation fog has received a great deal of attention in the past years for various reasons, often in connection with traffic safety. The necessity of realistic fog simulations has further increased since it is known that acid fog is responsible for damages to vegetation and forests [9]. Moreover, fog is an important aspect of the climate in certain regions [10]. Numerical modeling of fog onset and development has a long history. Fisher and Caplan [11] were possibly first in examining the feasibility of constructing a numerical model for fog and low stratus forecasting. Operational fog forecasting over large domain is extremely difficult. The reasons are: (i) Conventional coarse grid NWP models are not adequate for local scale fog prediction; (ii) Conventional NWP models are not specifically designed for fog prediction and the cloud parameterization schemes in the models function well only for clouds at high levels and not for fog near the surface [12-13]. Despite all the improvements in horizontal and vertical resolutions and the physics of NWP models, the prediction of fog and low clouds still remains a challenge. Because fog events occur on relatively short space and time scales, forecasters are faced with the very difficult task of having to formulate space or time specific skillful forecasts [14]. According to the pathways that can lead to the saturation of air, fog is classified into different fog types. A frequently occurring fog type, especially for relatively flat areas like Bangladesh, is radiation fog, which occurs in clear-sky conditions with relatively low wind speed. Bangladesh is mainly influenced by radiation and advection fog except some hilly areas. In these conditions air close to the surface cools from the evening transition onwards because the absence of clouds leads to strong radiation loss from air close to the Earth's surface [15-18], while low wind speeds obstruct a sufficient supply of sensible and latent heat toward the surface [19-20].

In the present study, an attempt has been made to predict fog over Bangladesh in 36 hours advance using WRF model based on the initial condition of 0000 UTC of 10 December 2014. It is found that the model simulated result is realistically well.

2. Experimental setup and Methodology

The NWP model used in this study is the Advanced Research Weather Research and Forecasting model version 3.4. The WRF model has been developed by the National Center for Atmospheric Research (NCAR) and provides a flexible and portable open-source community model for both atmospheric research and operational forecasting [21]. It is a limited-area, non-hydrostatic primitive equation model with multiple options for various parameterization schemes for different physical processes.

2.1 Experimental setup

The Advanced Research WRF dynamical core uses the Arakawa-C grid staggering for the horizontal grid and a fully compressible system of equations. The terrain following hydrostatic pressure with vertical grid stretching is followed for the vertical grid. The time–split integration uses the third-order Runge-Kutta (RK3) scheme with a smaller time step for acoustic and gravity wave modes. The Kain-Fritsch [22–23] cumulus parameterization scheme (shown in Table 1), the WRF different microphysics scheme (shown in Table 2), Yonsei University (YSU) planetary boundary layer scheme are used here. The rapid radiative transfer model [24] and the Dudhia scheme [25] are used for long and shortwave radiation, respectively. The Noah land-surface model represents the atmosphere-land coupling [26–27], which consists of four soil layers with an overlying vegetation layer. All the experiments are conducted with a single domain [Fig. (1)] of Lat: 12.00°-34.08°N & Lon: 79.45°-100.95°E, consisting of 480 × 540 grid points with 5km spatial resolution. Thirteen experiments are performed with different micro-physics schemes initialized from 0000 UTC of 10 December 2014 for 36 h predictions. The ECMWF Global Data Assimilation System (GDAS) analysis of 0.125° × 0.125° is used to prepare the initial and lateral boundary conditions for all the thirteen experiments. Grid Analysis and Display Systems (GRADS) and Matrix Laboratory (MATLAB) are used for visualization of the graphics.

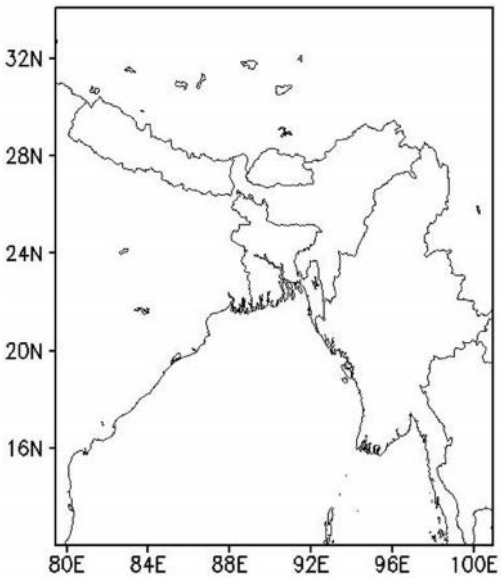

Figure 1: WRF model domain for the NWP study

Table 1: Model schemes used for fog prediction

No.	Characteristic Feature	WRF
01	Horizontal grid	Arakawa C grid
02	Map projection	Mercator
03	Time integration scheme	Third-order Runge–Kutta
04	Microphysics	All Schemes
05	Radiation (Short wave)	Dudhia scheme
06	Radiation (Long wave)	rrtm scheme [24]
07	Land Surface Model	unified Noah land-surface model [26]
08	Planetary Boundary Layer scheme	YSU
09	Cumulus parameterization scheme	Kain-Fritsch scheme
10	Dynamics	Non-hydrostatic with 3D Coriolis force

2.2Data Used

Model simulations are evaluated against VGHS (Hazrat Shahjalal int. Airport, Dhaka; Lat = 23.85°N & Lon=90.4°E), VGEG (Shah Amanat int. Airport, Chittagong; Lat=22.216667°N & Lon=91.8°E), VGSD (Sayedpur Airport; Lat=25.75°N & Lon=88.916667°E) and VGBR (Barisal Airport; Lat=22.75°N & Lon=90.36667°E) observations like 2 m air and dew-point temperature, relative humidity and visibility. The ECMWF generated global analysis with horizontal sampling of 0.125°X0.125° at four synoptic time hours of 0000, 0600, 1200, and 1800 UTC are used in WRF model.

Table 2: Different WRF micro-physics schemes used for fog prediction

Scheme	MP	Description
Kessler scheme	1	A warm-rain (i.e. no ice) scheme used commonly in idealized cloud modeling studies.
Lin et al. scheme	2	A sophisticated scheme that has ice, snow and graupel processes, suitable for real-data high-resolution simulations.
WRF Single-Moment 3-class scheme	3	A simple, efficient scheme with ice and snow processes suitable for mesoscale grid sizes.
Eta microphysics	5	The operational microphysics in NCEP models. A simple efficient scheme with diagnostic mixed-phase processes for fine resolutions (< 5km).
WRF Single-Moment 6-class scheme	6	A scheme with ice, snow and graupel processes suitable for high-resolution simulations.
Goddard microphysics scheme	7	A scheme with ice, snow and graupel processes suitable for high-resolution simulations. New in Version 3.0.
New Thompson et al. scheme	8	A new scheme with ice, snow and graupel processes suitable for high-resolution simulations. This adds rain number concentration
Milbrandt-Yau Double-Moment 7-class scheme	9	This scheme includes separate categories for hail and graupel with double-moment cloud, rain, ice, snow, graupel and hail.
Stony Brook University (Y. Lin) scheme	13	This is a 5-class scheme with riming intensity predicted to account for mixed-phase processes.
WRF Double-Moment 5-class scheme	14	This scheme has double-moment rain. Cloud and CCN for warm processes, but is otherwise like WSM5.
WRF Double-Moment 6-class scheme	16	This scheme has double-moment rain. Cloud and CCN for warm processes, but is otherwise like WSM6.
NSSL 2-moment scheme	17	This is a two-moment scheme for cloud droplets, rain drops, ice crystals, snow, graupel, and hail. It also predicts average graupel particle density, which allows graupel to span the range from frozen drops to low-density graupel.
NSSL 2-moment scheme	18	MP17+predict cloud condensation nuclei (CCN) concentration.

2.3 Development of Visibility algorithm

Initially Rapid Update Cycle (RUC) [28] and Forecast System Laboratory (FSL) [29] visibility algorithm show a large error in visibility forecasting. Moreover, Steolinga and Warner (SW99) [12] visibility methods implemented in UPP (Unified Post-processor) model is also not capable to detention this fog event and produce a very large error over the VGHS, VGEG, VGSD and VGBR stations.

So, a linear relation is established between observed visibility from in-situ temperature and dew point temperature using January-February-December data during 2012–2015 and applied to WRF Model predicted meteorological parameters. The relation is -

visibility $= -211 + 158 \times t_{2m} - 143 \times T_{d2m}$;

where, t_{2m} = 2m air temperature, t_{d2m} = 2m dew point temperature.

3. RESULTS AND DISCUSSIONS

3.1 Comparison between WRF model product and INSAT3D fog image

The special distribution of WRF model predicted visibility (visibility < 1000 m) using MP-1 (microphysics-1) valid for 0000 UTC of 11 Dec 2014 over Bangladesh is depicted in the Fig. 2 (a – b). It is found from the special distribution of WRF model predicted visibility using MP-1 and INSAT3D fog image that both has the similar signature except Rangpur, Tangail and Mymensingh regions. In case of other microphysics (MP-2, MP-3, MP-5, MP-6, MP-7, MP-8, MP-9, MP-13, MP-14, MP-16, MP-17 & MP-18) model predicted visibility and INSAT3D fog image represents the MP-1 with no appreciable change in patterns is shown in Fig. 3 (a-h) & Fig. 4 (i-h). But MP-7 does not capture the fog event over Rajshahi region reasonably well compared to INSAT3D image.

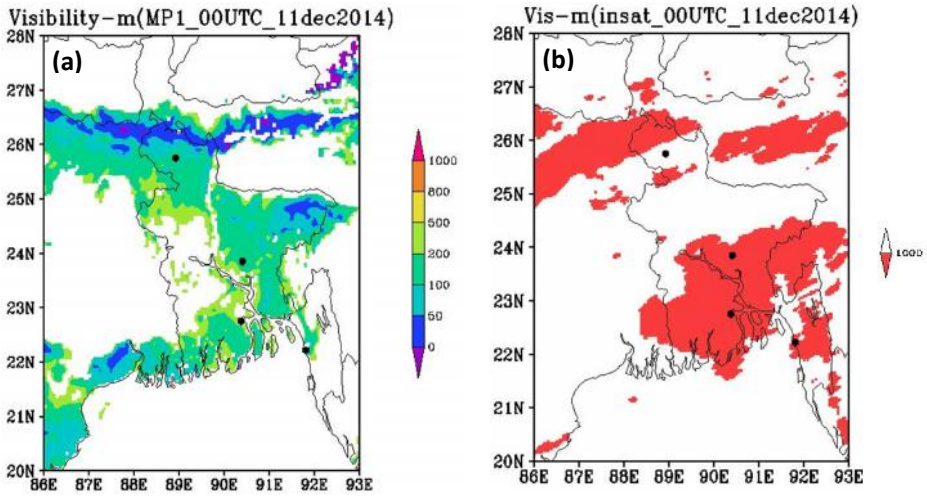

Fig. (2): 24 h predicted visibility of (a) MP-1 and (b) INSAT3D based on 0000 UTC of 10 Dec 2014

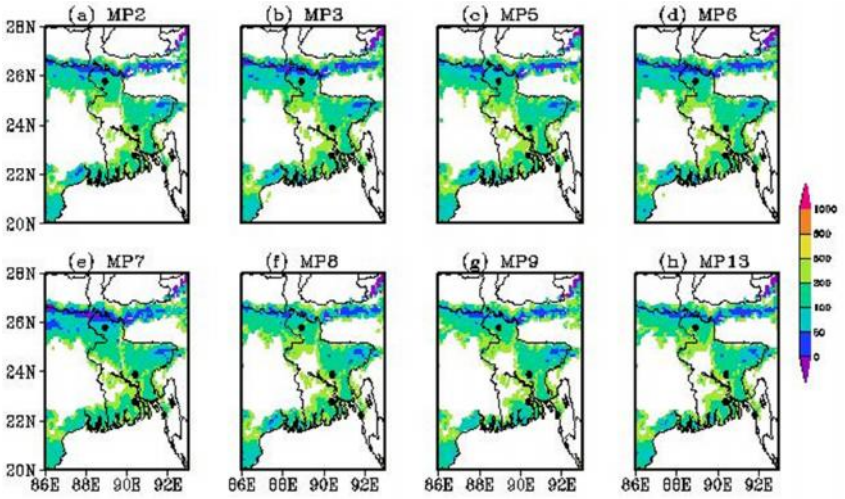

Fig. 3 (a-h): Spatial distribution of 24 h predicted visibility of MP-2, MP-3, MP-5, MP-6, MP-7, MP-8, MP-9 & MP-13 based on 0000 UTC of 10 December 2014.

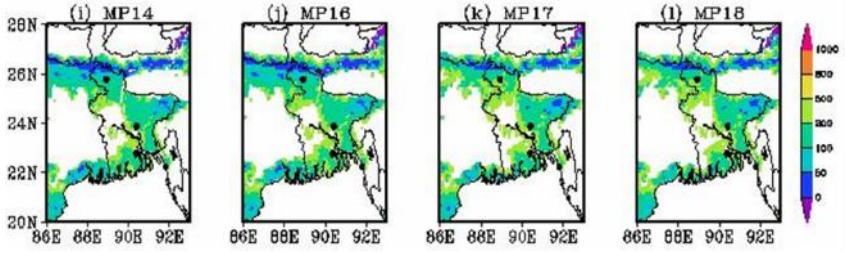

Fig. 4 (i-l): Spatial distribution of 24 h predicted visibility of MP-14, MP-16, MP-17 & MP-18 based on 0000 UTC of 10 December 2014.

3.2. Comparison of WRF model predicted visibility of VGHS, VGEG, VGSD and VGBR stations with in-situ and ECMWF output

Temporal distribution of temperature, relative humidity & visibility of WRF model predicted, in-situ measured and ECMWF analysed of VGHS, VGEG, VGSD and VGBR stations from 0000 UTC of 10 December 2014 to 1200 UTC of 11 December 2014 are shown in Fig. (5–8). 36 h temperature, relative humidity and visibility forecasts show that no major difference in the pattern is found when different micro-physics are used in WRF model. Low temperature and high relative humidity are found at the commencement of fog.

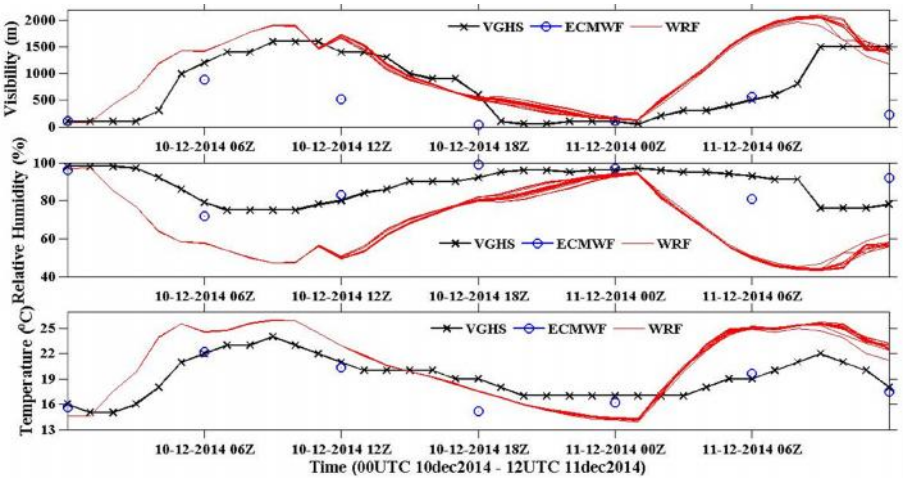

Fig. 5: Temporal distribution of temperature, relative humidity & visibility of WRF model predicted, in-situ measured and ECMWF analysed of VGHS stations from 0000 UTC of 10 December 2014 to 1200 UTC of 11 December 2014.

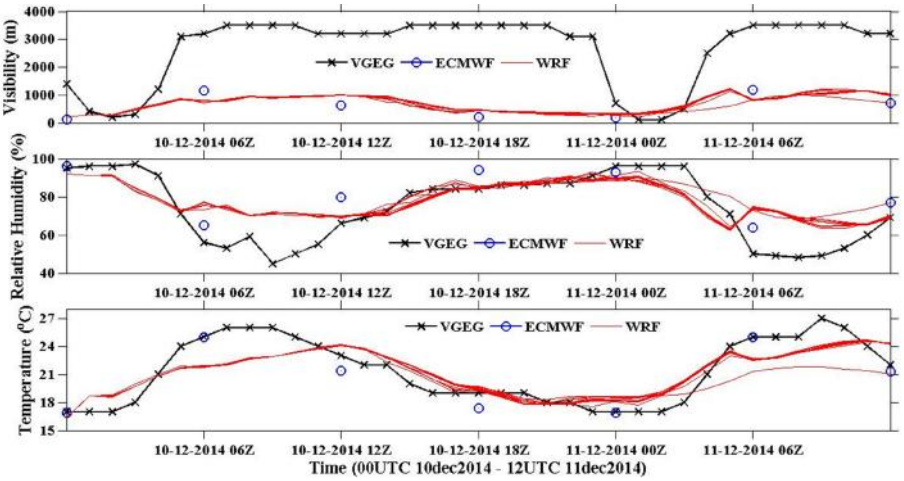

Fig. 6: Temporal distribution of temperature, relative humidity & visibility of WRF model predicted, in-situ measured and ECMWF analysed of VGEG stations from 0000 UTC of 10 December 2014 to 1200 UTC of 11 December 2014.

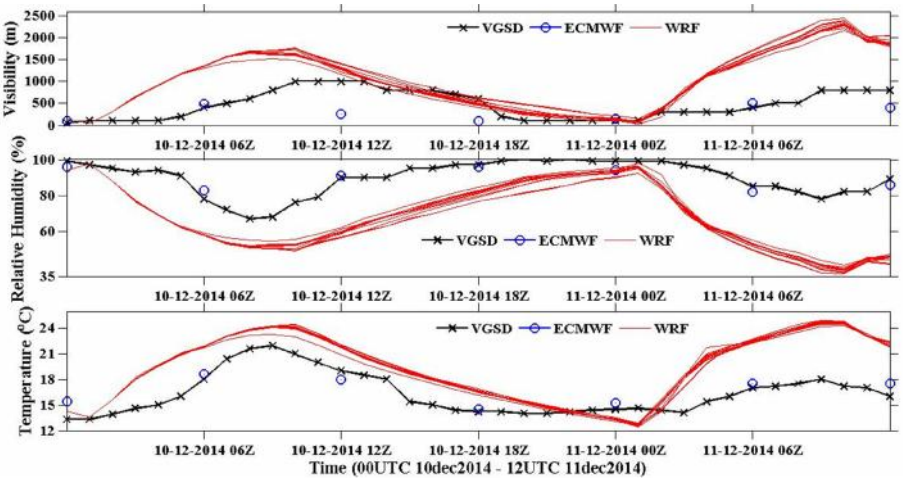

Fig. 7: Temporal distribution of temperature, relative humidity & visibility of WRF model predicted, in-situ me and ECMWF analysed of VGSD stations from 0000 UTC of 10 December 2014 to 1200 UTC of 11 December

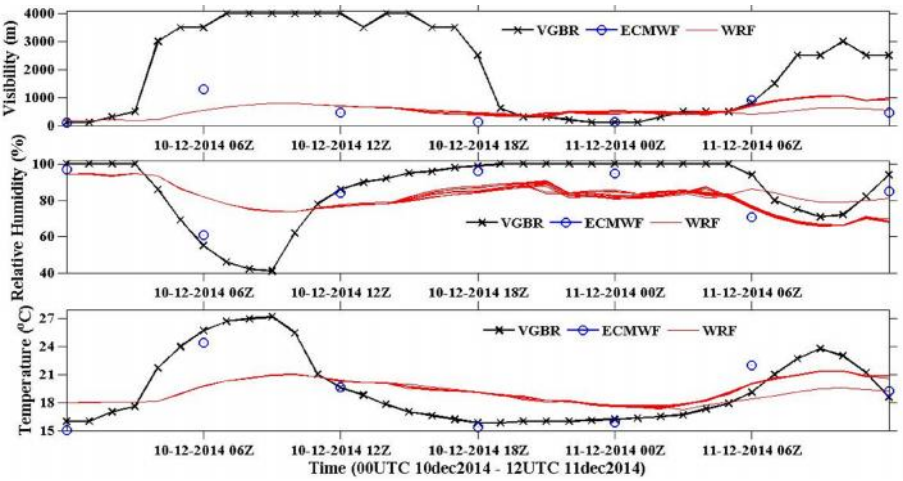

Fig. 8: Temporal distribution of temperature, relative humidity & visibility of WRF model predicted, in-situ measured and ECMWF analysed of VGBR stations from 0000 UTC of 10 December 2014 to 1200 UTC of 11 December 2014.

We found the dense fog at ~ 0200 UTC of 11 December 2014 which can be confirmed from visibility data. WRF model simulated fog is captured well at the stations of VGHS and VGSD. It indicates that WRF model is able to capture the necessary conditions for fog formation.

4. CONCLUSION

Fog forms, develops and dissipates as a result of complex interactions among various local microphysical, dynamical, radiative and chemical processes, boundary layer conditions and large-scale meteorological processes. In this study, all micro-physics schemes show no major difference in pattern predicted by WRF model. But the model is capable to capture the fog in terms of visibility realistically or unrealistically well.

REFERENCES

1. Brown R and Roach WT (1976): The physics of radiation fog: II-A numerical study. Q J R teorol Soc 102:335–354.
2. Gultepe I., Tardif R, Michaelides SC, Cermak J, Bott A, BendixJ, Muller M, Pagowski M, Hansen B, Ellrod G, Jacobs W, Toth G and Cober SG (2007): Fog research: a review of past achievements and future perspectives. Pure Appl Geophys 164:1121–1159.
3. Gultepe I., M. D. Müller, and Z. Boybeyi, 2006: A New Visibility Parameterization for Warm-Fog Applications in Numerical Weather Prediction Models. J. Appl. Meteor. Climatol., 45, 1469–1480.
4. Wang Binhua, 1983: *Sea Fog*. China Ocean Press, 352pp. (in Chinese).
5. LutgentsTarbuck, seventh edition.
6. Chun, Y.-S., K.-O. Boo, J.-Y. Kim, S.-W. Kim, H.-M. Cho, and S. Hong (1999): Analysis of the radiation fog at the Kimpo International Airport in autumn, J. of Atmos. Res., 16(1), 30-43.
7. Croft, P. J., R. L. P fost, J. M. Medlin, and G. A. Johnson, 1997: Fog forecasting for the southern region: A conceptual model approach. Wea. Forecasting, 12, 545–556.
8. Ellrod, G. P., 1995: Advances in the detection and analysis of fog at night using GOES multispectral infrared imagery. *Wea. Forecasting*, **10,** 606–619.
9. Bott A, Sievers U, Zdunkowski W (1990): A Radiation Fog Model with a detailed treatment of the interaction between radiative transfer and fog microphysics. J Atmos Sci 47:2153–2166.
10. Syed FS, Körnich H, Tjernström M (2012): On the fog variability over south Asia. Clim Dyn 39:2993–3005.
11. Fisher, E. L., and P. Caplan, 1963: An experiment in numerical prediction of fog and stratus. J. Atmos. Sci., 20, 425–437.
12. Stoelinga, T. G. and T. T. Warner, 1999: Non-hydrostattic, mesobetascale model simulations of cloud ceiling and visibility for an east coast winter precipitation event. *J. Apply. Meteor*., 38, 385-404.
13. Müller, M. D., M. Masbou, and A. Bott, Z. Janjic, 2005: Fog prediction in a 3D model with parameterized microphysics. Preprints, *World Weather Research Programme's Symposium on Nowcasting and Very Short Range Forecasting*, September 5-9, Toulouse, France.

14. Roquelaure, S., and T. Bergot, 2008: A Local Ensemble Prediction System (L-EPS) for fog and low clouds: Construction, Bayesian model averaging calibration, and validation. J. Appl. Meteor. Climatol., 47, 3072–3088.
15. Ha K J and Mahrt L (2003): Radiative and turbulent fluxes in the nocturnal boundary layer. Tellus 55A:317–327.
16. Savijärvi H (2006): Radiative and turbulent heating rates in the clear-air boundary layer. Q J R Meteorol Soc 132:147–161.
17. Edwards J M (2009): Radiative processes in the stable boundary layer: part I. Radiative aspects. Boundary-Layer Meteorol 131:105–126.
18. Steeneveld G J, Wokke M J J, Groot Zwaaftink C D, Pijlman S, Heusinkveld B G, Jacobs A F G, Holtslag A A M (2010): Observations of the radiation divergence in the surface layer and its implication for its parametrization in numerical weather prediction models. J Geophys Res 115:D06107.
19. Duynkerke, P. G., 1991: Radiation fog: A comparison of model simulation with detailed observations. *Mon. Wea. Rev.*, 119,324–341.
20. Duynkerke P G (1999): Turbulence, radiation and fog in Dutch stable boundary layers. Boundary-Layer Meteorol 90:447–477.
21. Skamarock W C, Klemp J B, Dudhia J, Gill D O, Barker D M, Duda M G, Huang X Y, Wang W, Powers W G (2008): A description of the advanced research WRF, Version 3. NCAR Technical Note, Boulder.
22. Kain, J. S., and J. M. Fritsch, 1990: A one-dimensional entraining/detraining plume model and its application in convective parameterization. J. Atmos. Sci., 47, 2784–2802.
23. Kain, J. S., and J. M. Fritsch, 1993: Convective parameterisation for mesoscale models: The Kain–Fritsch scheme. The Representation of Cumulus Convection in Numerical Models, Meteor. Monogr., No. 46, Amer. Meteor. Soc., 165–170.
24. Mlawer, E.J., S.J. Taubman, P.D. Brown, M.J. Iacono, and S.A. Clough (1997): Radiative transfer for inhomogeneous atmospheres: RRTM, a validated correlated-k model for the longwave, J. Geophys. Res., 102(D14), 16663-16682.
25. Dudhia J (1989): Numerical study of convection observed during the winter monsoon experiment using a mesoscale two-dimensional model. J Atmos Sci 46:3077–3107.
26. Chen F and Dudhia J (2001): Coupling an advanced land surface-hydrology model with the Penn State-NCAR MM5 modeling system. Part I: model implementation and sensitivity. Mon Weather Rev 129:569–585.
27. Chen F, Kevin W. Manning, Margaret A. LeMone, Stanley B. Trier, Joseph G. Alfieri, Rita Roberts, Mukul Tewari, Dev Niyogi, Thomas W. Horst, Steven P. Oncley, Jeffrey B. Basara, and Peter D. Blanken, 2007: Description and Evaluation of the Characteristics of the NCAR High-Resolution Land Data Assimilation System. *J. Appl. Meteor. Climatol.*, 46, 694–713.
28. Bang Cheol-Han, Ji-Woo Lee, Song-You Hong (2009) Predictability Experiments of Fog and Visibility in Local Airports over Korea using the WRF Model. J. KOSAE Vol. 24, No. E 2 pp. 92~101; Journal of Korean Society for Atmospheric Environment.
29. Doran, J.A., P.J. Roohr, D.J. Beberwyk, G.R. Brooks, G. A. Gayno, R.T. Williams, J.M. Lewis, and R.J. Lefevre (1999) The MM5 at the Air Force Weather Agency-New products to support military operations, The 8th Conference on Aviation, Range, and Aerospace Meteorology, Dallas, Texas, 10-15 January.

GROWING STOCK ESTIMATION IN FOREST TYPE GROUP-V OF HARIDWAR DISTRICT, UTTARAKHAND, INDIA, USING GEOSPATIAL TECHNOLOGY

Poonam[1], Ekta Singh[2], Dharmendra Singh[3]

[1]Forest Research Institute, Dehradun
[2]Forest Survey of India, Dehradun
[3]Indian Institute of Remote Sesning, [4]Kalidash Road, Dehradun
Email: *dharmbaghel01@gmail.com*

Abstract: The present study deals with combined usage of satellite remote sensing data and ground survey inventories to assess growing stock in per ha. and in the strata of forest type group-V. This exercise also yields three crown density classes i.e. more than 70% (VDF), between 70-40% (MDF) and between 40-10% (OF) for each forest sub-type comes under the forest type group-V. As per this estimation, based on IRS LISS-III satellite data of the year 2004, the total volume or growing stock per ha. of forest type group-V of different forest density classes of Haridwar district are 150.20 m^3 for VDF, 95.776 m^3 for MDF and 43.505 m^3 for OF. Result shows that about 1.56% of the total growing stock is contributed by VDF, 53% by MDF, 45.44% by OF. 81% of the total growing stock is stored in forest subtype 5B/C2 (Northern Dry Mixed Deciduous) and 5/1S2 (Khair Sissoo Forest). Pattern of growing stock accumulation is 5B/C2>5/1S2>5B/cC1>5/DS1. Forest subtype 5/DS1 (Dry Deciduous Scrub) is covering lowest area and thus showing lowest growing stock accumulation among all the subtype of the forest type group-V and need immediate conservation measures to be taken.

Keywords: Forest density, Satellite data, 5B/C2 (Northern Dry Mixed Deciduous), 5/1S2 (Khair Sissoo Forest).

1. Introduction

Forests are the most valuable natural resources because of its economic, environmental, aesthetic and recreational values along with its renewable nature [1, 2]. Due to ever increasing population and its inexorable needs, these resources are facing extreme pressure [3]. To facilitate sustainable forest resource utilization and its management and to reduce anthropogenic pressure, forest planner requires key information such as growing stock, stand density, stand height etc. [4]. Information on status of growing stock of the forest cover in the country is very important to obtain the gap in demand and availability of forest resources to sustain this demand [5]. Growing stock is also, key information required in forest policy formulation, [6, 7] however it is not possible to assess the growing stock at a given point in time for a given landscape with classical inventory methods [1]. Simultaneously it is not realistic too because of time and budgetary limits. Geospatial technology along with traditional field survey have been extensively applied in the field of forest inventories to estimate the growing stock [8, 9] at landscape level and have been found cost and time effective [10].

Applications of remote sensing and geographic information system (GIS) in forest inventories can be categorised in to three state of art: (1) observation or measurement, meaning using remotely sensed data in place of field observations or measurements; (2) estimation, meaning calculation of traditional inventory areal estimates such as forest area or volume per unit area; and (3) mapping [8]. Several work have already been done to assess forest parameters such as leaf area index (LAI), Growing Stock, Stand height, biomass etc. using field inventory incorporated remote sensing models [9-18].

FSI in 1995 attempted growing stock estimation at country level using a methodology which involved use of remote sensing data (satellite imagery as well as aerial photographs) and volume factors based on forest field inventory data [5]. Singh et al. have also used the satellite data for growing stock estimation in part of Doon valley [12]. Singh et al. and Singh & Singh have estimated above ground biomass in the forest of Jammu and Kashmir and in Rajpur Hills and Mussoorie hills of Uttarakhand respectively using remote sensing approach [9, 10]. Mackrobert & Tamppo

have reviewed all the aspect of forest parameter retrieval under National Forest Inventory (NFI) programme in geospatial domain [8]. Most of the studies related to the growing stock estimation have revealed that it varies with crown/forest density and forest type however very few studies are reported regarding growing stock accumulation at forest type group level [9, 10, 12]. As India itself is much diverse in its forest type with 6 major groups, 16 types, 46 sub-types and 221 ecologically stable formations [19], the distribution of growing stock among them would also be diverse. Knowing its distribution at landscape level, which is possible through geospatial technology, may help in formulating scientific management policies for the forest [10]. Present study highlights the application of satellite remote sensing technology and Global Positioning System (GPS) in quantification of forest growing stock in the forest type group-V (dominant forest type) in the Haridwar district of Uttarakhand, India. Results of this study would be applicable as baseline information for the forest managers and to assess biomass and carbon densities (both these parameters are growing stock dependent) in the subtypes of forest type group-V, as this is first of its kind study have been done with IRS P6 LISS-III satellite data in this area. Simultaneously it will also indicate about most vulnerable forest sub-type (forest sub-type with minimum coverage area and minimum growing stock) among forest type-V and which need immediate conservation.

Forest type group-V (Tropical dry deciduous forests)

Forest type group-V plays a key role in Indian environment as the maximum proportion of the countries forest area is occupied by them [18]. These forests (annual rainfall varies between 500mm to 1500mm at country level distribution, about 1100 mm reported at Hardwar area) have been degraded heavily during the past few decades because of increasing population pressure [1, 20, 21]. The effect is felt more as growth of these forests is slow and regeneration is poor. Information with respect to these forests, their type, quality and distribution is of prime need for adopting conservation measures, eco-balance and planning-cum-management aspect. They are distributed from southern portion (south Deccan plateau) of the country to the northern part of it, based on this they are categorised into southern Deccan plateau dry deciduous forest and Northern dry deciduous forest [21].

The general appearance of the northern tropical dry deciduous forest is very closely similar to that of its southern counterpart, differing most noticeably in the presence of certain conspicuous northern floristic constituents and the absence of some of the characteristic southern species, and in the typically rather different physiographic and soil which also affect the composition and structure to some extent. Variation in physiography, soil and vegetation composition and structure, builds distinctive physiognomy and unique structure in forest patches which make them unique from their surrounding vegetation. Based on these distinctive physiognomy and unique structure, forest type group-V of Haridwar district (northern dry deciduous forest) is categorised into four sub types viz. Dry Plain sal forest (5B/C1b), Dry deciduous scrub (5/DS1), and Northern dry mixed deciduous forest (5B/C2), Khair-sissoo forest (5/1S2) [19]. The peculiar characteristics of these forest sub types [5, 18, 20, 22] are listed in the table no. 1.

2. Materials and Methods

Study Area

Haridwar district, covering an area of about 2360 km², is the southwestern part of Uttarakhand state and is located in between Shiwalik Hills in the North and Northeast and Ganga River in the South within latitude of 29.58 degree north and longitude 78.13 degree east. However, since it is not cradled by the mountains, its weather is also affected by the conditions in other parts of Northern India. Mean height of the study area is 249.7 metres from the mean sea level [23]. Average yearly temperature varies from 16.2˚C to 28.5˚C. Annual rainfall is 2,374 mm.

The flora found in the area is diverse with distinct vegetation zones that include

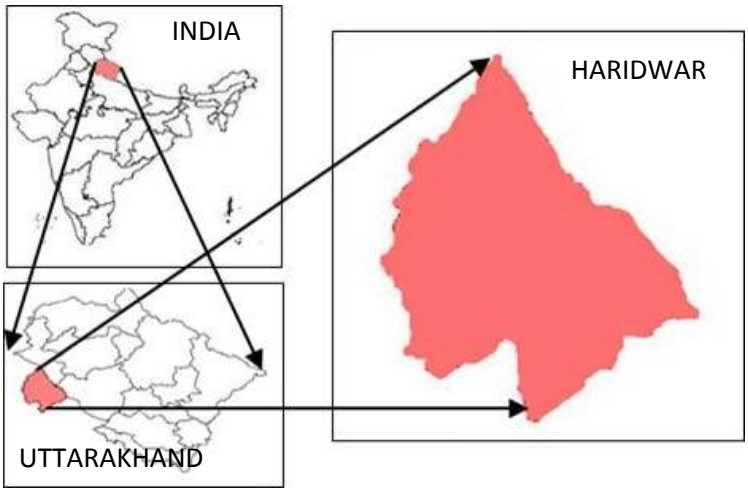

Fig 1: Location of the Study area

broadleaved deciduous forests, riverine vegetation and grasslands along with picturesque forests of pine trees that lend a unique charm to the environs.

Champion & Seth and further FSI have reported following four type of forest subtype in Haridwar district i.e. Dry plains Sal forest (5B/C1b), Northern dry mixed deciduous forest (5B/C2), Dry deciduous scrub (5/DS1) and Khair-sissu forests (5B/1S2) forest [19]. Being a pilgrims place in India it is highly affected by the population pressure (table 1).

Table 1: Subtypes and related characteristics of forest type-V of Haridwar District, Uttarakhand

Subtype	Distribution	Soil Type	Average annual Rainfall	Mean annual Temperature	Associates	Regeneration/ Remarks
Dry Plain sal forest (5B/C1b)	On flat ground, lower end of the bhabar, slightly above the bhabar-tarai	Top Soil Clayey, underlain by gravel or coarse sand	500-1500mm, mostly persist at lower limit	Maximum temperatures higher	*Terminalia tomentosa, Pterocarpus marsupium, Madhuca indica, Diospyros tomentosa, Aegle marmelos* etc.	Practically nil
Dry deciduous scrub (5/DS1)	Throughout the dry deciduous forest zone of India, mostly near thick habitations	Alluvial soil, Thin and gravelly	900-1150mm	24-27˚C	*Acacia catechu, Casearia tomentosa, Buchanania lanzan, Lannea coromandelica, Salmalia malabarica, Holarrhena, Dodonaea, Rabdia, Carissa, Zizypus xyopyrus, Zizyphus numularia, Gardenia turgida, Balanites aegyptiaca* etc.	Poor, Degradation is due to maltreatment mostly over felling, Overgrazing and annual fires.
Northern dry mixed deciduous forest (5B/C2)	Throughout northern India except in the eastern parts	Alluvial soil	Typical rainfall is 900 to 1,150 mm	24-27˚C	*Anogeissus latifolia, Diospyton melanoxylon, Miliusa tomentosa, Mitragyna praviflora, Bridelia retusa, Salmalia malbarica, Holoptelia integrifolia, Terminalia tomentosa, Shorea robusta, Bahuhinia racemosa, Boswellia serrate* etc.	Same as 5/DS1
Khair-sissoo forest (5/1S2)	Along the drainage pattern	Sandy or gravelly alluvium, New deposits, unstable, very porous, hot	500- 1300 mm	24-27˚C	*Dalgerbia sissoo* predominates, *Acacia catechu* etc.	Poor

Data Used

The satellite data from Indian Remote Sensing Sensor (IRS P6) LISS-III satellite data of Oct-Nov 2004, with a spatial resolution of 23.5×23.5 m made available by FSI (for the extraction Forest cover map of Haridwar district under its national Forest Cover Mapping, FCM project) and field data on forest type group-V, Species composition, crown density, DBH, and other field level observation and measurements was used in this study to assess growing stock.

Ancillary data such as topo-sheet of 1:50,000 scale (53K01, 53K02, 53K05, 53J04, 53F16, 53G13, 53G14, & 53G09) have been used for referencing satellite images. Forest type map of Haridwar district were made available by Forest Survey of India (FSI) was taken to couple it with forest density classes. Field Equipment such as Silva Ranger compass , Hega Altimeter, Diameter and linear measuring tapes, Diameter caliper, Nylon rope, Cloth flags,

Wooden pegs, GPS (Garmin-72) etc. have been taken to collect the ground information regarding growing stock estimation such as GBH, tree height plot location etc. Images obtained from space based plate form were processes in ERDAS/Imagine version 9.1.

Methodology

In compliance with the earlier mentioned objectives, a suitable Remote Sensing GIS based Methodology was adopted. The entire methodology of the present work have been categorised in the following three stage (a) Pre-field work, (b) Field data collection (c) Post field work. All these stages are elucidated below:

Pre-field work: The satellite data worked out in the present study were IRS-P6 LISS-III images with a spatial resolution of 23.5 m. After geometric correction in ERDAS IMAGINE 9.1 software by taking SOI toposheet as reference, the satellite images were mosaicked and Haridwar area was subset. The image was classified through Iterative self-organized data (ISODATA) classification algorithm into 30 odd classes. False colour composite (FCC) image of the study area was visually interpreted for spectral properties of various features like vegetation, water and other non-forest land covers, to classify the 30 pixel classes into various forest cover classes (such as OF, MDF and VDF) as well as water and non-forest classes by assigning a colour code to each of these classes.

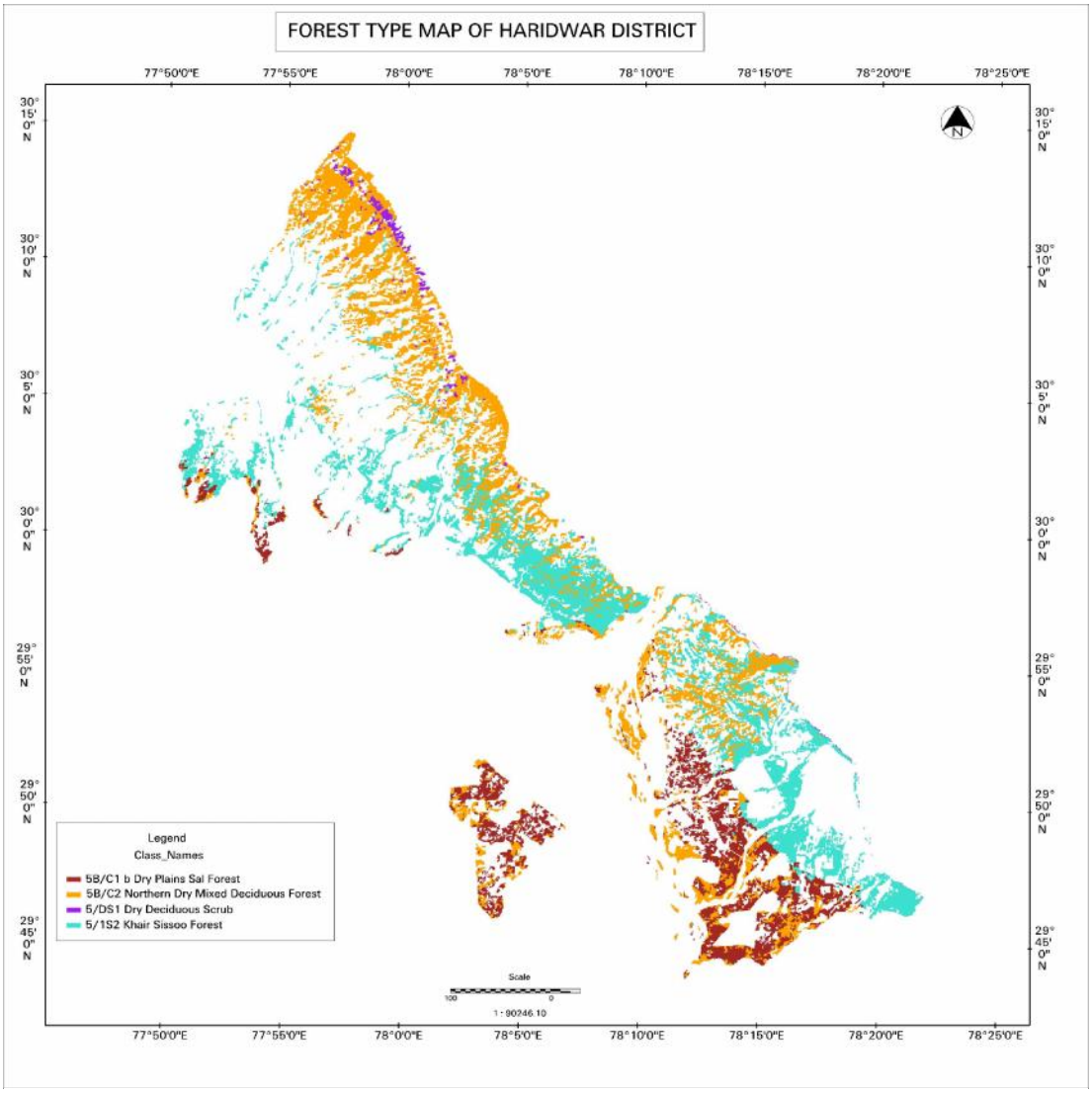

Fig 2: Forest type Map (Group-V) of Haridwar District

The on-screen visual image interpretation involves various image interpretation keys such as colour, Tone, texture, pattern, association and position with inputs from toposheets, ground truth information from earlier work and high spatial resolution Google Earth imagery. Forest density classes were sliced from the vegetation class of classified image, based on the tone and texture of the vegetation cover in the FCC (Dark red tone with coarse texture= VDF, Medium dark red tone with relatively less coarse texture=MDF and Light red tone with smooth or very less coarse texture=OF). Classified image raster attributes were recoded to assign a specific no. to each class was the next step of pre-field work. To remove "salt and pepper effect" from the classified maps "Clump" (connected neighbours=4) and "Eliminate" functions (with a patch of minimum 1 ha. area) were used over the recoded classified image. The output of this step was the preliminary forest cover map which we were planning to integrate with forest type group five after post-field corrections but forest type map (from FSI) of the study area were having various forest type group presents in it. The overall accuracy of the forest cover map was 86.84% and Kappa was 0.8443.

As our interest was in Forest type group Five (Tropical dry deciduous forest which is most dominant and vulnerable to degrade), it has been recoded in such a way that all the forest sub-type of this group found separate code such as one, two, three and four and rest as zero (Figure 2). A subset of preliminary forest cover (Figure 3) equal to the forest type group-V was made for the stratified random sampling strategy preparation.

Field Data Collection: Field sampling strategy was based on the stratified random sampling method, however due to less variation in plot level growing stock (VDF, MDF and OF) only 29 plots were laid. The plots were laid down in such a way that all the plots are equally distributed in different forest density classes based on ratio fraction (percentage of coverage area by different density classes). GPS (Garmin 72) was used for determining positions. Randomly selected inventory points on forest density map with latitude/longitude were generated automatically

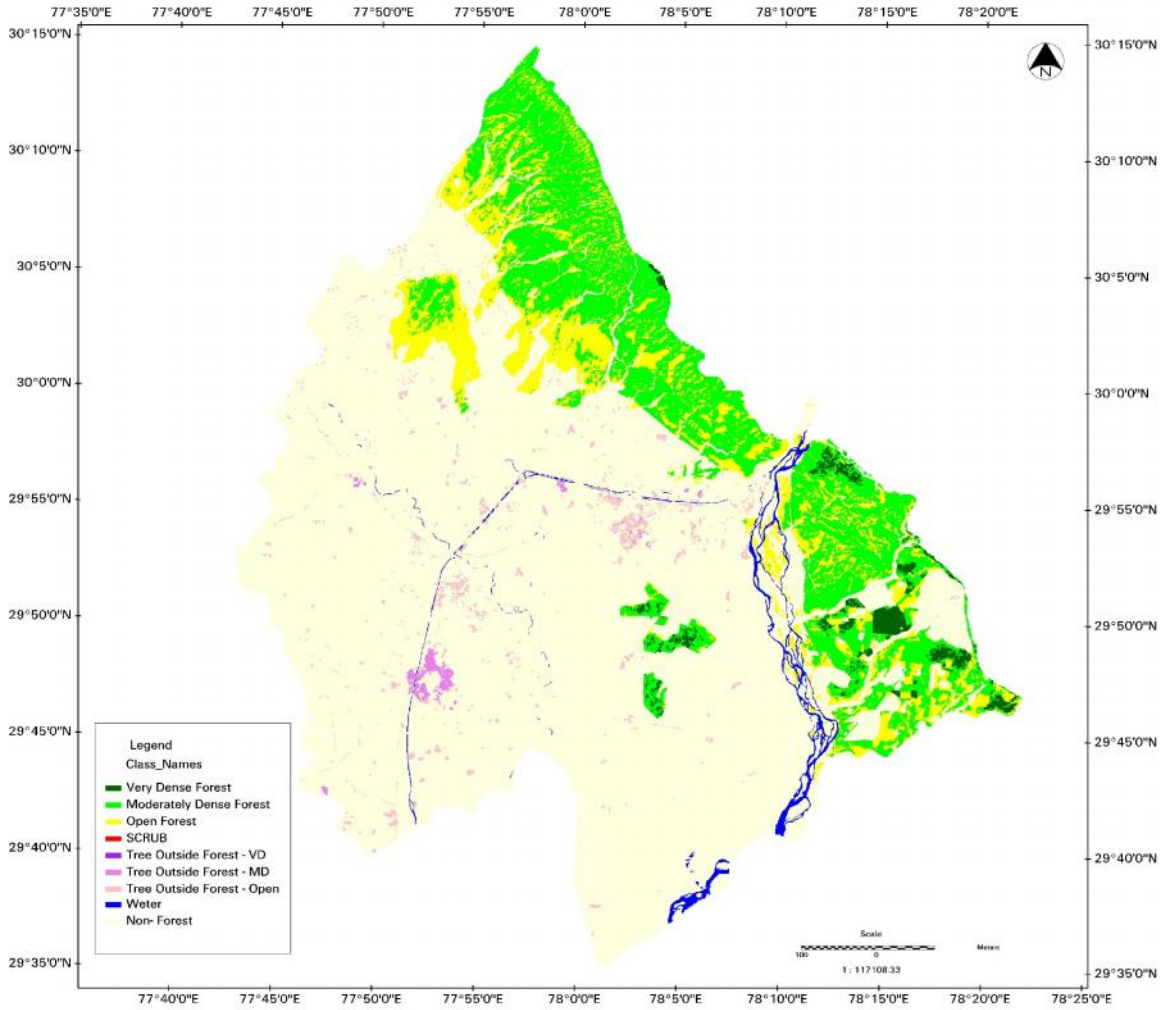

Fig 3: Forest Cover Density map of the Haridwar district, Uttarakhand

using ERDAS Imagine software. With the use of GPS, we easily determined the distance and the direction of the selected inventory points on the ground. The randomly selected inventory points (n=29) have been well distributed on the forest density map (5 in VDF, 13 in MDF and 12 in OF). Standard method of laying plot for field inventory work by FSI has been applied for this study. The plot centre reached after covering desired distance and bearing from the reference point represents the centre of the plot of 0.1 ha. (i.e. the point of inter section of two diagonals i.e. NE to SW and NW to SE of the plot). The length of each diagonal measures 44.72 m. After fixing plot centre the NE at 45^0, SE at 135^0, SW at 225^0, NW at 315^0 corners of the plot have been fixed by measuring 22.36 m. horizontal distance. The dimensions of the plot i.e. all sides have been measured 31.62 m. horizontal distance. Anatomy of the growing stock measurement plot is given in the figure 4. All the plants (GBH>15 cm) within the vicinity of the plot were measured individually and listed in the field form along with their individual heights.

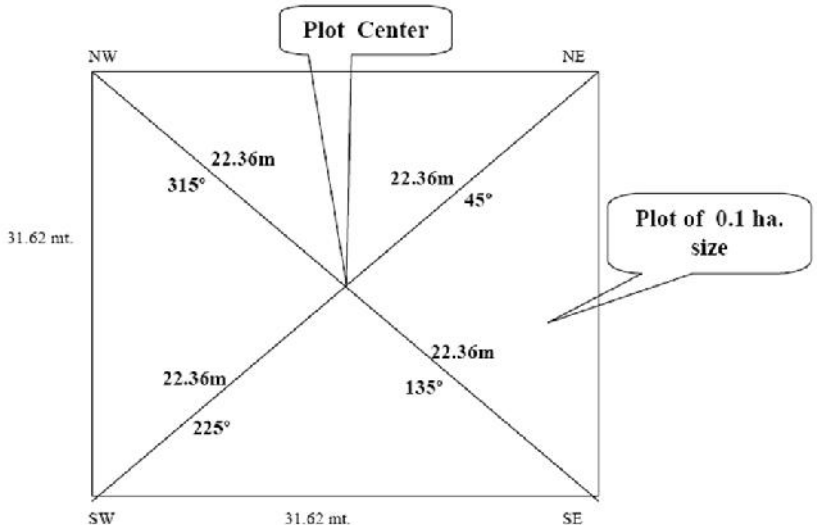

Fig.4: Growing Stock inventory sample plot

Post-field Work: On the basis of Fieldwork, ground truth and available data and knowledge, the finalization of forest cover mapping work was done and further analysis was carried out. Incorporation of more information in the forest density map from ground has made it more accurate. Data collected from the field inventory was analysed in the Microsoft excel 2008. Both the thematic data layers i.e. Forest type (Figure 2 and Forest cover (Figure 3) were subjected to the matrix function of the ERDAS Imagine 9.1 to create a composite layer having distribution of density classes in the forest type group-V. The output of matrix function was forest type density map (Figure 5). A total of 12 combinations (4 forest sub-types×3 forest density classes) have been made and area of each combination was used as multiple factor for the volume estimation under respective combination of particular density class. The mean volume or growing stock from the sampled plot under individual density classes i.e. Mean volume of VDF, MDF and OF, were multiplied by multiple factor of their respective forest type density class.

Table 2: Species and site specificVolume equations used to calculate volume

Species	**Volume Equations**
Acacia catechu	$V=0.16609-2.78851D+17.22127D^2-11.60248D^2$
Diospyros species	$V=0.06206-1.43609D+9.778164D^2$
Eucalyptus species	$V=0.02894-0.89284D+8.72416D^2$
Holarrhena antidysenterica	$V=0.17994-2.78776D+14.44961D^2$
Lagerstroemia parviflora	$V=0.10529-1.68829D+10.29573D^2$
Mallotus philippinensis	$V=0.14749-2.87503D+19.61977D^2-19.11630D^2$
Shorea robusta	$\surd V=0.16306+4.8991D-1.57402\surd D$
Tectona grandis	$V=0.08847-0.46936D+11.98979D^2+1.970560D^2$

Computation of volume for each individual tree come inside a sample-plot were carried out using species and site specific volume equations developed by FSI in 1996 (Table 2). In this way the total and per hectare growing stocks for forest type group five in different density classes of the forest cover of the study area have been calculated respectively. The growing stock calculated, is for 0.1 hectare because the Sample plot was laid out in the field of 0.1 ha area. The growing stock per hectare has been computed by up scaling method with the multiple factor of 10 (i.e. by multiplying 10 with the growing stock of 0.1 ha.). The same has been expended for the forest type group five using area as multiple factor.

3. Results and Discussion

Forest Cover Density

The total geographical area of Haridwar district is 2, 36,000 ha. The forest cover (Fig. 3) in the district, based on interpretation of satellite data of Oct-Nov 2004, is 61,900 ha, which is 26.23 % of the district's geographical area. It includes VDF, MDF, OF, TOF-MDF, TOF-OF, Water and Non-Forest (includes settlement fellow land, forest blanks etc.) classes.

Forest cover having canopy density 70% or more than 70% is classified as VDF. Forest cover having canopy density 40% or more and less than 70% of the per unit ground area have been considered as MDF. OF forest were those forest patches having canopy density 10% or more and less than 40%.

The forest patches situated in the city and those are outside the natural forest areas are termed as TOF. They have been further classified in to MDF and OF-TOF. The areas of TOF classes were added in the respective density classes of natural forest which gave forest cover in terms of forest canopy density classes. The district has 2,600 ha very dense forest, 35,400 ha moderately dense forest and 23,900 ha open forest.

Growing Stock Statistics from Field

Table 3 is showing plot level vegetation parameters. From this table a clear variability can be seen in the plot level diameter. OF is having less diameter (236.39 cm) as compared to the MDF (533.45 cm) which have less diameter than VDF forest (700.76) at plot level. Similar variations are seen in the total volume at plot level. OF, MDF and VDF have 4.35±4 m^3 (Mean± standard deviation), 9.58±6 m^3 and 15.02±6 m^3 respectively. Variation in the volume and diameter at plot level came from no. of trees occurring in the plot. OF, MDF and VDF forest are having average 11±4, 25±6 and 34±11 no. of trees.

Table 3: Per plot mean diameter and volume derived from field inventory points (n=29)

Per plot (0.1 ha) mean Diameter (cm.) and Volume (m^3)			
FTD	Diameter	Volume (Growing Stock)	Average No of Plant
OF	236.39±12.21	4.35±4	11±4
MDF	533.45±12.04	9.58±6	25±6
VDF	700.76±8.70	15.02±6	34±11

The mean parameters for the individual tree given in table no. 4 are representing less variation in the diameter, Basal area and volume irrespective of the forest density. This is the no. of trees per unit area, which create variation in the volume per ha. (Table 3).

Table 4: Mean Parameters of Individual tree from different density classes

Forest Density	**Diameter (cm)**	**Basal Area (m^2)**	**Volume (m^3)**
OF	20.55	0.04	0.37
MDF	21.49	0.04	0.32
VDF	20.79	0.05	0.45

Individuals present in VDF forest having mean diameter 20.97cm for individual tree. Similarly individual tree of MDF forest is having mean diameter 21.49 cm and individual tree of OF 20.55cm. Mean basal area for the individual tree from VDF, MDF and OF is 0.05, 0.04 and 0.04 m^2 respectively. However mean volume is showing

little variation. Mean volume for individual tree from VDF is highest (0.45 m^3) followed by OF (0.37 m3) and MDF (0.32 m^3). Average growing stock is estimated 28.9481 cubic meters. The average growing stock/ha in Very dense forest is much higher (150.20 m^3) than the average growing stock/ha in case of moderately dense forest (95.78 m^3) and Open forest (43.50 m^3) at plot level.

Growing Stock of Forest Type Group-V

Total forest cover area under the forest type-V was estimated 28843.05 ha. Combined area of the forest cover under different forest sub-type was highest in the MDF and lowest in VDF. Among the forest sub-type 5B/C2 is covering highest geographical area (12289.69 ha) covered by forest type-V in Haridwar district. Area coverage of the 5/1S2 is second highest (10881.69 ha) area under the forest type-V. Forest sub type 5B/cC1 is covering 4908.75 ha area. Forest sub-type 5/DS1 is covering lowest area (762.92 ha) among all. The areas (ha) under each forest sub-type are given in table no. 5.

Table 5: Area in different density classes of the forest type-V

Forest Type Group (V)/ Forest Cover Density (Area in ha.)	**VDF**	**MDF**	**OF**
5B/C2 Northern Dry Mixed Deciduous	238.54	9115.64	2935.51
5/1S2 Khair Sissoo Forest	494.44	5302.25	5085.00
5B/cC1 Dry Plains Sal Forest	425.37	3048.66	1434.72
5/DS1 Dry Deciduous Scrub	0.00	430.67	332.25
Total	**1158.35**	**17897.21**	**9787.48**

Table 6: Growing Stock or Volume in m^3 of different forest sub type under different canopy density classes.

Forest Type Group (V)	**Volume in m^3 under VDF**	**Volume in m^3 under MDF**	**Volume in m^3 under OF**
5B/C2 Northern Dry Mixed Deciduous	10376.49	873278.31	440913.60
5/1S2 Khair Sissoo Forest	21508.14	507955.55	763767.00
5B/cC1 Dry Plains Sal Forest	18503.60	292061.63	215494.94
5/DS1 Dry Deciduous Scrub	0.00	41258.19	49903.95
Total	**50388.23**	**1714553.68**	**1470079.50**

Based on mean volume of per ha plot from different density classes, the growing stock of each forest sub-type coming under forest type-V is estimated (table no. 6). Estimates are revealing that almost 53% of total volume (3235021.40 m^3) is accumulated in the MDF followed by OF (45%) and VDF (1.5%). Growing stock was showing following pattern in different forest type: 5B/C2>5/1S2>5B/cC1>5/ DS1. Forest sub-type 5B/C2 is having highest (873278.31 m^3) growing stock in MDF forest cover (table no. 6) followed by in OF (440913.60 ha) and VDF (10376.49 ha). Forest sub-type 5/1S2 (Khair -Sissoo Forest) is accumulating highest growing stock in OF (763767.00 m3) followed by in MDF (507955.55 m3) and VDF (21508.14). Forest sub-type 5B/cC1 (Dry Plains Sal Forest) is having highest growing stock in MDF followed by OF and VDF. 5/DS1 (Dry Deciduous Scrub) is having highest growing stock in OF followed by MDF. There is no growing stock for VDF for 5/DS1. The total growing stock in 5/DS1 is lowest among all the forest sub-type and it covers less area also that is why it need immediate conservation strategies.

Discussion

Information on Growing stock is vital for scientific management of forests. In the past, this information was obtained entirely on the ground by taking a full stock of every forest cover over a certain diameter class. Collection of ground data is not only time-taking and expensive, but it is difficult in inaccessible areas and becomes out-dated at the time of completion of the project.

However, the use of aerial photograph, supplemented by limited ground data was found quite convincing in the assessment of growing stock. The use of aerial photograph can be replaced with recent satellite remote sensing data.

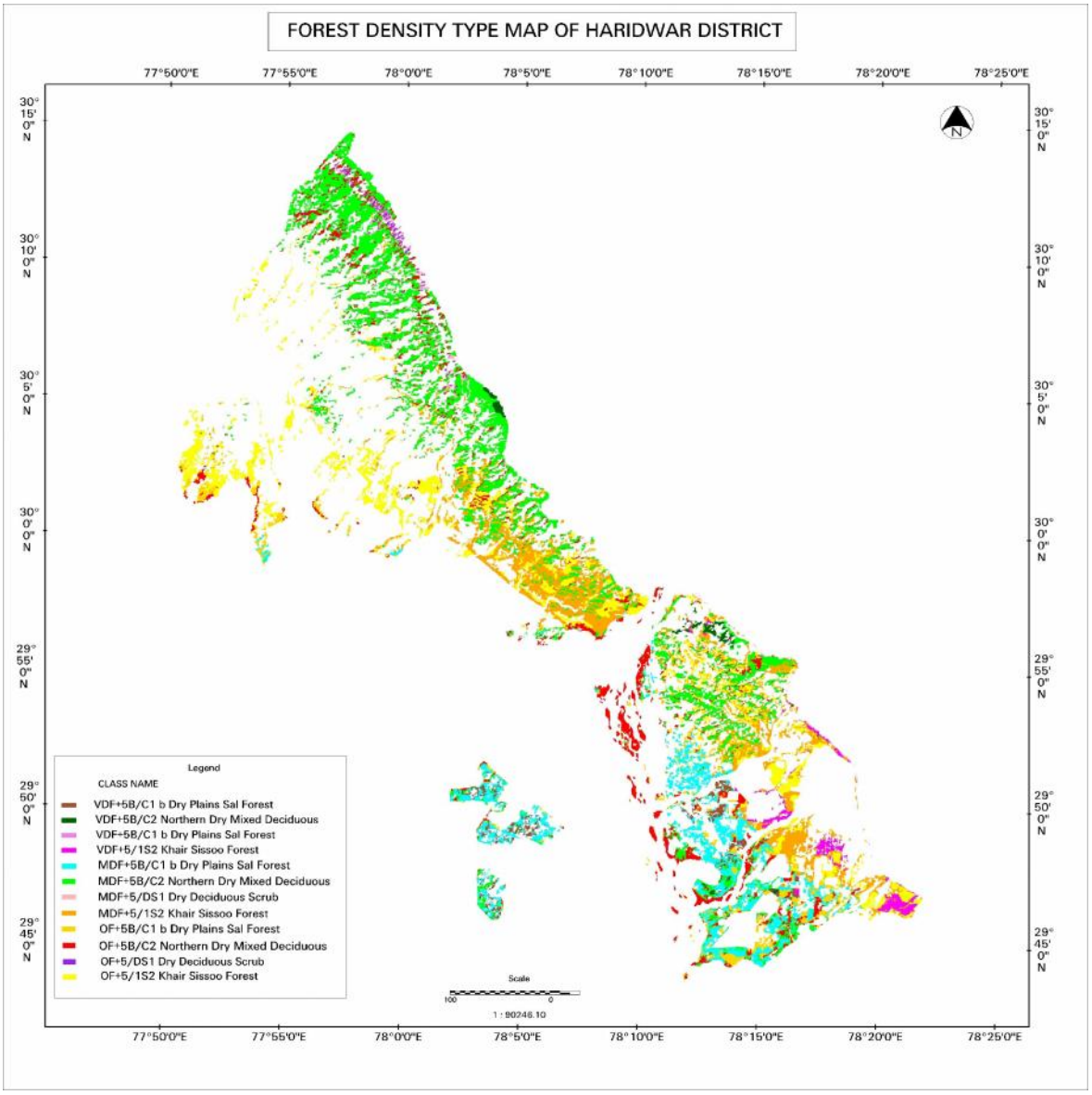

Fig 5: Forest Type Density Map

The methodology used in the present study is same as used in initial estimations except that due to use of better quality of satellite data, improved method of interpretation and improved cartographic resolution, growing stock could be estimated in forest cover patches down to 1 ha in extent as against 25 ha limitations in earlier estimations. The present study deals with combined usage of satellite remote sensing data and ground survey inventories. Incorporation of field inventory in remote sensing technology may support observation, measurement, estimation and mapping of forest biophysical, biochemical and other health related parameters [8, 9, 11, 24]. Strata obtained from remote sensing data such as forest density map, forest type map, species map etc. may overcome budgetary constraints and deliver précised accuracy [8]. Taking this in view present study utilizes forest cover derived from IRS LISS-III data and forest type from FSI. The results expected to be more accurate as the sampling was done on the stratified map of the Forest density classes [8].

Total 29 plots were laid on the ground for the growing stock estimation of forest type group-V. Measurement taken from the ground (for trees only) were analysed in Microsoft excel software environment. Matrix of forest density and forest type has given 12 combinations (i.e. 3 forest density classes×4 forest subtype of forest type group-V). Areas of each combination were used as multiple factor to extrapolate the plot level growing stock to the landscape level. This gives growing stock distribution in different forest sub-type density classes.

The no of trees in the open forest are less as compared to the MDF and VDF. Thus the total volume at the plot scale is less in OF. MDF have moderate plot level volume and VDF have highest plot scale volume. However the average volume of the individuals in the forest of Haridwar district is almost similar in all the density classes. This is also little less as compared to the mature forest of the same type which generally have diameter (DBH) greater than 20 cm and thus volume more than 0.49 m^3 obviously. This is showing that the forest type group-V of Haridwar district is having potential to grow and might be preserved for the optimum timber yield. The result outputs of this study are able to deliver valuable information for management purposes. Simultaneously it may also be used as baseline information for the assessment of growing stock, biomass and carbon under different density classes of forest subtype of forest type group-V in near future.

4. Conclusions

- Remote sensing has enormous potential and it was possible to classify the forest in different types and density classes. Digital image analysis, unsupervised classification and onscreen visual interpretation of the remote sensing data IRS LISS-III (hybrid approach of classification), resulted in forest cover map of the study area including three density classes viz. OF, MDF and VDF along with their coverage area, with reasonable accuracy.
- Creation of database that is of primary requirement for the inventory and growing stock estimation is possible. Thus it can be concluded that the application of modern tools and procedures such as remote sensing technology combined with GIS can be a major input for the quantification of growing stock which is non-destructive and cost-effective [8].
- Mean diameter, Basal area and growing stock obtained from the sampled individuals i.e. average of diameter, basal area and growing stock from all the individuals of all the plots is less as compared to the mature forest of similar type group. This shows that the forest of Haridwar district comes under the forest type-V is having potential to grow with large prospective to sequester carbon over several decades [25] and might be preserved for the optimum timber yield. Simultaneously it is obtained that which is the most considerable subtype regarding its conservation. Subtype having less growing stock and spread in less area are considered as unhealthy and needs immediate conservation measures. Present study have shown vulnerability to the dry deciduous scrub (5/DS1) forest sub-type, as it is covering very less percentage (2.65%) of total forest cover and also have low growing stock.
- Further, result output of this study will be used for the management planning of the forest and can be of great help to the forest Departments in the enhancement, updating and diversifying the forestry knowledge at the state and national levels.
- Use of matrix map of forest density and forest type will give more accurate estimation of growing stock as suggested by McRoberts & Tomppo. Nigam also investigated the application and evaluation aspects of remote sensing and GIS in the biomass estimation and have given similar conclusion.

Acknowledgement

Authors are thankful to the Dr. Anmol Kumar, Director Journal FSI for providing forest type data required under this study. Authors are also thankful to Dr. Sunil Chandra Deputy Director, FSI and Mr. Devi Singh STA, FSI for their valuable suggestions and support during the research work.

References

1. Mahto B. 2001. Paper presented at the 22nd Asian conference on remote sensing, 5-9 November 2001, Singapore. Copyright (c) 2001 Center for remote imaging, sensing and processing (CRISP), National Universitynof Singapore; Singapore Institute of Surveyores and Valuers (SISV); Asian Association on Remote Sensing (AARS).
2. Moore R, Williams T, Rodriguez E & Cymmerman JH. 2011. Quantifying the value of non-timber ecosystem services from Georgia's private forests. Final Report submitted to the Georgia Forestry Foundation, 2-44.
3. Shaheen H, Qureshi AR, Ullah Z & Ahmad T. 2011. Anthropogenic pressure on the western Himalayan moist temperate forests of Bagh, Azad Jammu & Kashmir. Pakistan Journal of Botany 43(1): 695-703.
4. Franklin SE. 2001. Remote Sensing for Sustainable Forest Management. Lewis publisher, 1-409.
5. Indian State of Forest Report 2011 (ISFR-2011), 2012. Forest survey of India, 1-286.

6. Vidal C, Lanz A, Tomppo E, Schadauer K, Gschwantner T, di Cosmo L & Robert N. 2008. Establishing forest inventory reference definitions for forest and growing stock: a study towards common reporting. *Silva Fennica* 42(2): 247–266.
7. FAO. 2010. Developing effective forest policy A guide. Available online on http://www.fao.org/docrep/013/i1679e/i1679e00.pdf. Accessed on date 07-05-2014.
8. McRoberts RE & Tomppo EO. 2007. Remote sensing support for national forest inventories. *Remote Sensing of Environment* 110 (4): 412–419.
9. Singh S, Patil P, Dadhwal VK, Banday JR & Pant DN. 2012. Assessment of above ground phytomass in temperate forests of Kashmir Vally, J&K, India. *International journal of Ecology and Environmental Science* 38 (2-3):47-58.
10. Singh D & Singh S. 2013. Hyperspectral Data Application for Above Ground Biomass Estimation in Doon Valley, Uttarakhand. In: *Proceedings*: ISG-ISRS National Symposium-2013 Dec. 4-6, 2013. Andhra University, Visakhapatnam 530003.
11. Asner GP. 1998. Biophysical and Biochemical Sources of Variability in Canopy Reflectance. *Remote Sensing of Environment* 64: 234-253.
12. Rai SN & Chauhan KVS. 1998. Distribution and Growing Stock of Bamboos in India. *Indian Forester* 124(2):89-98.
13. Singh IJ, Das KK, Pant DN & Thee N. 2004. Quantification of Forest stock using remote sensing and GIS. *Journal of the Indian Society of Remote Sensing* 32(1):113-118.
14. Shvidenko A, Schepaschenko D, Nilsson S & Bouloui Y. 2007. Semi-empirical models for assessing biological productivity of northern Eurasian forests. *Ecological Modelling* 204(1–2): 163–179.
15. Chhabraa A, Palriab S & Dadhwala VK. 2002. Growing stock-based forest biomass estimate for India. *Biomass and Bioenergy* 22(3):187-194.
16. Patenaude G, Milne R & Dawson TP. 2005. Synthesis of remote sensing approaches for forest carbon estimation: reporting to the Kyoto Protocol. *Environmental Science & Policy* 8(2): 161‑178.
17. Kindermann GE, McCallum I, Fritz S & Obersteiner M. 2008. A global forest growing stock, biomass and carbon map based on FAO statistics. *Silva Fennica* 42(3): 387–396.
18. Lausch A, Pause M, Merbach I, Zacharias S, Doctor D, Volk M & Seppelt R. 2012. A new multiscale approach for monitoring vegetation using remote sensing-based indicators in laboratory, field, and landscape. *Environmental Monitoring and Assessment* 185(2):1215-35.
19. Champion HG & Seth SK. 1968. Revised Classification of Forest Types in India, Manager of Publications, Government of India, New delhi.
20. Ashutosh S, Pandey D, Kaur T & Bajpai RK. 2010. Knowledge-based remote sensing and GIS approach for forest type mapping in Kathua district, Jammu and Kashmir. *Tropical Ecology* 51(1): 21-29.
21. Web: http://www.indianetzone.com/39/indian_dry_deciduous_forests.htm.
22. Pandey R, Mall TP & Singh RK. 2008. Forest types of Katarniaghat Wildlife Sanctuary- a biogeographic classification. *Environment Conservation Journal* 9(3): 83-87.
23. Web: http://haridwar.nic.in/pages/display/86-about-district.
24. Hansen PM & Schjoerring JK. 2003. Reflectance measurement of canopy biomass and nitrogen status in wheat crops using normalized difference vegetation indices and partial least squares regression. *Remote Sensing of Environment* 86:542-553.
25. Haripriya GS. 2000. Estimates of biomass in Indian forests. Biomass and Bioenergy 19(4): 245‑258.

DEW DROP 02(2016) 25-30

Thunderstorms Patterns in Bangladesh using long-term Synoptic Observation

Fatima Akter[1*] and Md. Abdul Mannan[2]

[1]*Department of Geography, University of Dhaka, Bangladesh*
[2]*Bangladesh Meteorological Department, Agargaon, Dhaka*
Corresponding author's e-mail: Fatima.geo.bd@gmail.com

Abstract: The objective of this paper is to analyze thunderstorm scenario of Bangladesh based on the thunderstorm (TS) days and thunderstorm frequency data obtained from Bangladesh Meteorological Department (BMD) during between 1976 and 2005. A range of statistical techniques such as trend analysis is used to carry out this work using spreadsheet and Surfer software. Analysis reveals that Northeastern part of Bangladesh is the most vulnerable to this locally occurring phenomenon. Monthly and seasonal TS occurrences analysis exhibits that the month of May had the maximum thunderstorms during study period while monsoon witnessed the highest TS occurrence in terms of seasonal distribution. Annual occurrence of TS analysis reveals a spectacular figure, Bangladesh experienced more than 62 days thunderstorm per year from 1976 to 2005. In addition, trend analysis demonstrates that TS occurrence is decreasing in February, April and May, whereas seasonal result is positive during all seasons (e.g. pre-monsoon, monsoon, post-monsoon and winter). During February to October, the maximum TS days are observed in the northeastern part, particularly in Sylhet region of the country. However, annual TS frequency is 164, on an average for the entire Bangladesh. This study is expected to contribute significantly to the understanding of the spatial and temporal variation of thunderstorm occurrences in Bangladesh which eventually helpful for future management of this locally occurring natural hazards.

Keywords: *Thunderstorms, Meteorology, Instability, TS days, TS frequency, Bangladesh*

1. Introduction

Thunderstorms are meso-scale phenomena, usually generated from cumulonimbus clouds, and are characterized by lightning discharges. They are, often, accompanied by strong gusts, hail, heavy rains and sometimes turn to tornado. A number of literatures suggest that every year Bangladesh experiences enormous damage to crops, lives and properties by these strong violent revolving gusty winds. It is postulated that pre-monsoon months are the most suitable time for these thunderstorms to occur, mostly from northwesterly direction which is popularly known as Nor'westers [1]. Generally, abrupt fall in air pressure due to differential heating, local atmospheric instability resulted from adequate supply of moisture, are believed to be the major factors contributing to the development of local severe storms, including thunderstorms across the country [2]. These thunderstorms during pre-monsoon bring heavy shower which is also said to be beneficial for agriculture when rising temperature along with dry weather produce dry spells throughout the country, however, damage from such storms can also be massive. Since these storms have both positive and negative effects on the environment, the climatology of these meso-scale phenomena has received little attention compare to other natural hazards such as flood and cyclone [3]. The study of inter-annual variability and trend of thunderstorm occurrences is not only important for operational meteorologists but also imperative to develop effective countermeasures for agricultural planning in Bangladesh [4].

A number of studies have been attempted to document the spatial and temporal variation of thunderstorms and their mechanism in relation to atmospheric instability in India and Bangladesh [5, 6, 7]. In a study [8] frequency distribution of thunderstorms in Bangladesh investigated. Using secondary data from 1950 to 2005, the study analyzed the pattern of fatalities and damage to agriculture in Bangladesh [9]. According to this study, each year the losses of properties from these storms are significant. The study [9] also demonstrated that Bangladesh is very much vulnerable to local severe storms, and the probable climatic change may trigger more frequent events [10] which might have detrimental effects on the people and economy of the country. The damages by the single severe local storms are located in the very small area compared with those in the cyclones and floods. However, as the occurrence frequency of the severe local storms is much larger then that of cyclones and floods, the total damage amount cannot be negligible [11]. Although a few studies attempted earlier to document the frequency of thunderstorms in the country, most of them are from meteorological point of view and very few and only severe climatological and case studies were only reported [12]. A study pertaining to geographic distribution of thunderstorms in terms of spatial-temporal patterns may serve better and deemed to fulfill the gap. Hence, the objective of this study is to examine the spatial and temporal variation of thunderstorm frequencies in

Bangladesh using synoptic observation from 1976 to 2005, which can be used to discern the pattern of thunderstorm days and frequencies across Bangladesh over a long-term perspective.

2. Methodology and data used

To understand thunderstorm frequencies, Bangladesh Meteorological Department's (BMD) long-term synoptic records were primarily used. The 3-hourly weather data from BMD archive was accessed and investigated. However, it may be noted that since specific time of an occurrence of a thunderstorm was not pinpointed in the record, the study sorted out the records using daily meteorological data from all meteorological observatories. As some of the BMD stations were inoperative for a few years, those stations were not considered for computation in this study. Spreadsheet software such as MS-Excel and Earth Science/GIS software Surfer 8.0 were employed to carry out the analysis. Linear statistical technique was used characterize the pattern of thunderstorm occurrences in Bangladesh.

3. Result & Discussion

3.1 Temporal distribution of thunderstorm days

The number of TS days is shown in Table 1 which signifies that the number of TS days was the highest in May followed by the months of June and September. Note that, the lowest TS days were in December. Seasonal analysis revealed that the highest number of TS day was in monsoon followed by pre-monsoon, and the lowest was in winter. During break or weak monsoon phase, meso-scale systems are formed and create thunderstorm activities in Bangladesh due to the presence of sufficient moisture and insolation. In addition to this, western disturbances frequently reach Bangladesh and meets with the monsoon flow which associates cool and dry air, and the air from southerly monsoon flow is characterized by moist and warm. Therefore, two different types of air are mixed during this period and believed to generate thunderstorm clouds in Bangladesh [7]. The longer duration of monsoon than that of pre-monsoon could be a reason to the development of thunderstorms in the country [13]. Average annual number of TS day for entire country was found to be more than 62 days in every year (Table 2). Monthly variation of thunderstorm occurrences revealed an increasing tendency of the occurrences in January during the study period. However, a decreasing trend for the same month was also noticed during 1976-1985. Similar fact was true for the month of June. In other words, decreasing trend of thunderstorm occurrence was found in June but from 1986-1995, the occurrence was much higher. Trend analysis also revealed that March and July-December experienced increasing trend while February was in downward trend (Table 3).

Table 1: Monthly distribution of TS days in Bangladesh

Month	Frequency of TS (Days)
January	0.5
February	1.7
March	4.3
April	8.8
May	12.1
June	10.2
July	7.3
August	7.4
September	9.6
October	5.2
November	0.6
December	0.2

Table 2: Seasonal and annual distribution of TS days in Bangladesh

Season	Frequency of TS (Days)
Winter	2.2
Pre-monsoon	23.5
Monsoon	31.4
Post-monsoon	5.2
Annual	62.3

Further analysis of seasonal and annual distribution revealed that the frequencies of TS days are on the rise during the study period. The rate of increment in winter, pre-monsoon, monsoon and post-monsoon seasons were about +0.0146, +0.1781, +0.4075 and +0.1145 in every year, respectively. However, during 1996-2005, the numbers of TS days were in decreasing trend in the months of February, May, June, September and November. In contrast, from 1976 to 2005, TS days were found to be decreasing in February, April and May. A summary of the trend of seasonal and annual occurrences of TS days are presented in Table 4.

3.2 Spatial distributions of thunderstorm days

Fig. 1(a) depicts the spatial distribution of thunderstorms days in Bangladesh. A close examination shows that in January, numbers of TS days were comparatively higher in the northwestern and northeastern tips of the country, however in February, higher TS days were observed in the northeast region followed by west-central part of the country. The highest number of TS days (18 to 22) was observed in April to July in the Sylhet region too. A pocket of second highest number of TS days was observed in the west-central part of the country during June. The number of TS days gradually decreases from the northeast to the western part of the country. The lower number of TS days were found in the southeastern and south-central parts of the country while the lowest values being prevailed in Noakhali, Feni, Chittagong and Cox'Bazar regions.

The distribution pattern of TS days in August and September are much resembled to July. In October, the highest number TS days were found in Madaripur region and the south central parts of the country followed by Srimongal area. In November and December, lowest occurrences were observed in the northwestern tip of the country. The higher annual number of TS days was found in the northeastern part followed by west-central part of the country, with the maximum annual TS days (146) was found in Sylhet region. This is due to the orographic effect and frequent meeting of warm and cold air masses in different seasons of the year [14]. Note that the lower annual number of TS days were observed in the northwestern and southern parts of the country.

Table 3: Temporal variation of monthly thunderstorm

Months	Period 1976-2005
January	0.0077
February	-0.0134
March	0.0266
April	-0.0716
May	-0.0089
June	0.0421
July	0.033
August	0.0185
September	0.052
October	0.0833
November	0.0053
December	0.0006

Table 4: Periodic trend of occurrences of TS days per year in Bangladesh

Range of Year	Winter	Pre monsoon	Monsoon	Post monsoon
1976- 1985	-0.0494	0.0209	-0.1759	0.0482
1986 -1995	0.2159	-0.1197	1.0574	0.3056
1996 – 2005	-0.0356	0.127	-0.246	0.039
1976 - 2005	0.0146	0.1781	0.4075	0.1145

3.3 Temporal pattern of thunderstorm (TS) frequency

Analysis revealed that the monthly average frequency of TS were the highest in May (> 30) followed by June (25) and September (23), but the lowest frequency was observed in December (0.4). The average TS frequencies in winter, pre-monsoon, monsoon and post-monsoon were 4.96, 63.96, 82.79 and 12.10, respectively, and the annual average of TS frequency was 164 during the study period. Further to the above analysis, monthly TS frequency was carried out and found that in January the number of thunderstorm occurrences were in increasing trend (0.0093/ year) but in February it showed a decreasing trend with a rate of –0.0546/year. Again in April, May, June, July, August and September, the rates of TS frequency were negative which corresponds to the values of –0.3958, -0.1436, -0.1645, -0.135, -0.1277 and -0.0531/year. Conversely, in

October, November and December, the trends of TS frequency were 0.1495, 0.0059 and 0.0043, respectively (Fig. 1(b)).

Nation-wide average TS frequency in winter and pre-monsoon seasons was computed and found that the occurrence of thunderstorms were decreasing, indicating the rates of -0.0176 and -0.0262/year but in other seasons the trends were quite positive (Table 5). Hence, the study signifies that further investigation is crucial to unveil the relationship of climate change and the occurrence of local severe storms in the region.

Table 5: Periodic trend of TS frequency per year in Bangladesh

Range of Year	Winter	Pre-monsoon	Monsoon	Post-monsoon
1976- 1985	-0.1576	-0.9834	-3.0087	-0.0635
1986 -1995	0.4997	0.5211	3.0002	0.7275
1996 – 2005	-0.1374	0.039	-0.5544	0.0233
1976 - 2005	-0.0176	-0.0262	0.0364	0.1967

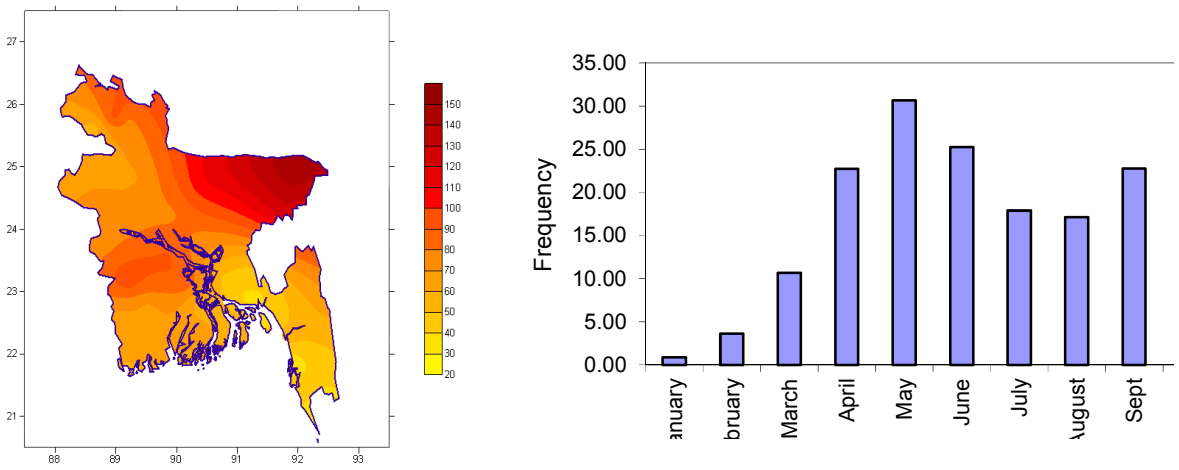

Fig. 1: (a) spatial distribution of annual TS days and (b) monthly distribution of TS frequency in Bangladesh during 1976-2005

Spatial distribution of monthly TS frequency demonstrated that the highest TS frequencies were observed in Sylhet (northeastern part of Bangladesh) during the month of January and February. However, a pocket of second highest TS frequencies were observed in the west-central part of the country. In March and April, the TS frequencies were higher compared to the previous months across the country. From mid-March to April the temperature in Bangladesh rises sharply compared to the preceding months (i.e., winter months) and this variation is particularly common in the northwestern part. Presence of warm and moist air in the lower layer of the atmosphere is essential for the development of nor'westers [15]. This might be explained to the highest occurrences of thunderstorms in northeastern part of Bangladesh. In contrast, the TS frequencies are gradually decreased from east to west for instance; higher TS frequencies were observed in northeastern part of Bangladesh in May. Note that relatively lower occurrences of thunderstorms were observed in western and southern parts of the country [13] as this part of Bangladesh is relatively flat landscape and experiences southerly flow during most of the time of a year. The westerly circulation system rarely extended up to this part in Bangladesh and meet with easterly flow. From June to August, the spatial pattern of TS frequency was slightly different than that of winter and monsoon months. The higher TS frequencies of these months were recorded in the northeastern part, but the lower TS frequencies

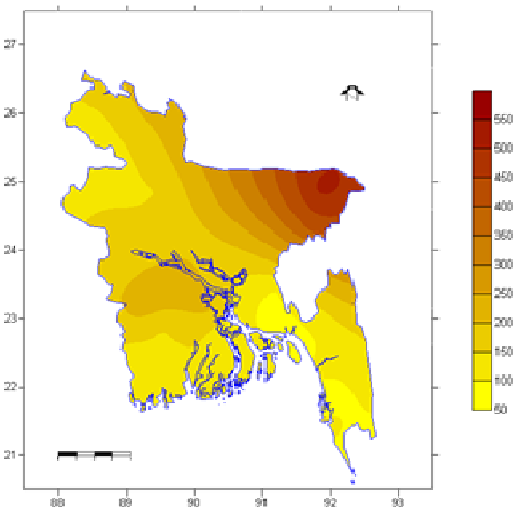

Fig. 2: Spatial distribution of annual TS frequency in Bangladesh for 1976-2005

were observed in the Noakhali, Chittagong and Cox's Bazar areas. On the other hand, in September, the monthly TS frequencies were lower than that of June, July and August. In October, the distribution pattern of TS frequency was also different, for example, the higher TS frequencies were found in the northeastern and west-central parts whereas in November and December, the thunderstorm occurrences were infrequent across the country. Thus, the distribution pattern is somehow found to be irregular.

3.4 Spatial distribution of annual thunderstorm frequency of Bangladesh

Spatial distribution of the annual TS frequencies showed that higher TS occurrences were in the northeastern part of Bangladesh. The maximum annual TS frequency (512/year) was observed in Sylhet. This is due to the orographic effect and more frequent meeting of warm and cold air masses in this region [16]. The second highest TS frequencies were observed in the west central region whereas lower TS frequencies of thunderstorm occurrence were observed in the northwestern and southern parts of the country. It may be noted that the lowest thunderstorm frequencies were observed in Noakhali. The annual average thunderstorm frequency for entire country was 164 days (Fig. 2) and very similar result with the other researchers [13].

4. Conclusions

This study attempted to analyze spatio-temporal distribution of thunderstorm occurrences in Bangladesh using long-term synoptic records from 1976 to 2005. Thunderstorms have an adverse socio-economic impact on life and livelihoods in Bangladesh. The analysis of TS days and frequency showed that the distribution of thunderstorm occurrences in Bangladesh is uneven. Both the distribution of thunderstorm days and thunderstorm frequencies are maximum in May followed by June. The lowest thunderstorm days as well as lowest frequency of thunderstorm occurrences are observed in December. During pre-monsoon season, thunderstorms are mostly associated with nor'westers, resulting massive damage to properties such as agricultural crops [17]. The damage and causalities caused by this type of natural phenomena are very high, which supposed to exhibit a substantial risk for the people. Hence, to diminish risk from this disaster, this study would provide a basis to advance knowledge in terms of geography of local severe storms in Bangladesh. A better planning to save life and property can now be prepared using the spatial and temporal distribution of thunderstorms in the country. As mentioned earlier, the probable climate change may have considerable impact on the occurrences and distribution of local severe storms, therefore further study considering local climatology would be of help in understanding the factors associated with their occurrences.

Acknowledgement

The author is indebted to Dr. Samarendra Karmakar, Former Director of Bangladesh Meteorological Department, Dhaka to provide necessary data available at BMD.

References

1. Afroze, S. and et al., 1981: Investigation of Nor'westers and Tornadoes in Bangladesh by weather satellite pictures, Nuclear Science and Applications, Vol. 12, 13 (B), pp.100-104
2. Debsarma, S. K., 2004: Post mortem (analysis) of the nor'wester that hit Dhaka on 14 April 2003, SAARC Meteorological Research Centre (SMRC), Dhaka, Bangladesh
3. Ono, Y., 1997: Risk Factors in Mortality from tornados-a case study of the May 13, 1996 tornado in Bangladesh. An unpublished M. S. dissertation, Kent State University, Kent, Ohio
4. Ayoade, J. O., 1983: Introduction to Climatology for the Tropics, John Wiley & Sons, pp. 88-89.
5. Chowdhury, M. H. K. and Karmakar, S., 1986: Pre-monsoon nor'westers in Bangladesh with case studies, Proceedings of the Seminar on Local severe Storm, Bangladesh Met. Dept., held on 17-21 January 1985.
6. Karmakar, S., 2000: Probabilistic extremes of thunderstorm days over Bangladesh during pre-monsoon season, Journal of Bangladesh Academy of Sciences, 2, 2, pp. 225-238.
7. Karmakar, S., 2001: Climatology of thunderstorm days over Bangladesh during pre-monsoon season, Journal of Bangladesh Academy of Sciences, 3, 1, pp. 103-112.
8. Karmakar, S. and Alam, M., 2005: On the probabilistic extremes of thunderstorm frequency over Bangladesh during pre-monsoon season, Journal of Hydrology and Meteorology (SOHAM-Nepal), 2, 1, pp. 41-47.
9. Peterson, R. E. and Dewan, A. M., 2002: Damaging nor'westers in Bangladesh, Paper presented at the 21st Conference on Severe Local Storms, American Meteorological Society, San Antonio, Texas.
10. Yamane, Y., T. Hayashi, A. M. Dewan and F. Akter, 2010: Severe local convective storms in Bangladesh: Part II.: Environmental conditions; Atmospheric Research, Vol. 95, Issue 4, March 2010, pp. 407-418

11. Hayashi, T and Yamane, Y., 2009: Meteorological condition of Tornadoes in Bangladesh, Proceedings of the International Forum on Tornado Disaster Reduction for Bangladesh - to Cope with Neglected Severe Disasters -13-14 December2009, Dhaka, pp 60-72
12. Peterson R .E. and K. C. Mehta, 1981: Climatology of Tornadoes of India and Bangladesh, Arch. Met. Geophy. Bokl., Ser. B 29, pp 345-356
13. Ferdousi, N., M. N. Islam and M. N. Ahsan, 2008: Characteristics of Nor'wester in and around Bangladesh, proceedings of the SAARC Seminar on Nor'westers and Tornadoes over the SARRAC Region and their Forecasting and Preparedness, Dhaka pp.123 – 135
14. Mannan, A. and Karmakar, S., 2006: On the study of gusty wind, rainfall and instability of the troposphere associated with local severe storms during pre-monsoon season in Bangladesh, The Atmosphere, Bangladesh Abhawa Karmakarta Parisad (BAKP), Dhaka, Vol. 3, pp. 39-45.
15. Climate, Natural Hazard, Nor'wester in Bangladesh, 2008: Available at: http://my.opera.com/nielsol/blog/2008/05/08/norwesters-in-bangladesh
16. Ahsan, M. N., M. N. Islam and N. Ferdousi, 2008: A Diagnostic study on Synoptic and environmental conditions favourble for the formation in and around Banglades using MM5 Model, proceedings of the SAARC Seminar on Nor'westers and Tornadoes over the SARRAC Region and their Forecasting and Preparedness, Dhaka pp. 143-156
17. Peterson, R.E., A. M. Dewan and K.C. Mehta, 2001: Destructive Thunderstorms in Bangladesh, Journal of Wind Engineering**,** Vol. No**.**89; pp**.** 369-371

A Study of the Trend, Track and Frequency of Monsoon Depression over the Bay of Bengal

M. A. K. Mallik[1, 2*], M. A. M. Chowdhury[2], Shamsuddin Ahmed[1], M. N. Ahasan[3], Md. A. E. Akhter[4], S. M. Q. Hassan[1], Md. Omar Faruk[1] and Md. Arif Hossain[1]

[1]Bangladesh Meteorological Department, Agargaon, Dhaka, Bangladesh
[2]Department of Physics, Jahangirnagar University, Savar, Dhaka, Bangladesh
[3]Feni University, Feni, Bangladesh
[4]Khulna University of Engineering and technology, Khulna, Bangladesh
[*]Corresponding author E-mail: mallikak76@yahoo.com

Abstract: Monthly, annual and seasonal frequencies of monsoon depression that occurred over the area extending from 5°N to 35°N and 65° E to 100°E are examined for the period 1891–2013. The analysis revealed a significant decreasing trend in monthly, annual as well as seasonal frequency of depressions in the monsoon season. The frequency of depression in the monsoon season also shows a dressing trend. The tracks indicate that the westward propagation of monsoon depressions has an increasing trend. On the decadal time scale, frequencies of monsoon depressions show a decreasing trend.

Keywords: Monsoon Depression, Track and Frequency

1. INTRODUCTION

During the summer monsoon season over Bangladesh and India (June–September), a series of low-pressure systems form over the Head Bay of Bengal and move in a west, north-west, north or northeast direction across the northern India, Bangladesh and Myanmarland mass. Generally, these low-pressure systems have three closed isobars at 2 hPa intervals on a mean sea level pressure chart and they cover 4–5° latitude/longitude square; they are known as monsoon depressions. These systems have surface winds up to 16 ms^{-1} and they produce widespread rain, with the heaviest over the south-west quadrant [1]. Some of the depressions fill up before reaching north-west India, while others move along the monsoon trough and finally merge with the seasonal low-pressure area over northwest India. A few of them may recurve northwards and move to the foothills of the Himalayas. With the formation of depressions over the Head Bay of Bengal, the monsoon becomes active over many parts of Bangladesh and India. The monsoon trough, which runs from Pakistan to the Head Bay of Bengal, oscillates to the north and south about its mean position. On some occasions, during the northward movement of a monsoon depression, the monsoon trough swings northwards to the foothills of the Himalayas [2], and this results in a considerable decrease in rainfall over most parts of the country. This situation is often known as the break monsoon condition. However, during the formation and movement of a monsoon depression, the monsoon trough remains either in its normal position or shifts slightly southwards [3]. After formation, Indian monsoon depressions propagate to the west-northwest atan average speed of about 2 ms^{-1} and have a lifetime of about 3-5 days [4].Records from the India meteorological Department (IMD) and Bangladesh Meteorological Department (BMD) show that an average of about 6 monsoon depressions formed each summer (June-September) in the Indian sub-continent region (5-35°N and 65-100°E) over the last century.
In the present work, an attempt has been made to analyze the frequency of depression formed in the Bay of Bengal (BoB) and the number of depression that crossed the coast, on monthly, seasonal and yearly basis for the period of 1891–2013. The frequency of depressions that crossed the different coasts and that weakened with their 5 year moving average is also discussed. The objective of this work is to identify the track, frequency and the trend of the depression formed over the BoB in the southwest summer monsoon season.

2. EXPERIMENTAL SET UP, DATA USED AND METHODOLOGY

The annual and seasonal frequencies monsoon depressions for the period 1891–2013 were extracted from the atlas of tracks of storms: depressions published by the India Meteorological Department (IMD) and from the special weather bulletin of Bangladesh Meteorological Department (BMD).

3. RESULTS AND DISCUSSION

3.1. Monthly and seasonal trend analysis of monsoon depression

The monthly and seasonal frequency, the linear trend and 05 year moving average of monsoon depression of June, July, August, September and June-July-August-September (JJAS) from 1891–2013 formed in the Bay of

Bengal (BoB) are depicted in Fig. (1-5). The linear trend and 05 year moving average of the month June indicates an increasing trend and no appreciable change in nature respectively and it has a decreasing trend in the month of July, August and September. But it is not statically significant in the time series of monthly monsoon disturbances.

The linear trend and 05 year moving average shows a decreasing trend [Fig. 5] and the value of R^2 is very low for June, July, August, September and JJAS are characterized by statistically insignificant.

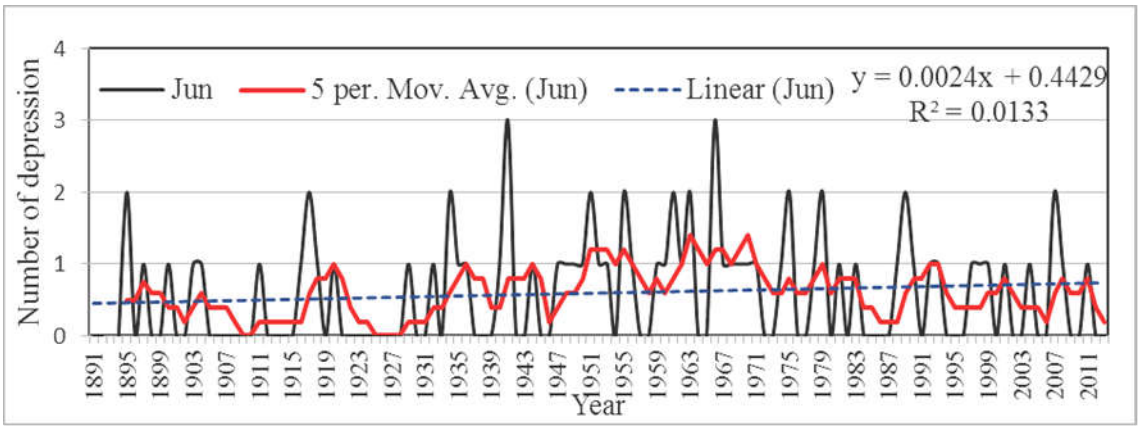

Fig. 1: Frequency of the depression of June over the BoB in 1891-2013.

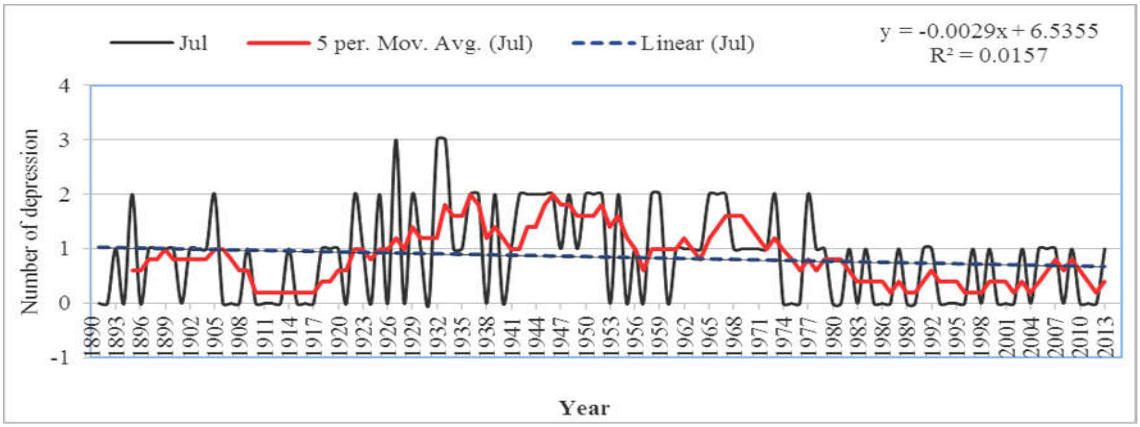

Fig. 2: Frequency of the depression of July over the BoB in 1891-2013.

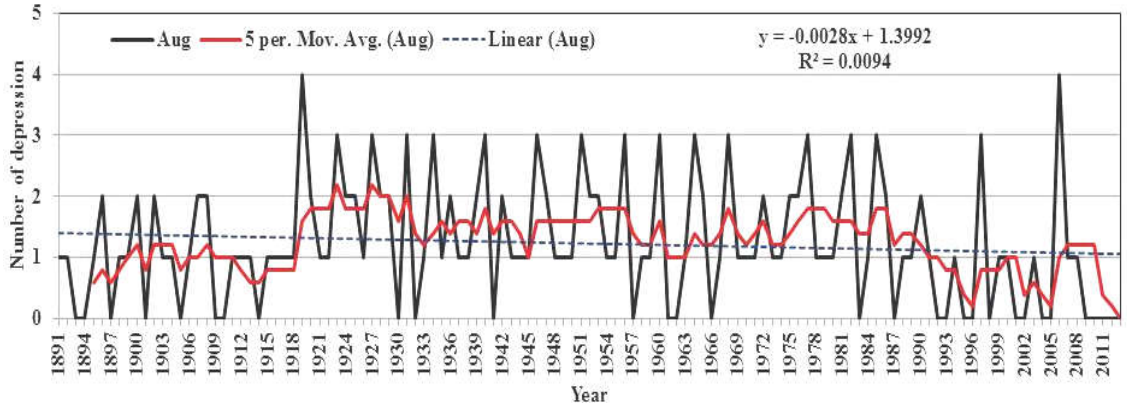

Fig. 3: Frequency of the depression of August over the BoB in 1891-2013.

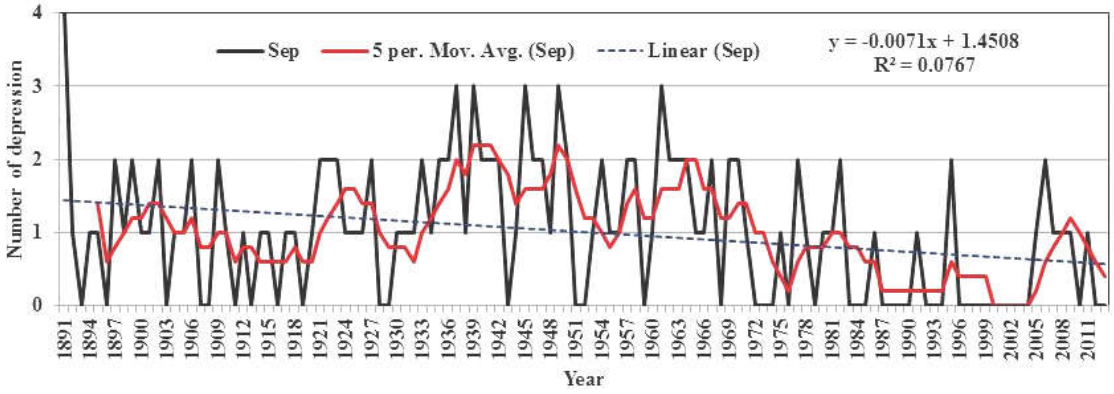

Fig. 4: Frequency of the depression of September over the BoB in 1891-2013.

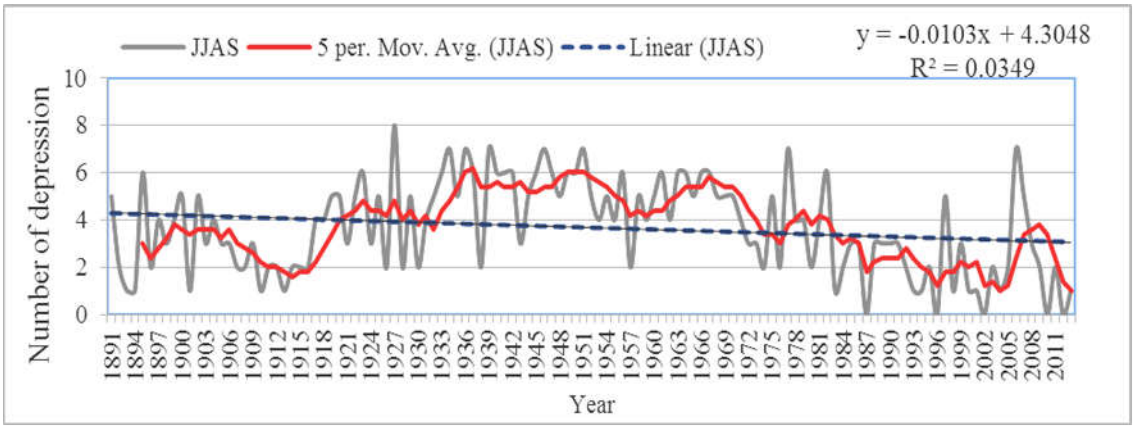

Fig. 5: Frequency of the depression of JJAS over the BoB in 1891-2013.

3.2 Monthly decadal trend analysis of monsoon depression

The monthly decadal frequency and the linear trend of monsoon depression of June, July, August and September from 1891–2013 formed over the BoB are illustrated in [Fig. (6-9)]. The linear trend of the month June shows an increasing trend than that of others months which have a decreasing trend. But it is not statically significant. The decadal frequency also represents that after 1970 it is characterized by a steep decreasing tendency

for the month of June, July and September except August. In August the frequency decreases after 1990 onwards.

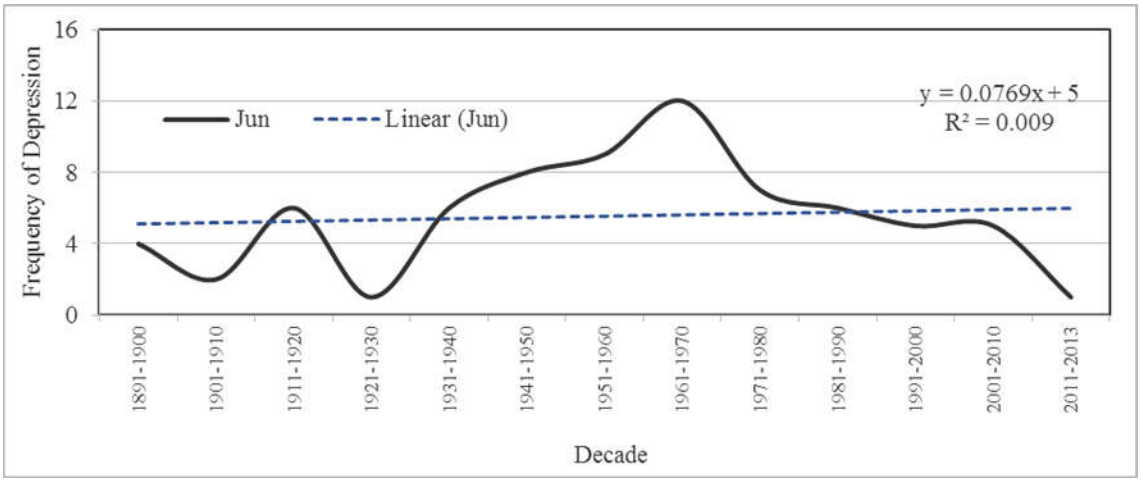

Fig. 6: Decadal frequency of the depression of June over the BoB in 1891-2013.

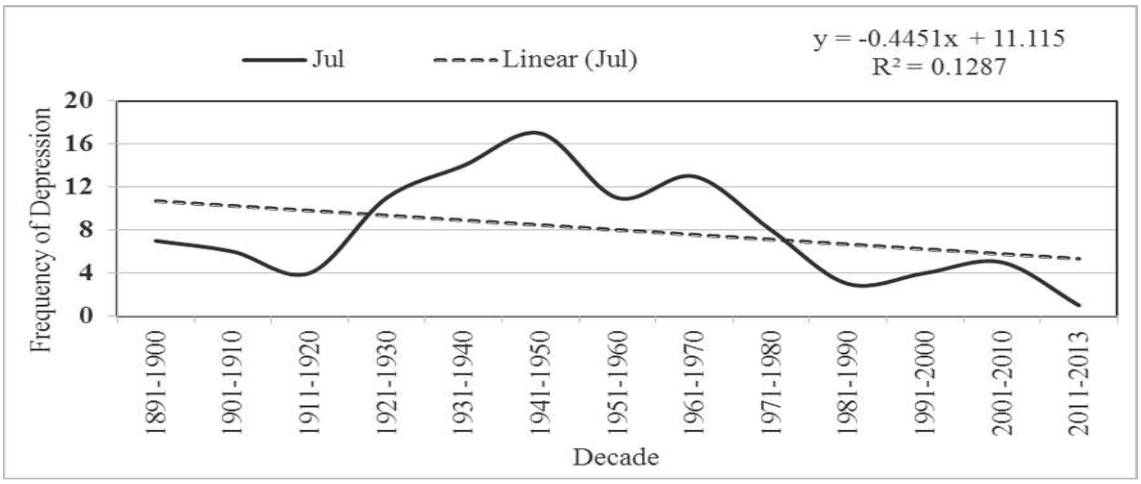

Fig. 7: Decadal frequency of the depression of July over the BoB in 1891-2013.

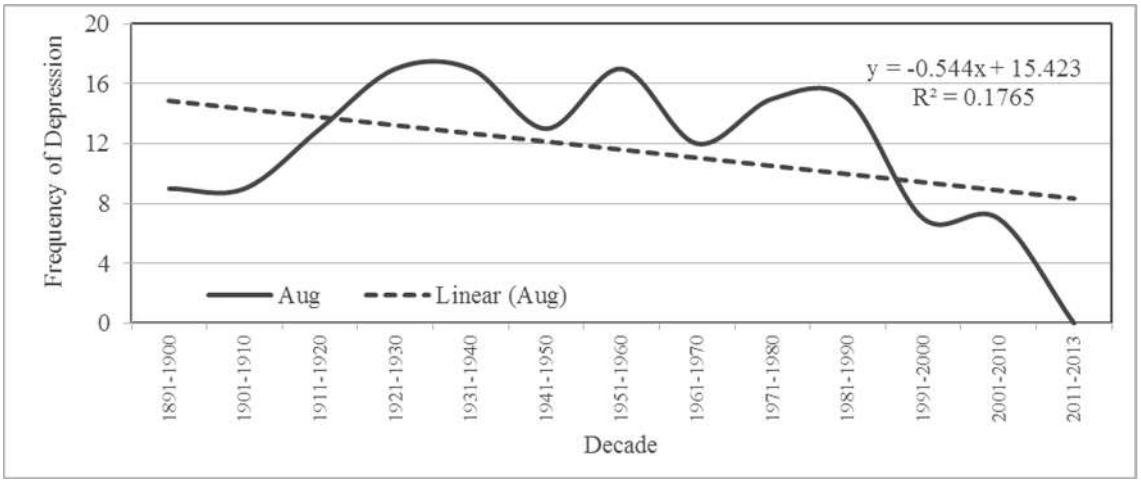

Fig. 8: Decadal frequency of the depression of August over the BoB in 1891-2013.

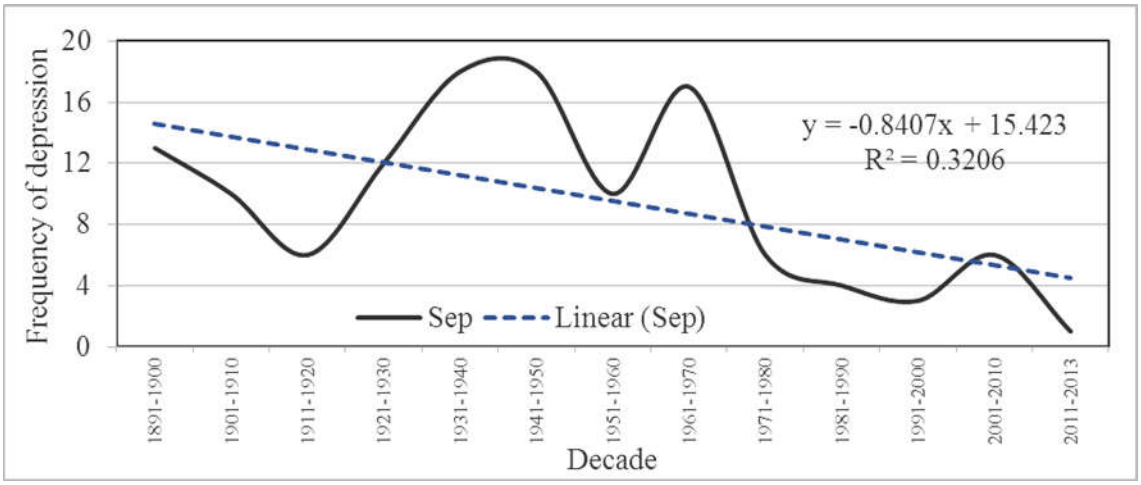

Fig. 9: Decadal frequency of the depression of August over the BoB in 1891-2013.

3.3 MONTHLY DECADAL SEASONAL TRACKS OF MONSOON DEPRESSION

Seasonal and monthly decadal track of monsoon depression of JJAS, June, July, August, and September from 1891–2013 formed in the Bay of Bengal (BoB) are demonstrated in [Fig. (10-11)]. The linear trend of the month

June shows an increasing trend than that of other months which have a decreasing trend and it is not statically significant. The decadal frequency also represents that after 1970 it is characterized by a steep decreasing tendency for the month of June, July and September except August. In August the frequency decreases after 1990 onwards.

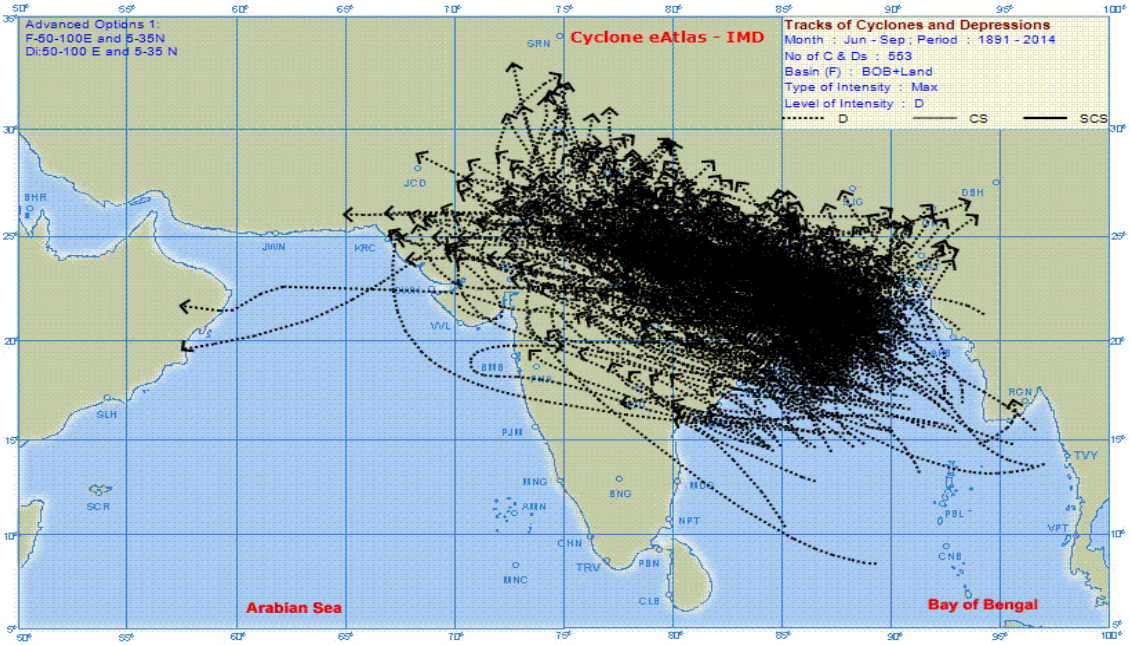

Fig. 10: Track of the depression of JJAS over the BoB in 1891-2013.

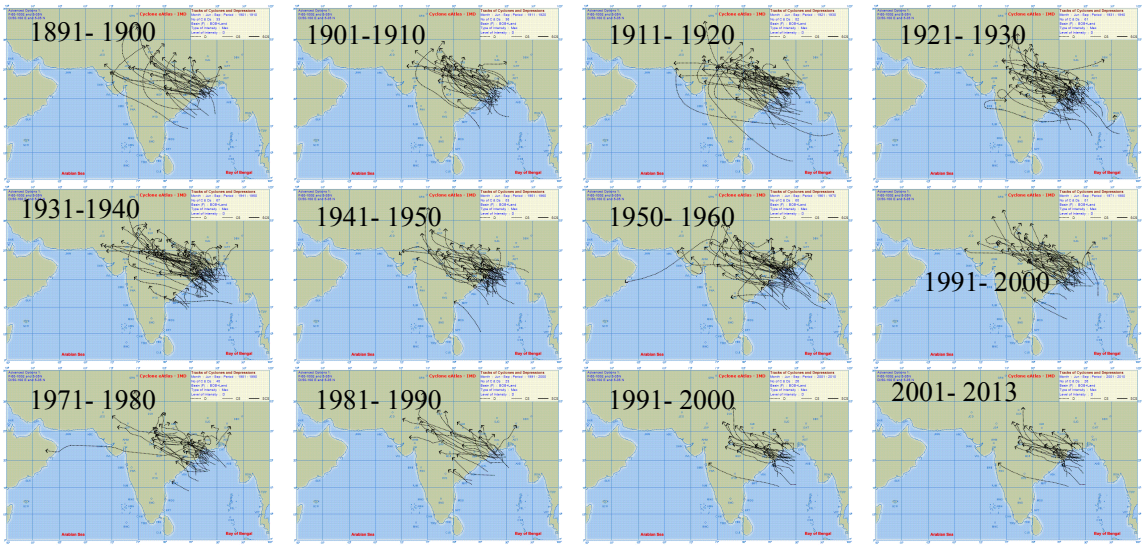

Fig. 11: Decadal Track of the depression of JJAS over the BoB in 1891-2013.

4. CONCLUSION

Studies on the occurrence of monsoon depressions over long period such as 1891 to 2013 show a significant decrease of their seasonal frequencies. Also, examinations of monthly and decadal frequencies indicate that the decreasing trend was maximum in September followed by August and July. In June it shows a slightly increasing trend. From the constructed track it is seen that the common moving direction of monsoon depression is northwestwards and a few depression recurved and move northeastwards and some followed to the northward direction.

ACKNOWLEDGEMENT

The authors wish to thank Mr. Shah Alam, Director of Bangladesh Meteorological Department and all the officers and staff of this Department for their help and cooperation during the work in providing the relevant data. The authors are also thankful to India Meteorological Department (IMD) for the storm track prediction eAtlas.

REFERENCES

1. Rao, Y. P. (1976). Southwest monsoon. *Meteorological Monograph*, *Synoptic Meteorology*, No. 1/1976, India.
2. Asnani, G. C. (1993). Tropical Meteorology. Published by Prof. G. C. Asnani. 1202 pp.
3. Mooley, D. A. & Shukla, J. (1987).Variability and forecasting of the summer monsoon rainfall over India. In: *Monsoon.*
4. Ding, Y., and D. Sikka (2006), Synoptic systems and weather, in *Springer Praxis Books*, pp.131–201, Springer Berlin Heidelberg.

DEW DROP 02(2016) 37-52

A study on the prediction of Heavy Rainfall occurs during monsoon season in Bangladesh

Md. Abdul Mannan[1*], Md. Abdul Mannan Chowdhury[2], Samarendra Karmakar[3], Shamsuddin Ahmed[1] and Md. Abdur Rahman[1]

[1]Bangladesh Meteorological Department, Agargaon, Dhaka,Bangladesh
[2]Jahangirnagar University, Savar, Dhaka Bangladesh
[3]Bangladesh Centre for Advanced Studies (BCAS), Dhaka, Bangladesh
[*]Corresponding author: mannan_u2003@yahoo.co.in, mamannanbmd2015@gmail.com

Abstract: During 21-28 June 2015 widespread heavy rainfalls occur over southeastern and southern coastal parts of Bangladesh which had significant impact on the socio-economic activities of these areas. To understand the associated behaviour with the event and to make it predictable, WRF-ARW model (version: 3.2.1) with the grid resolution of 9 km considering Ferrier (FR) microphysics (MPs) schemes combined with the Kain-Fritsch (KF) cumulus scheme (CP) is used. It is found that a low pressure system positioned over Bangladesh during 23-27 June 2015 was the cause for this event. Analysis also reveals that the favourable environmental condition in terms of surface and upper air relative humidity (RH) and moisture flux (MF), convective available potential energy (CAPE), Total Static Energy (TSE) and Level of Conditional Instability (LCI) were associated with the system for the occurrence of heavy rainfall (HR). But the model simulated average and maximum rainfalls during the days of HR are higher than observation. The frequency of the simulated Cat-III, Cat-IV and Cat-V rainfalls are quite comparable with the 0.25°x0.25° gridded observed rainfall. Accordingly, the skill scores of Probability of Detection (PoD) for the frequency of Cat-III and its higher amounts of rainfall are found high during 21-25 June and it is the maximum on 25 June. Similarly, PoD for the frequency of Cat-IV and its higher amounts of rainfall is the highest on 25 June when the system was well organized over Bangladesh.

Key words: CAPE, heavy rainfall, LCI, moisture flux and TSE.

1. INTRODUCTION

Bangladesh is situated at the interface of two different environments, with the Bay of Bengal to the South and Himalayas to the north. Due to its geographical position, Bangladesh experiences highest amount of country average monsoon and annual rainfall among the SAARC countries [1]. Bangladesh is also an agricultural country and agriculture is the foundation of the economy in Bangladesh which largely depends on the rainfall from the monsoon. The life and livelihood of the inhabitants of Bangladesh depend directly and indirectly on the monsoon rainfall as the fertility of cultivable land as well as the stability of land resources depend highly on the activities of the monsoon. Most of the development endeavours especially those of physical infrastructure like roads, flood control dams, irrigation canals and so on are dictated by the monsoon and the most of natural disasters are also associated with the behavior of the monsoon [2]. The economy of the country and fate of the people are therefore closely tied up with the good monsoon rain which occurs during June to September. Moreover, the monsoon season is characterized by the occurrence of heavy rainfall causing extensive damage to crops, live stocks and properties associated with loss of valuable lives [3].

Heavy rainfall in Bangladesh during monsoon season are mainly governed by the activities of southwest or summer monsoon system i.e., position, formation and intensity of monsoon trough and monsoon lows or monsoon depressions [3, 4]. Monsoon Trough (defined as MT) is an elongated area of a low pressure running parallel to the Himalayan Mountains in a west to east direction. MT is depicted by a line on a weather map showing the location of minimum sea level pressure within the monsoon region. It extends up to 5-6 km above mean sea level (AMSL) tilting southwards with height [5, 6]. When the eastern end of the MT swings southwards and dips into the northern most Bay of Bengal, conditions become favourable for the formation of a monsoon depression (defined as MD), the most important synoptic system during monsoon. Rainfall is heavier in the southern side of the MT. The belt overlain by the MT itself receives only modest rainfall, and rainfall increases on either side (south and north) of the MT [5, 7]. Monsoon depressions (MD) are more intense than monsoon lows. For a low pressure area to be a depression there should be at least two closed isobars present within a 5º square [5, 7]. MD is known as cold core system, which reaches its highest intensity at well above mean sea level (1-2 km AMSL). Though most of the depressions are cold core, some depressions cannot be

bracketted into warm or cold core categories. These are probably of a baroclinic type and exist in the presence of the large zonal wind shear. In a well developed depression, region of maximum ascent, convergence and rainfall coincide in the west of the centre and conversion of potential energy and kinetic energy takes place through a thermally direct vertical circulation [5, 7].

Heavy to very heavy rainfall frequently occurs in the vicinity of MDs. Rainfall is the heaviest in the left forward (i.e., southwest) sector of a west moving depression and sparse in the northeastern sector [5, 7]. For northward moving systems, the heaviest rainfall occurs in the northern sector. Heavy rain in the field of MD is confined to a narrow belt of 2-3° width and 7° lengths. When a depression develops over the Head Bay in June and July, the monsoon gets strengthened over the west coast as well. When it moves inland, the activity may get reduced but might intensify again when the systems move closer to the west coast [5, 7]. But the problem of forecasting heavy rainfall is difficult since it involves a quantitative precipitation forecast, recognized as a challenging task [5, 8]. Simulation of active mesoscale systems such as monsoon depressions and heavy rainfall episodes during monsoon season, with high-resolution mesoscale models such as the fifth-generation PSU/NCAR mesoscale model (MM5), has been attempted by many researchers [5, 9-12]. The study of heavy rainfall over Bangladesh territory is also very limited and insufficient [5]. Mannan et al. showed that the WRF model with the initial and boundary conditions from NCEP are able to simulate high intensity rain bands over Bangladesh during monsoon season [13, 14]. Mannan et al. also showed that the simulated location specific rainfall only up to three days are highly correlated with the observed rainfall [15].

Hence, a study is undertaken to investigate predictability of heavy rainfall by calculating Moisture Flux (MF), Convective Available Potential Energy (CAPE), Total Static Energy (TSE) and Level of Conditional Instability (LCI) as defined in the chapter 2 to detect as predictive tools. Accordingly, consecutive heavy rainfall event occurred during 21-28 June 2015 in Bangladesh has been chosen and simulated as the event had significant socio-economic impacts on the life and livelihood of the inhabitants of the occurrence areas with the aim to guide the operational forecasters.

1.1 Description of the event

A monsoon low formed over West Central Bay and adjoining Northwest Bay of Bengal on 17 June 2015. It intensified into well marked low over the same area on 19 June. The system then moved north-northwestwards and concentrated into a depression over Northwest Bay and adjoining West Central Bay on 20 June when its central location was at latitude 19.5°N and longitude 85.5°E. It moved further northwestwards and crossed Orissa Coast of India at about 0900 UTC of 21 June. The system then changed its direction of movement and moved northwards first and then northeastwards and finally reached Bangladesh and adjoining areas on 25 June and persists over the same area up to 27 June. It weakened into a well marked low on 28 June and moved oppositely towards northwest to Sub-Himalayan West Bengal and then to Bihar of India. During this period monsoon was active to very active over Bangladesh territory and strong to vigorous over North Bay.

1.2 Recorded rainfall during 21-28 June 2015

As per the record available at Bangladesh Meteorological Department (BMD), high amounts of rainfalls are recoded in Bangladesh during 21-28 June 2015. For the interest of the study the frequency of the recoded rainfall has been calculated based on World Meteorological Organization (WMO) acceptable operational use classification in BMD as given in Table 1. It is found that the frequency of Cat-III rainfall varies from 3 to 9 with the maximum on 27 June 2015. Similarly, the frequency of Cat-IV rainfall varies from 2-13 with the maximum on 26 June followed by 24 June. The frequency of Cat-V varies highly from 1-15 with the highest on 25 June followed by 23 June. The rainfall averaged over 35 rain gauge locations vary from 18.1 to 87.9 mm during the mentioned period. The maximum country average rainfalls of 87.9 mm followed by 65.4 mm are found respectively on 25 June and 24 June 2015 [Table 2]. The maximum amounts of rainfall recorded during 21-28 June are respectively at Teknaf, Kutubdia, Sitakunda, Cox's Bazar, Chandpur, Cox's Bazar, Teknaf and Mongla [Table 2].

Table 1: Classification of rainfall used under the study [2, 16]

Intensity (mm/day)	Category of rainfall	Defined as	Comments
Non-measurable amount	Trace	-	Operationally used classification in Bangladesh
1 - 10	Light	Category-I (Cat-I)	
11 - 22	Moderate	Category-II (Cat-II)	
23 - 43	Moderately heavy	Category-III (Cat-III)	
44 – 88	Heavy	Category-IV (Cat-IV)	
≥ 89	Very heavy	Category-V (Cat-V)	

Table 2: Frequency of HR, average rainfall (mm) & maximum rainfall (mm) in Bangladesh during 21-28 June 2015

Parameter		Dates in June 2015							
		21	22	23	24	25	26	27	28
Frequency of rainfall	Cat-III	5	3	6	6	7	7	9	3
	Cat-IV	2	9	6	11	9	13	5	3
	Cat-V	1	6	8	5	15	5	1	1
Average rainfall		19.4	50.6	51.3	65.4	87.9	59.4	29.4	18.1
Maximum rainfall		98	173	182	467	288	263	243	91

1.3 Spatial distribution of rainfall in Bangladesh

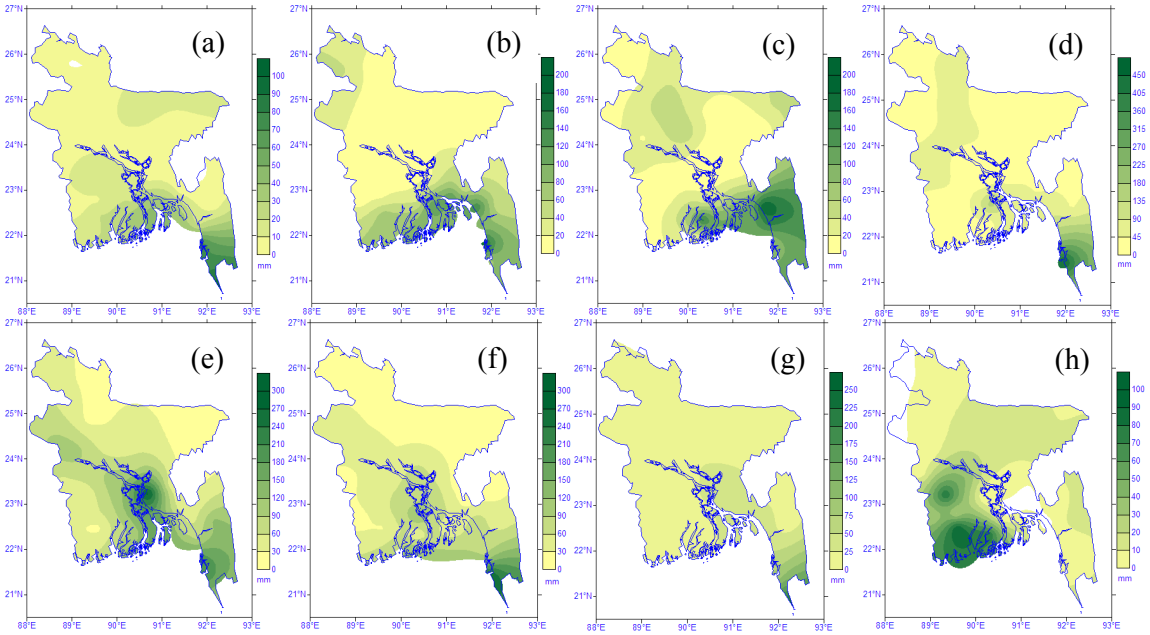

Fig. 1: Spatial distribution of observed rainfall in Bangladesh: (a) 21 June, (b) 22 June, (c) 23 June, (d) 24 June, (e) 25 June, (f) 26 June, (g) 27 June and (h) 28 June 2015

Fig. 1 depicts the spatial distribution of the observed (rain gauge) rainfall during 21-28 June 2015. It shows that the HR of Cat-III, IV and V occur only over extreme southeastern part of Bangladesh and its adjoining areas during 21 June. The zone of HR expands towards north along with the intensification of the system and covers southern part of Bangladesh during 22-26 June 2015. The zone of HR shrinks and the frequency of HR of Cat-III, IV and V decreases during 27 June and found only over extreme southeastern part of Bangladesh. It is recorded only over southwestern part of Bangladesh on 28 June 2015. Spatial distribution of rainfall also reveals that the higher amounts of rainfall are mainly concentrated over the southern part of Bangladesh during 21-24 June 2015; it extends up to south-central part during 25 June and southeastern part of Bangladesh during 26-27 June. High amounts of rainfall are witnessed only over southwestern part and adjoining western part of Bangladesh during 28 June 2015.

2. METHODOLOGY

WRF ARW model (version: 3.2.1) with the grid resolution of 9 km is used to diagnosis the event using Ferrier (FR) microphysics (MP) schemes with the combination of Kain Fritsch (KF) cumulus scheme (CP). The selected combination of CP and MP for the experiments is named as KFFR. The coverage area of model domain is 12-30ºN and 80-100ºE. The topography in the model is obtained from USGS land covers data set. NCEP data have been provided at every 6 hrs as initial and boundary conditions. The model has been run continuously during 0000 UTC of 21 June to 29 June 2015 considering 27 sigma levels in the vertical direction. The parameters of mean sea level pressure (MSLP), horizontal and vertical distribution of wind field, relative humidity (RH), moisture flux (MF), convective available potential energy (CAPE), convective rain and non-convective rain etc. are considered for the analysis. GrADS software is used for displaying the simulated and derived parameters of the model and rainfall of TRMM.

In addition the Total Static energy (TSE) and Level of Conditional Instability (LCI) are calculated and analyzed for justifying their relation with the heavy rainfall in Bangladesh. The Total Static Energy (TSE) is the total energy within an atmosphere of a parcel of air without taking the small KE (due to microscopic motion) into account. Mathematically, TSE [17] can be defined as-

$$TSE = C_p T + gz + Lq \quad \text{.....(1)}$$

Where, C_p=1004.64 $JK^{-1}kg^{-1}$ and z is the gepotential height and the term 'gz' is the geopotential, if it is accepted that g does not vary in the vertical column. The right hand terms represents respectively the enthalpy, gepotential and latent energy of the parcel. The average TSE in the troposphere is calculated between the 850 hPa and 300 hPa levels. The vertical profile of TSE is used to determine if the atmosphere is conditionally unstable.

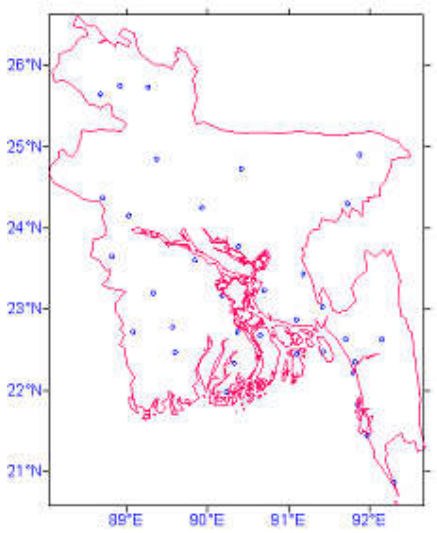

Fig. 2: Rain gauge locations of BMD

To calculate LCI [17] the following formula is used:

$$LCI = TSE_{850hPa} - TSE_i \quad \text{.....(2)}$$

Where, LCI varies between 700 hPa and 400 hPa. For the atmosphere to be conditionally unstable up to 400 hPa, the LCI must be positive for i= 700 hPa to 400 hPa. Finally, simulated result (i.e., frequency of heavy rainfall of Cat-III, IV and V), maximum rainfall and the country average rainfall are verified with the observation by calculating the Mean Absolute Error (MAE) so that the predicted result can be utilized by the operational forecasters. The MAE can be defined as [2, 18-20]:

$$MAE = \frac{1}{N}\sum_{i=1}^{N}|F_i - O_i| \quad \text{.....(3)}$$

Where, F_i denotes the forecast (or simulated) value and O_i denotes the observed value of any parameter. As stated by Murphy and Winkler [21] and by Doswell [18] forecast verification is an essential component of a forecasting system, since it provides a measure of the quality and value of a numerical forecast. The forecast skills of Probability of Detection (PoD) [2, 19-20, 22] and Percentage Correct (PEC) [2, 19-20, 22] are calculated for Cat-III, Cat-IV and Cat-V rainfall at rain gauge locations for all of the experiments using Table 3 [23] and the equations 4-5 [24-26].

Table 3**:** Contingency table [2, 23]

		Observation		
		Yes	No	Total
Forecast	Yes	Hits (A)	False alarms (B)	Forecast Yes (A+B)
	No	Misses (C)	Correct non-events (D)	Forecast No (C+D)
	Total	Observed Yes (A+C)	Observed No (B+D)	Total (A+B+C+D)

Where, the sum of these frequencies represents the total number of the forecast-observation pairs N=$A+B+C+D$

$$POD = \frac{Hits}{Hits + Misses} = \frac{A}{A + C} \quad \text{.....(4)}$$

The range of POD is 0 to 1 but its perfect score is 1. It is sensitive to hits, but it ignores false alarms.

$$PEC = \frac{A + D}{A + B + C + D} = \frac{A + D}{N} \quad \text{.....(5)}$$

The magnitude of PEC varies from 0 to 1 but its perfect score is 1. Its gives maximum score if everything is correct.

The False Alarm Ratio (FAR) is the measure of the predicted 'yes' event actually did not occur. It can be defined as-

$$FAR = \frac{B}{A + B} \quad \text{.....(6)}$$

The range of FAR is 0 to 1 but its perfect score is 0. It is sensitive to false alarms, but it ignores misses.

The result obtained through the methodology is formulated in chapter 3.

3. RESULTS AND DISCUSSION

3.1 Mean Sea Level Pressure (MSLP) and wind at 10 m

Simulated MSLP and wind field at 10m height reveals that the depression formed over the Bay of Bengal crossed Orissa coast of India on 21 June 2015. It then moved north-northeastwards to West Bengal and adjoining area of India. The system then weakened slightly and moved further eastward and positioned over Bangladesh and adjoining area and reached Bangladesh territory on 24 June. In continuation of the movement, the system reached northeastern part of Bangladesh and adjoining area at 0000 UTC of 25 June and intensified further. After that it returned back and moved west-northwestwards following the monsoon trough. The successive positions of the system are depicted trough MSLP and wind fields in Fig. 3.

3.2 Relative humidity

Simulation indicates that the RH at 2m height was high over North Bay of Bengal and adjoining coastal areas of Bangladesh during 21-28 June 2015. The strong band of high RH appeared and persisted at the same level over Bangladesh during 23-27 June which moved with the movement of the low pressure system but the high RH band continuously persisted over the southern coastal region of Bangladesh (Fig. 4). This situation may be accelerated the heavy rainfall activity over Bangladesh during the observed period.

Similarly, the spatial distributions of RH at different upper levels of atmosphere at 0000 UTC of 25 June 2015 are depicted in Fig. 5. Fig. 5 illustrates that the higher RH concentrated over the surroundings of the low pressure system covering southern coastal region of Bangladesh and adjoining North Bay of Bengal. This situation extended vertically up to 200 hPa level is the indication of strong vertical profile of RH and the existence of sufficient moisture or advection of sufficient moisture over Bangladesh for the occurrence of heavy rainfall.

The vertical profiles of simulated area average RH of Bangladesh during 21-28 June 2015 is illustrated in Fig. 6. It is also found that the RH was high and almost steady in the layer of surface to mid-troposphere over Bangladesh during the observed period which was 90% and above during 22-26 June. The average RH in the layer of 950-500 hPa were 89, 91, 95, 93 and 90% respectively during 22, 23, 24, 25, 26 and 27 June 2015. RH decreased sharply in the layer above of 500 hPa to 25-30%. Persistence of high RH in the layer of surface to 500 hPa level was the signature of high instability leading to strong convection over the area of the occurrence of heavy rainfall.

Vertical profile of RH along 21.0ºN at 0600 UTC (east-west direction over southern part of Bangladesh) of each day under study demonstrates the strong vertically extended moisture content which varied along zonal direction

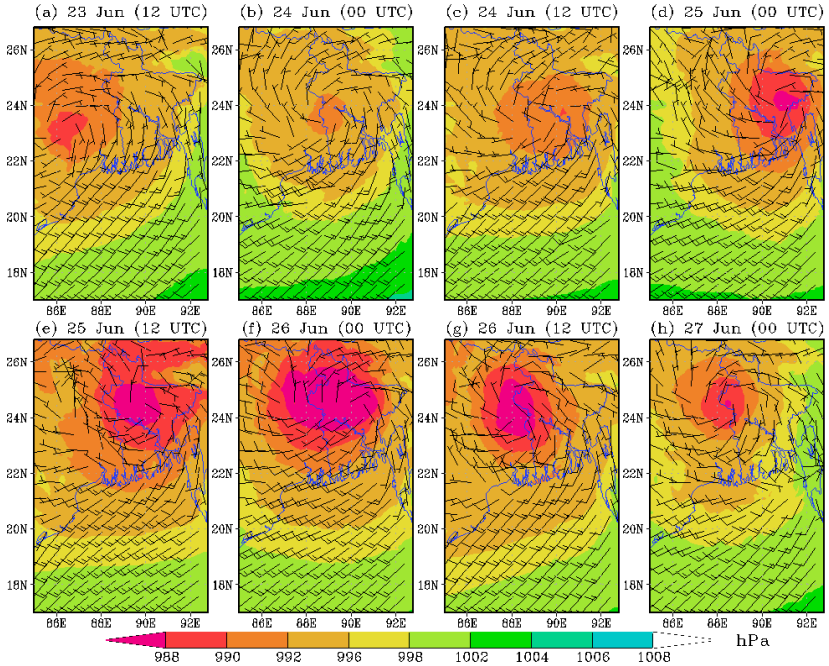

Fig. 3: MSLP and wind (at 2 m) fields for KFFR at (a) 1200 UTC of 23 June, (b) 0000 UTC of 24 June, (c) 1200 UTC of 24 June, (d) 0000 UTC of 25 June, (e) 1200 UTC of 25 June, (f) 0000 UTC of 26 June, (g) 1200 UTC of 26 June and (h) 0000 UTC of 27 June 2015

(Fig. 7). It is also found that the sufficient moisture content had uplifted due to convection as well as advected up to 400 hPa level and it's above temporarily for saturating the lower troposphere. In particular, the moisture profile was very strong with high vertical extension during 22-26 June when high amounts of rainfall consequently more numbers of Cat-III, Cat-IV and Cat-V rainfall were observed.

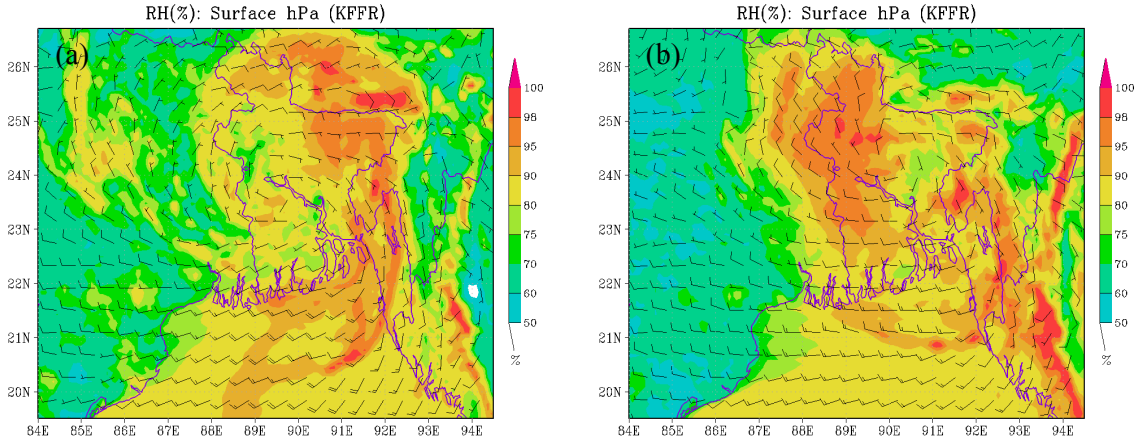

Fig. 4: Spatial distribution of RH at 2m height over Bangladesh at 0600 UTC of (a) 24 June and (b) 25 June 2015

.

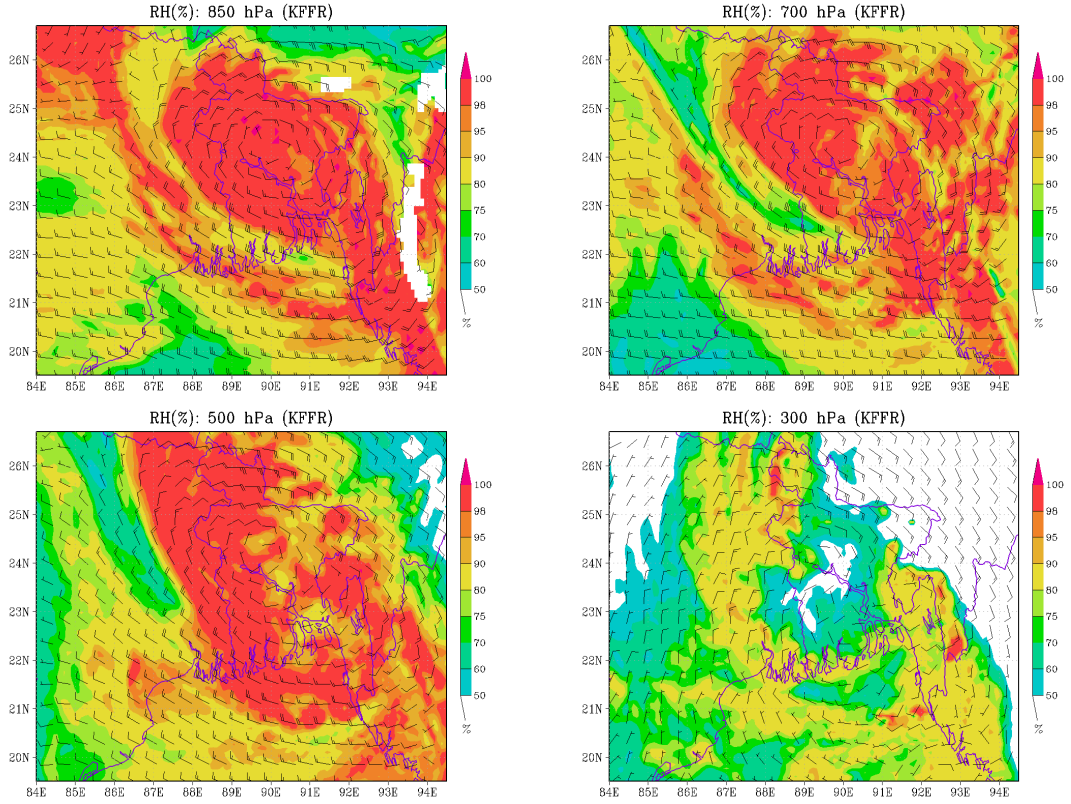

Fig. 5: Spatial distribution of RH at (a) 850, (b) 700, (c) 500 and (d) 300 hPa levels at 0000 UTC of 25 June 2015

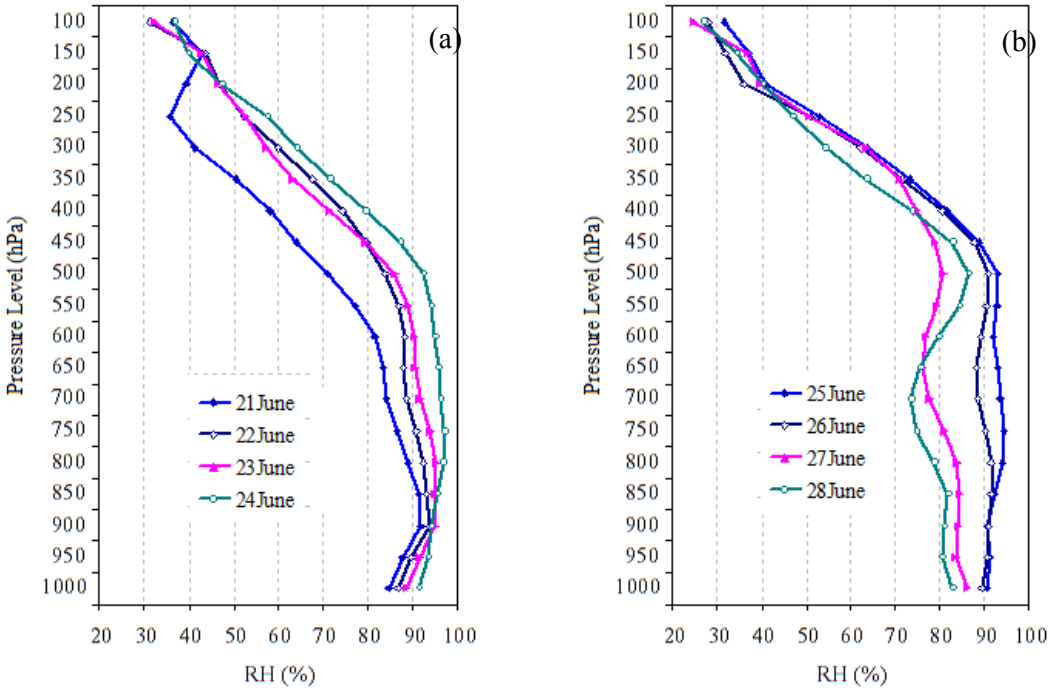

Fig. 6: Vertical distribution of area average simulated RH over Bangladesh during (a) 21-24 June and (b) 25-28 June 2015

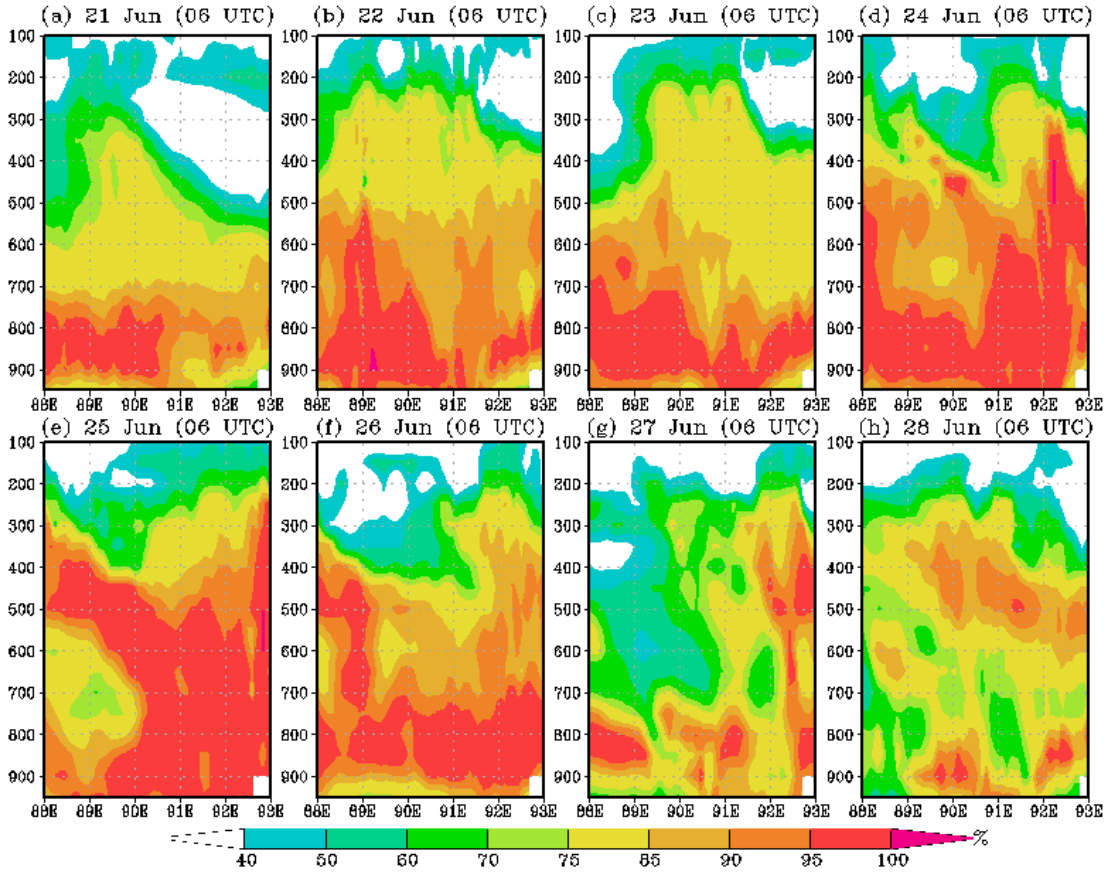

Fig. 7: Vertical distribution of simulated relative humidity (RH) at specified time along 21ºN over Bangladesh during 21-28 June 2015

3.3 Moisture Flux

Simulated result reveals that the deep moisture flux (MF) persisted over Northwest Bay of Bengal and adjoining areas during 21-26 June 2015 at lower levels of the troposphere, i.e., at 900 hPa. When the system positioned over Bangladesh, moisture accumulated over Bangladesh land mass and the intense MF persisted over the surrounding areas of the low pressure system which covered southern part of Bangladesh and adjoining North Bay of Bengal following the flow pattern associated with it (Fig. 8). As a result, the band of deep MF persisted surroundings to the low pressure system over Bangladesh during the days when the maximum number of heavy rainfall was recorded over southern part of Bangladesh.

Similar pattern of the distribution of MF is found at upper air standard levels upto 500 hPa (Fig. 9). This situation further indicates the presence and advection of high moisture content in the lower to mid-troposphere over Bangladesh. This situation may be responsible for the occurrence of heavy rainfall.

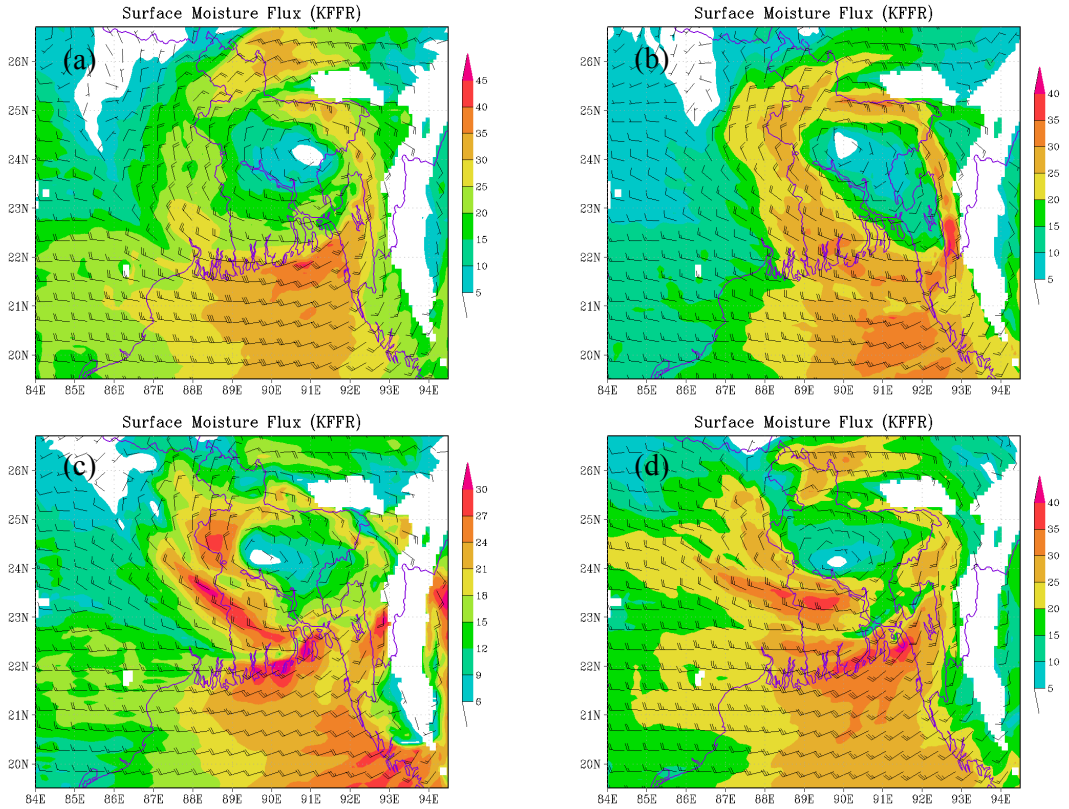

Fig. 8: Spatial distribution of moisture flux for KFFR over Bangladesh at 900 hPa at (a) 0000 UTC, (b) 0600 UTC, (c) 1200 UTC and (d) 1800 UTC of 25 June 2015.

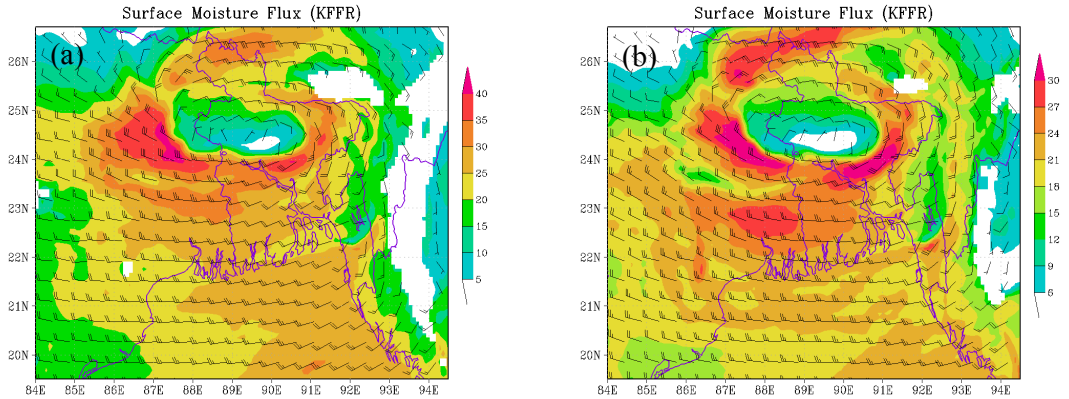

Fig. 9 (a-b): Spatial distribution of MF for KFFR at (a) 900 hPa and (b) 850 hPa at 0000 UTC of 26 June 2015

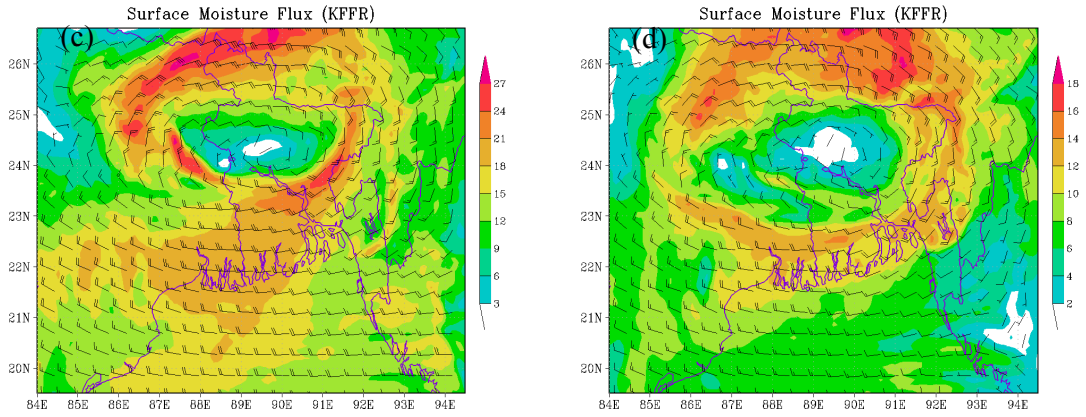

Fig. 9 (c-d): Spatial distribution of MF for KFFR at (c) 700 hPa and (d) 500 hPa at 0000 UTC of 26 June 2015

3.4 Convective Available Potential Energy (CAPE)

Moderate to quiet strong CAPE near to surface level persisted over the southwestern and southern side of the low pressure system during the observed period (Fig. 10). Analysis also reveals that the CAPE field was quiet strong over southern coastal areas of Bangladesh during 24-25 June 2015 when heavy rainfall was recorded. Moderate to high values of CAPE at the lowest level of troposphere during the observed period is found over Bangladesh. But the band of intense CAPE persisted over the surrounding areas of the low pressure system including southern part of Bangladesh and adjoining Bay areas (Fig. 11).

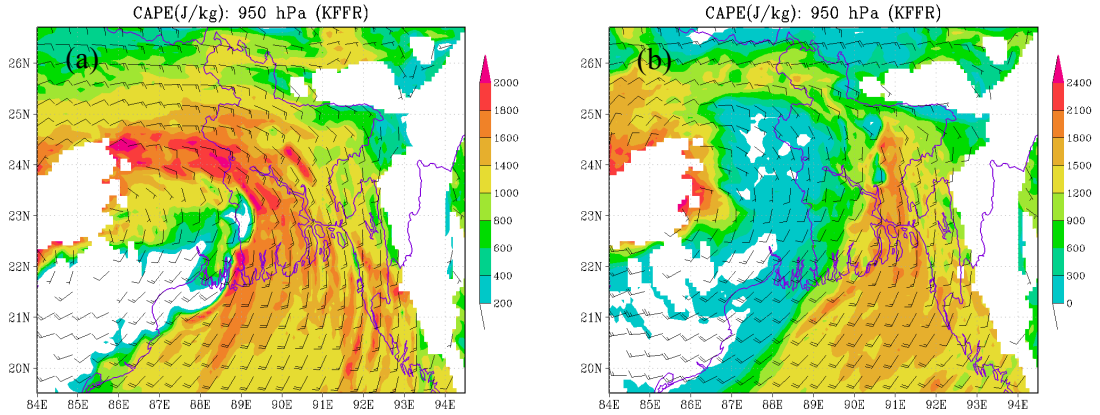

Fig. 10: Spatial distribution of CAPE for KFFR at (a) 0600 UTC of 22 June and (b) 0600 UTC of 23 June 2015

Spatial distribution of CAPE at upper levels depicts the existence of moderate to quiet strong CAPE surrounding to the circulation associated with low pressure system in the layer surface to mid-troposphere over Bangladesh during 22-27 June 2015. It is also found that the strong band of CAPE field persists over southwestern and southern side of the circulation system and was over southern part of Bangladesh where heavy rainfall was recoded (Fig. 11). Vertical profile reveals that the area average CAPE over Bangladesh decreased rapidly with height and it was about to zero above of 500 hPa level (Fig. 12).

Vertical distribution of CAPE over Bangladesh along 21.0ºN at 0600 UTC of each day under study illustrates that the CAPE prolonged upto 850 hPa but there were short lived deep layered CAPE during 22-26 June (Fig. 13). This situation indicates the short durable high convection within the period of study along the west-east direction over southern part of Bangladesh where heavy rainfalls are recorded.

3.5 Total Static energy (TSE)

Spatial distribution of the integrated TSE within the layer of 850-300 hPa has been calculated at 0000 UTC of each day to be used as the predictor (Fig. 14). It is exposed that the integrated TSE was high over and surroundings to the system during the observed period and the maximum intense TSE traveled with the movement of the system. It is also observed that TSE was high over Bangladesh and its adjoining areas during

23-27 June when the low pressure system was over Bangladesh is the indication of the strong association of TSE with the monsoon system which is caused for occurrence of HR over Bangladesh.

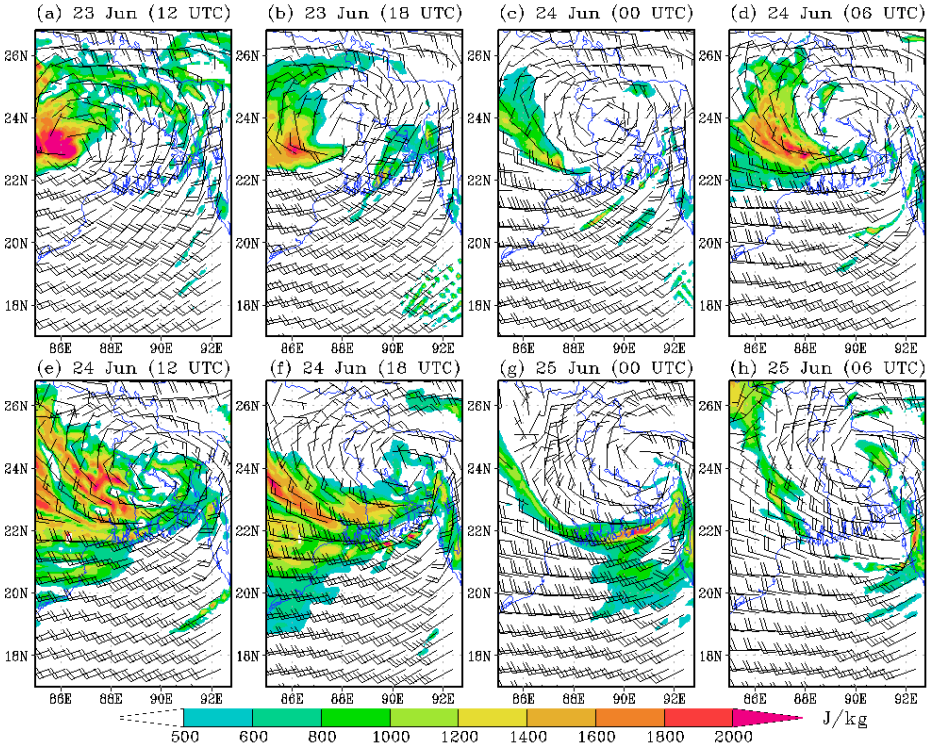

Fig. 11: Spatial distribution of CAPE for KFFR at (a) 0600 UTC of 22 June, (b) 0600 UTC of 23 June, (c) 1200 UTC of 23 June, (d) 0600 UTC of 24 June, (e) 0600 UTC of 24 June and (f) 1800 UTC of 25 June 2015

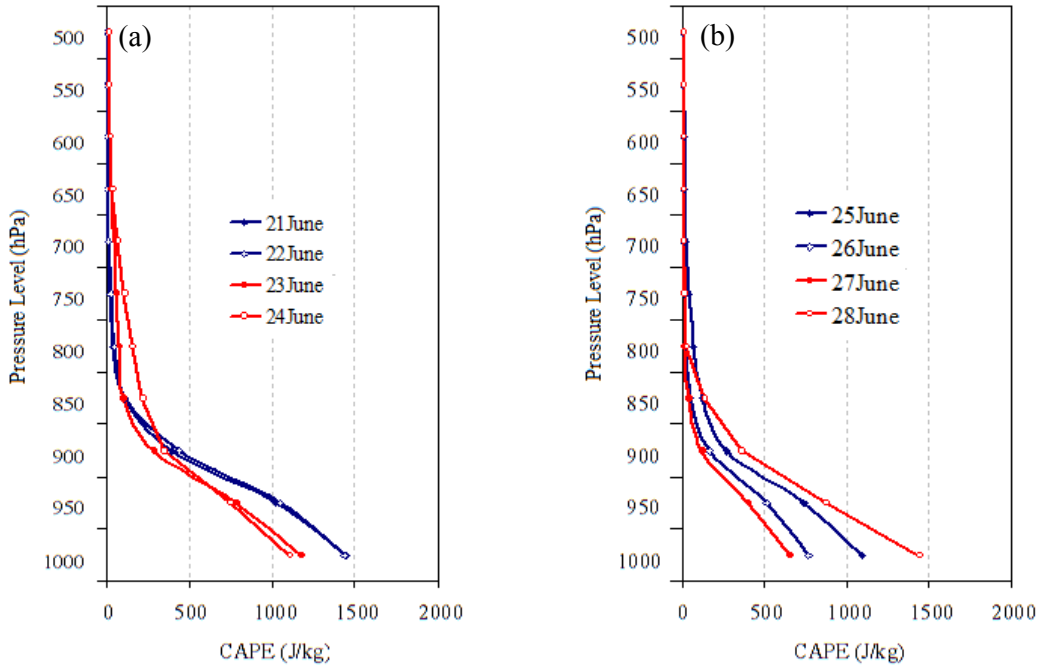

Fig. 12: Vertical profile of the area average simulated CAPE (J/kg) for KFFR over Bangladesh during (a) 21-24 June and (b) 25-28 June 2015

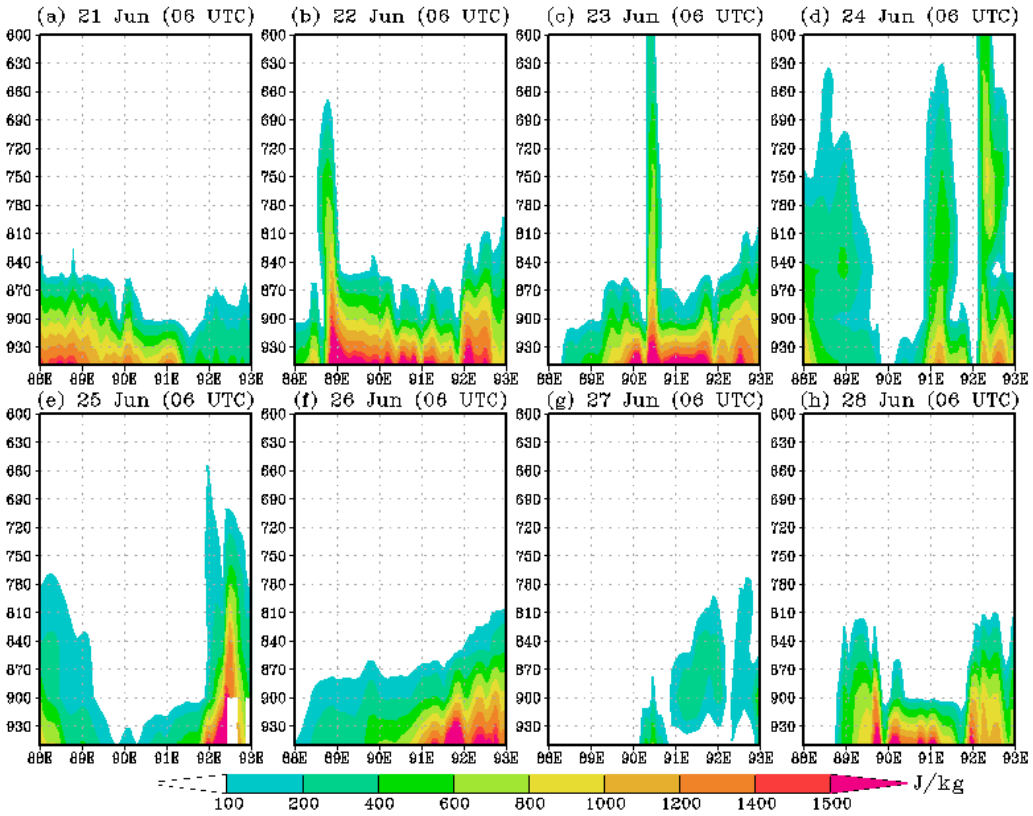

Fig. 13: Vertical distribution of simulated CAPE (J/kg) for KFFR at specified time along 21ºN over Bangladesh during 21-28 June 2015

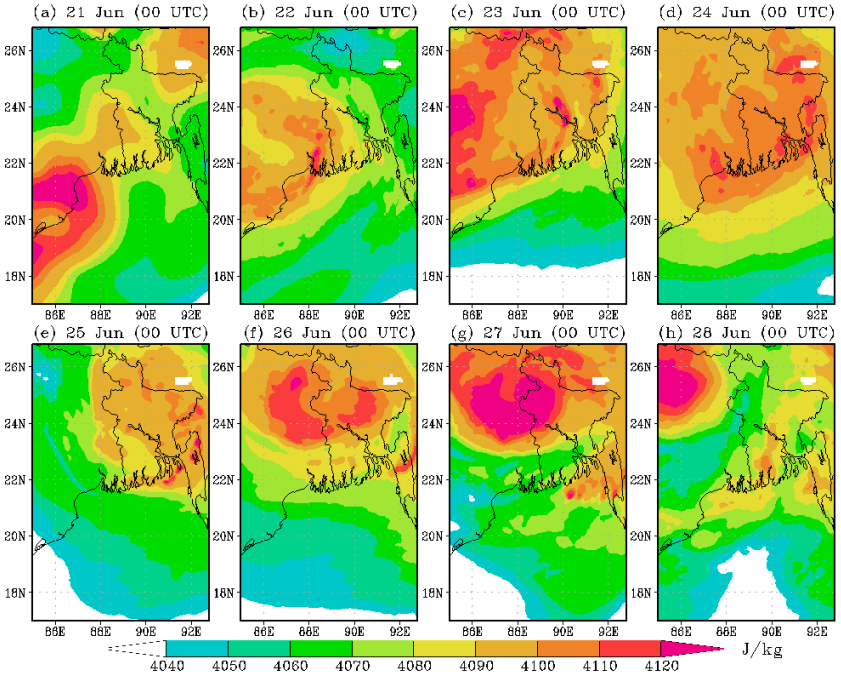

Fig. 14: TSE of 850-300 hPa fields for KFFR at (a) 1200 UTC of 23 June, (b) 0000 UTC of 24 June, (c) 1200 UTC of 24 June, (d) 0000 UTC of 25 June, (e) 1200 UTC of 25 June, (f) 0000 UTC of 26 June, (g) 1200 UTC of 26 June and (h) 0000 UTC of 27 June 2015

3.7 Level of Conditional Instability (LCI)

Analysis indicates that the zone of positive LCI, is the indicator of the conditionally unstable atmosphere, persisted surroundings to the system which moves with the movement of the system. In continuation of this, the zone of positive LCI located over Bangladesh and its adjoining areas during the period of HR. The maximum positive LCI is also found over Bangladesh during the days of HR recorded in Bangladesh (Fig. 15).

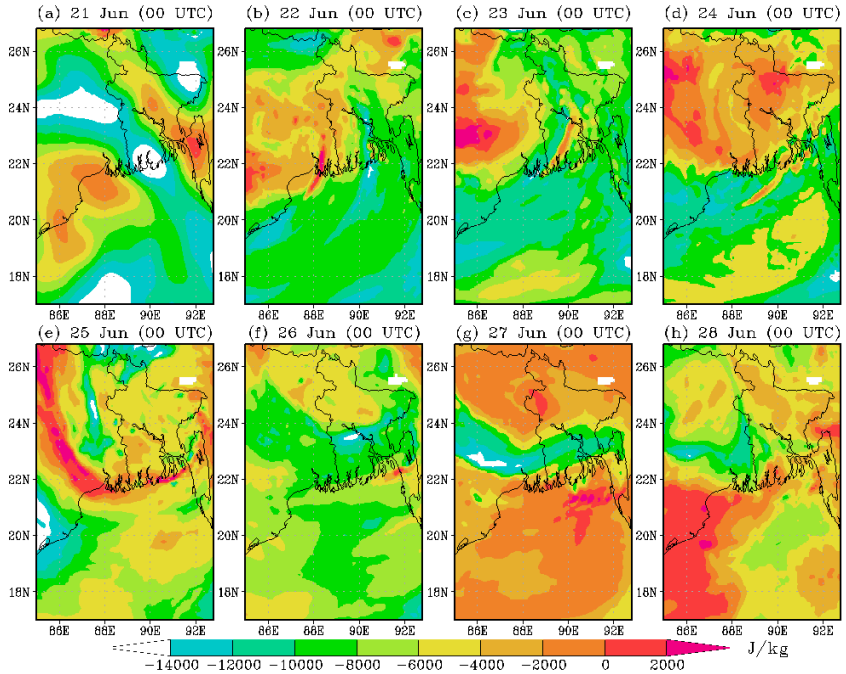

Fig. 15: LCI of 850-400 hPa fields for KFFR at (a) 1200 UTC of 23 June, (b) 0000 UTC of 24 June, (c) 1200 UTC of 24 June, (d) 0000 UTC of 25 June, (e) 1200 UTC of 25 June, (f) 0000 UTC of 26 June, (g) 1200 UTC of 26 June and (h) 0000 UTC of 27 June 2015

3.8 Simulated Rainfall

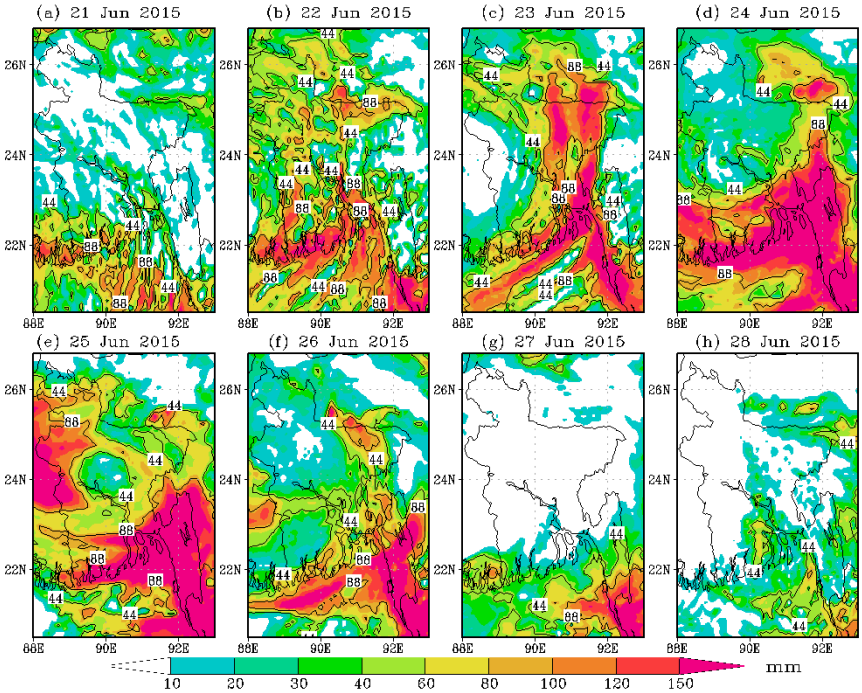

Fig. 16: Model Rainfall for (a) BMJFR, (b) BMJKS, (c) BMJLN, (d) BMJTH, (e) BMJWSM3, (f) BMJWSM5, (g) GDFR, (h) GDKS during 7-8 September 2011

Model simulates isolated Cat-III and Cat-IV rainfalls over extreme southwestern part of Bangladesh and adjoining North Bay of Bengal on 21 June 2015. Simulated Cat-III and Cat-IV rainfall covered more segment of Bangladesh during 22 June. Isolated Cat-V rainfalls are also simulated on this day. Model simulates widespread Cat-IV and Cat-V rainfall over southern part of Bangladesh and adjoining areas and northeastern part of Bangladesh. Cat-IV and Cat-V rainfalls are found over extreme southeastern part of Bangladesh during 27 and 28 June 2015 (Fig. 16).

3.9 Model rainfall validation

Out of eight consecutive HR days, the frequency of simulated Cat-III rainfall are comparable to the observation in four days; higher in one day and lower during the remaining three day. Simulated Cat-IV rainfall frequencies are comparable to the observation in four days, higher in one day and lower in the remaining days. Simulated Cat-V rainfall frequencies are equivalent in two days, lower in two days and higher in the remaining days. Similarly, the simulated station average rainfall (averaged over 35 stations) of BMD are analogous to observed station average rainfall in six days, higher in one day and lower in other day. In addition, simulated maximum rainfalls based on the rainfall of rain gauge locations are higher than observation in most of the days.

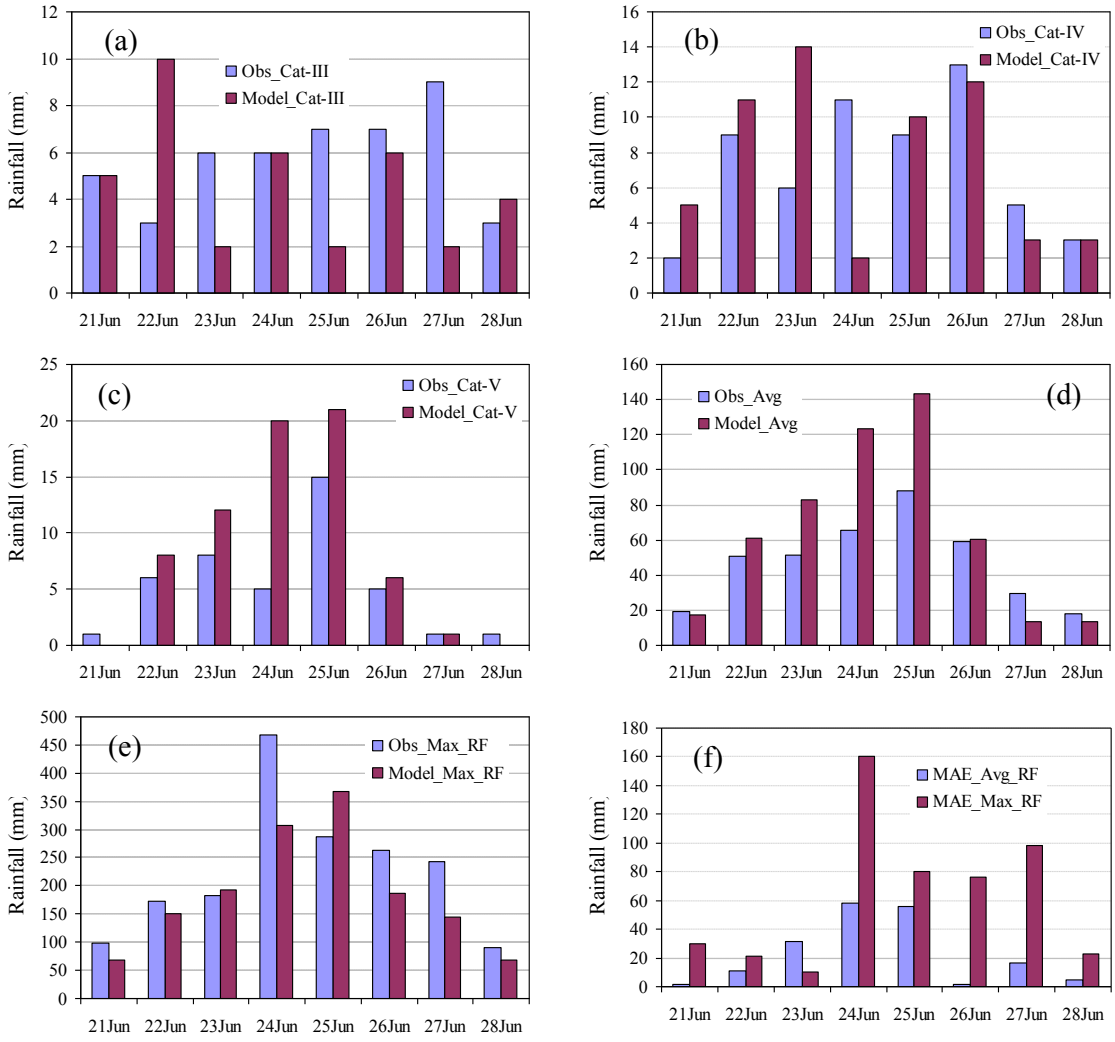

Fig. 17: Comparison of simulated (KFKR) frequency of (a) Cat-III, (b) Cat-IV and (c) Cat-V rainfall with observation; (d) station average and (e) maximum rainfall with observation; (f) MAE for station average and maximum rainfall during 21-28 June 2015

3.10 Prediction skill of the model

Comparison of the frequency of Cat-III simulated rainfall with the 0.25°x0.25° grid observed rainfall reveals that the magnitude of the skill score of PoD was quite high during 21-25 June but it was maximum with 0.42 on

25 June and decreased afterwards. Similar pattern of the score is found for FAR with the maximum of 0.64 on 25 June. The maximum PEC score of 0.41 is found on 27 June which followed by 0.38 on 25 June (Fig. 18a). Similarly, comparison of the frequency of simulated Cat-III rainfall with TRMM rainfall reveals that the magnitude of the skill score of PoD was high during 21-25 June with the maximum magnitude of 0.39 on 25 June and decreased afterwards. Comparison of the frequency of simulated Cat-IV rainfall with the 0.25°x0.25° grid observed rainfall reveals that the magnitude of the skill score of PoD was rather high during 24-27 June with the highest 0.38 on 25 June (Fig. 18b). The score of FAR was higher during 22-26 June but it was the maximum of 0.58 on 25 June (Fig. 18c). The maximum PEC score of 0.34 was on 27 June which is followed by 0.33 on 24 and 28 June. Similarly, the FAR was higher during 24-26 June with the highest of 0.46 on 25 June (Fig. 18d). The skill score of PoD of 0.31 for simulated Cat-IV rainfall evaluating with TRMM rainfall was also highest on 25 June and then on 24 June. Similarly, FAR of 0.37 was the highest on 25 June and then on 24 June. Therefore, it may be conclused that the model performance was relatively satisfactory during the mature and organized stage of the system.

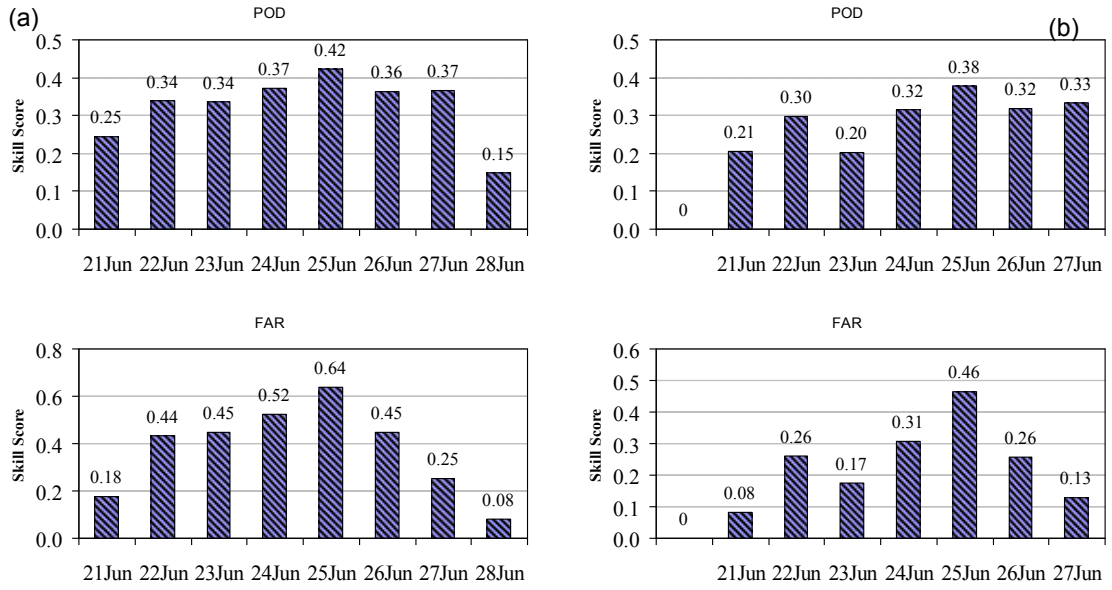

Fig. 18: The prediction skill of PoD for (a) Cat-III and (b) Cat-IV rainfall and FAR for (c) Cat-III and (d) Cat-IV rainfall during 21-28 Jun 2015.

4. CONCLUSION

The following conclusions may be drawn from this study:

i. Model efficiently identifies the genesis, intensity and track of the low pressure system which was positioned over Bangladesh during 23-27 June 2015 and responsible for the occurrence of heavy rainfall

ii. Surface and upper air RH, vertical profile of the area average (coverage area: lat. 20.5-27.0°N and lon. 88.0-93.0°E) RH, vertical profile of RH along 21.0°N specified the presence and advection of sufficient of moisture as required for the event.

iii. Deep moisture flux associated with the system in the lower levels over the southern and southeastern parts of Bangladesh during the days of heavy rainfall may be the source of heavy rainfall.

iv. Presence of quiet strong CAPE at surface level and its spatio-temporal variability is the indicator of short durable high convection over the areas of heavy rainfall.

v. The signature of High TSE within the layer of 850-300 hPa is found associated with the system and it was over Bangladesh and its adjoining areas during the days of HR. In the same way, the signature of the maximum positive LCI is found over Bangladesh. TSE and LCI may therefore be considered as predictors in addition to moisture flux and CAPE.

vi. Model simulates isolated Cat-III, Cat-IV and Cat-V rainfalls over southwestern, southeastern and northeastern parts of Bangladesh during the observed period but the simulated maximum rainfalls based on the rainfall of rain gauge locations are higher than observed rainfall in most of the days.

vii. The frequency of the simulated Cat-III, Cat-IV and Cat-V rainfalls compared with the 0.25°x0.25° grid observed rainfall are quite comparable. Assessment of the frequency of Cat-III rainfall and higher amounts with 0.25°x0.25° grid observed rainfall reveals that the skill score of PoD is found quite high during 21-25 June with the maximum magnitude of 0.42 on 25 June. Similarly, PoD for the frequency of Cat-IV and its higher amounts of rainfall is 0.38 is the maximum highest on 25 June.

References

1. SMRC Report, 2006: Rainfall over SAARC region with special focus on tele-connections and long range forecasting of Bangladesh monsoon rainfall, monsoon forecasting with a limited area numerical weather prediction system, SMRC Report No-19.
2. Mannan, M. A., Chowdhury, M. A. M, Karmakar, S., Ahmed, S. and Mason, S. J., 2015: Rainfall prediction over northeastern part of Bangladesh during monsoon season, Dew-Drop- A Journal of Meteorology and Geo-Physics, Vol 1(1), 14-25, Bangladesh Meteorological Department, Dhaka, Bangladesh.
3. Wahiduzzaman, Md., 2012: ENSO connection with monsoon rainfall over Bangladesh, Int. Journal of Applied Sciences and Engineering Research, Vol. 1, No. 2, 2012, ISSN 2277-9442.
4. Ahasan, M. N., Chowdhury, Md. A. M. & Quadir, D. A., 2010: Variability and Trends of Summer Monsoon Rainfall over Bangladesh, Journal of Hydrology and Meteorology, Vol. 7, No. 1, SOHAM, Nepal.
5. Mannan, M. A., Chowdhury, M. A. M, Karmakar, S., Ahmed, S. and Mason, S. J., 2015: Numerical simulation of heavy rainfall event occurred over Bangladesh using WRF model, The Atmosphere- A Journal of Meteorology and Geo-Physics, Vol 5(1), 47-60, Bangladesh Meteorological Department, Dhaka, Bangladesh.
6. Prasad, K., 2005: Monsoon Forecasting with a limited area numerical weather prediction system, SAARC Meteorological Research Centre (SMRC), Scientific Report No.-11, p. 82.
7. Y. Raj, 2003: Weather systems associated with Indian summer monsoon, Proceedings of Training Seminar on Summer Monsoon and Prediction Techniques, Katmandu, Nepal, 19–40, 2003.
8. Charles, A. D., 1993: Scientific approaches for very short-range forecasting of severe convective storms in the United States of America, In: International Workshop on Observation/Forecasting of Meso-scale Weather and Technology of Reduction of Relevant Disasters pp 181-188.
9. Bohra, A. K., 2006: Swati Basu, E. N. Rajagopal, G. R. Iyengar, M. Das Gupta, R. Ashrit, and B. Athiyaman, Current Science **90** (9), 1188.
10. Litta, A. J., Chakrapani, B. and Mohankumar, K., 2004: Meteorol. Appl. **14**, 291, doi:10.1002/met.31.
11. Das, S., 2002: Mesoscale and cloud resolving scale simulation of a heavy precipitation episode and associated cloud system using MM5 model, INDO-US Workshop on Weather and Climate Modeling, New Delhi, India.
12. Jenamani, R. K., Bhan, S. C. and S. R. Kalsi, 2006: Current Science **90**, 1344.
13. Mannan M. A., Chowdhury, M. A. M, Karmakar, S., Ahmed, S. and Mason, S. J., 2013: Application of NWP Model and its validation in prediction of Heavy Rainfall in Bangladesh, Journal of Engineering Science (JES), Faculty of Civil Engineering, KUET, Khulna, Bangladesh, Vol 4(1), 127-140.
14. Mannan M. A., Chowdhury, M. A. M. and Karmakar, S., 2014: Use of NWP Technique for understanding the characteristics of heavy rainfall over northeastern part of Bangladesh and adjoining areas during pre-monsoon season, The Atmosphere- A Journal of Meteorology and Geo-Physics, Vol 4(1), 41-51, Bangladesh Meteorological Department, Dhaka, Bangladesh.
15. Mannan M. A., Chowdhury M. A. M, Karmakar, S., Ahmed, S. and Mason, S. J., 2015: Variability of Heavy rainfall in Bangladesh and its prediction using NWP Model, Proceedings of the 5th International conference on Water and Flood Management (ICWFM 2015), Institute of Water and Flood Management, BUET, Dhaka, Bangladesh, 493-504.
16. Mannan M. A. and Karmakar, S., 2008: Climatic features of Heavy Rainfall activities in monsoon season and its socio-economic impact in Bangladesh, Proceedings of SAARC Seminar on Application of Weather and Climate Forecasts in the Socio-economic Development and Disaster Mitigation, 5-7 August, 2007, Dhaka, Bangladesh, pp 95-115.
17. Triegaart, D. O., Van Heerden J. And Steyn P. C. L., 1991: Anomalous precipitation and floods during Frebrury 1988, S. Afr. Weath. Bur. Tech. Paper, Vol 23, 25, S. Afr. Weath. Bur., Private Bag X97, Pretoria 0001.
18. Doswell III, C. A., 1996: Verification of forecasts of convection: Uses, abuses, and requirements. Proc. of the 5th Australian Sever Thunderstorm Conference, Avoca Beach, New South Wales, Australia.
19. Aneja, N. and George, T., 2014: Verification of Forecasts from High Resolution Numerical Weather Prediction Model, Research Journal of Applied Sciences, Engineering and Technology, 8(10), pp 1255-1258, ISSN: 2040-7459; e-ISSN: 2040-7467.

20. Doswell, C. A., Davies, -J. R. and Keller, D. L., 1990: On Summary Measures of Skill in Rare Event Forecasting Based on Contingency Tables, Weather Research and Forecasting, 5, pp 576-585 (1990).
21. Murphy, A. H, and R. Winkler, 1987: A general framework for forecast verification. Mon. Wea. Rev., **115**, 1330–1338.
22. Kaufmann, P. Schubiger, F. and Binder, P., 2003: Precipitation Forecasting by a mesoscale numerical Weather prediction (NWP) model: eight years of experience, Hydrology and Earth System Sciences, 7(6), pp 812-832.
23. Wilks, D. S., 1995: Statistical Methods in the Atmospheric Science. Academic Press, San Diego, 467 pp.
24. SMRC Report, 2006: Rainfall over SAARC region with special focus on tele-connections and long range forecasting of Bangladesh monsoon rainfall, monsoon forecasting with a limited area numerical weather prediction system, SMRC Report No-19.
25. Ahasan, M. N., Chowdhury, M. A. and Quadir, D. A., 2008: Few aspects of the flood disaster caused by heavy rainfall over Bangladesh, Proceedings of SAARC Seminar on Application of Weather and Climate Forecasts in the Socio-economic Development and Disaster Mitigation, 05-07 August, 2007, Dhaka, Bangladesh, p. 79-94.
26. Mannan, M. A., Ahasan, M. N. and Alam, M. S., 2014: Study of Severe Thunderstorms over Bangladesh and its surrounding areas during pre-monsoon season of 2013 using WRF-ARW model, Proceedings of the seminar on high impact weather events over SAARC Region, Co-published by Springer, P.O. Box 17, 3300, AA Dordrecht, The Netherlands with Capital Publishing Company, New Delhi, India, 3-20, ISBN: 978-93-81891-12-4

Tropical Cyclone Track Predication Using INSAT-VHRR Data

Md. Abdur Rahman[1], P.C. Joshi[2] and B.M. Rao[2]
[1]*Bangladesh Meteorological Department, Agargaon, Dhaka-1207*
[2]*Satellite Application Centre, Ahmedabad, India.*
Corresponding Author E-mail: rra_rahman@yahoo.com

Abstract: Three hourly INSAT-IR imageries of three cyclones formed in the Bay of Bengal and Arabian Sea (North Indian Ocean) during the period 1992–1999 have been analyzed. The present study was carried out with a view to improve the cyclone track predication in this region. Cloud top temperature (CTT) maps were prepared to know the time and the turning angle of the track of cyclone. It was observed that the rotation in the major structural cloud features as seen from the cloud top temperature maps associated with these cyclones in the North Indian Ocean is followed with a chance in direction of their movement. But this method is effective only when the cyclone is severe and when the major cloud feathers persist for a reasonably longer time. In this study, only the direction of movement is forecast consider a uniform speed of the cyclone.

Key words: CTT, VHRR, BoB.

1. Introduction

Tropical cyclones are intense low-pressure systems in the atmosphere which are conceived over warm Oceans, born among torrential thunderstorms and maintained by the convergence of moisture towards the central regions from far away. Bangladesh is located on the largest delta region in the world with funnel shaped alluvial plain between the Himalayas and the Bay of Bengal. A typical mature cyclone is a warm core vortex in the atmosphere having cyclonic circulation in the lower troposphere and anticyclonic in the upper troposphere. There is an eye - at the centre which is cloud free having very light winds or no wind at all (Fig. 1).A "wall cloud" made up of tall cumulonimbus clouds below which strongest surface winds and heaviest rain intensity of the cyclone are found. Beyond the wall cloud, surface wind speeds decrease gradually with the radial distance from the centre and rainfall is confined to the regions covered by the inward spiraling cloud-bands. Strong winds, heavy rainfall and storm surges associated with the cyclones are the main phenomena which are responsible for causing the damage. The issue of warning about the impeding cyclones in time helps to reduce the loss of lives that the cyclone causes. Several factors like astronomical tide, shallow bay, funneling coastal configuration, low flat terrain, reduces devastating coastal areas bordering the North Bay of Bengal, killing thousands of people over there. Bakergonj cyclone of 1876, Bhola cyclone of 1970 and Chittagong cyclone of 1991 are such examples, each killing lakh of people in Bangladesh. It is observed that the severe cyclone occurs mostly during the pre-monsoon (March – May) and post-monsoon (September –December) period. The most important element is to forecast the future track of the tropical cyclone. Where and when it will cross the coast is also an important factor. Most of the cyclones move westwards, some have West-Northwest and some in Northwest direction, while others initially move in Northwest direction and after then turns towards North and sometime Northeast to East and cross Bangladesh coast or Burma. These are called the re curving cyclones and their track forecasting are somewhat difficult and often involves large error.

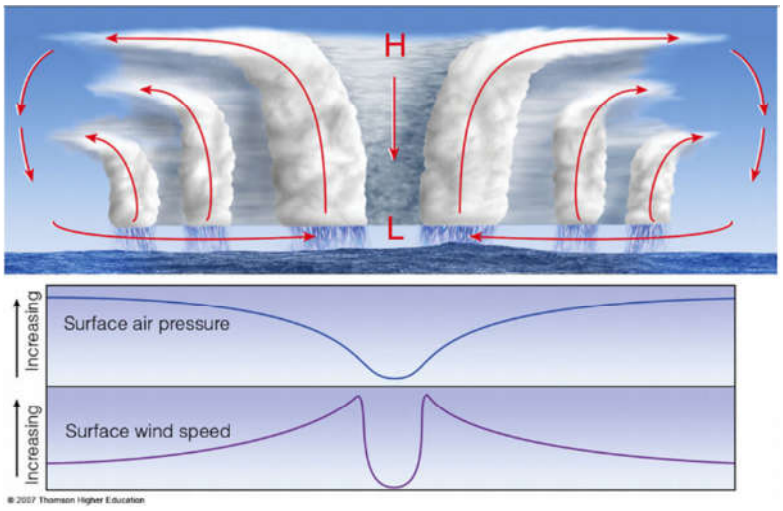

Figure: 1 Structure of Tropical Cyclone

2. Cyclone Track Prediction Techniques

The preparation of tropical cyclone forecast involves an analysis of available observations to determine the behavior of the cyclone followed by an application of various techniques to estimate its future behavior. Track prediction techniques are grouped in two categories, Subjective and deterministic.
The following shows the different track prediction techniques-

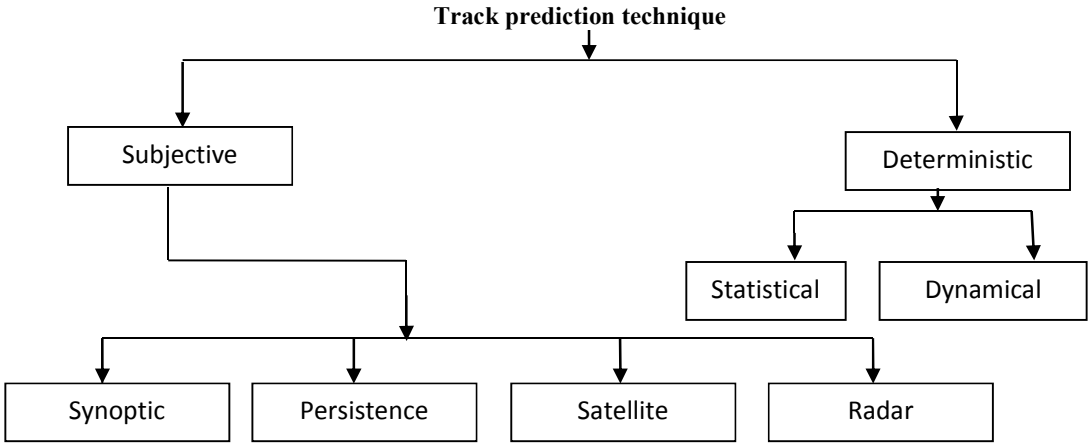

Figure: 2 Different Track prediction techniques

Analysis of aircraft reconnaissance data if available is important. The quality of these analyses has a marked impact on the forecast accuracy, particularly in the short range forecast. Today the forecasting offices are equipped with large number of track prediction techniques. These track prediction techniques are currently used worldwide and are divided into the following categories:

a) Persistence technique
b) Climatological technique
c) Persistence and Climatological techniques
d) Synoptic technique
e) Surface geostropic steering technique
f) Upper air steering technique
g) Satellite technique
h) Dynamical technique

Studies have been made which attempt to relate past change in cloud features associated with tropical cyclones to future change in the direction of movements. Certain assumptions for use of other techniques are necessary to obtain the speed of movement in order to arrive at 12 or 24 hours forecast location. In tropical cyclone analysis, cloud image from geostationary satellite have proved to be more useful than those of polar-orbiting satellites. The geostationary satellite like INSAT enables the analyst to view the tropical cyclone or disturbances over the ocean from the same relative position at successive time, making it easier to follow the storm centre. The movement of the cyclone can generally be inferred from satellite pictures making use of the fact that the cloudiness often extends ahead in the direction of movement of the tropical cyclone [1]. In this studies, INSAT-VHRR infrared imageries have been analyzed and using these images, CTT maps are prepared to know the turning of the cyclone and the result were compared with the actual track of the cyclone.

3. Experimental Set Up, Data Used & Methodology

3.1 Data Used

The three cyclones, formed in the Bay of Bengal (BoB) and Arabian Sea during the period 1992 to 1999 were selected for the present study. The cyclones are –

3i) The Bangladesh Cyclone (November, 1992)
3ii) The Gujarat cyclone (June, 1998)
3iii) The Orissa cyclone (October, 1999)

Data from infrared imageries provided by VHRR onboard INSAT satellite are used. INSAT VHRR measures the radiance emitted by the surface and the clouds in infrared region (10.5–12.5 μm) at 11 kilometer resolution. For each cyclone, three hourly data are used. Figure (5) and (6) shows the Bangladesh cyclone, figure (8) and (9.) represent the Gujarat cyclone while figure (11) and (12) exhibit the Orissa cyclone respectively.

The estimation of cloud top temperature from infrared data is based on the principal that thick clouds and sea surface radiate energy equivalent to the blackbody [2]. The infrared channel data of equivalent blackbody temperature give representations of the structure of clouds and the circulation features surrounding them. For every IR image, a picture print out was prepared by assigning different characters to certain ranges of gray values. Thus a two dimensional map of cloud top temperature for the area covered by the cyclones are obtained. These features are then analyzed for every three hour interval. The tracks of the cyclones available from the Indian Daily Weather Report (IDWR) published by Indian Meteorological Department (IMD) are analyzed to find out the relation between the cloud features and the turning in the future track of the cyclone.

3.2 Experimental Set Up & Methodology

It is true that if we look at two or three hourly intervals of satellite imageries of a tropical cyclone in the intense stage, a distinct similarity in appearance mostly in its features close to the centre is observed. It was known from earlier studies by Fett and Brand that the environmental flow field around a tropical cyclone is an important factor in determining the cyclone motion [3]. If there is a turning in the upper air flow, then the front edge of the central cloud features first reaches the turning point and the features start turning with the wind flow. Depending upon the size of the cloud structure and the speed of its movement, the centre of the cloud system reaches the turning point after a certain period of time and the whole system start turning with the wind flow [4]. This time lag between turning of the features and that of the whole system is shown in figure below.

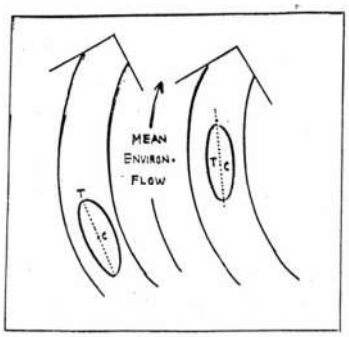

Fig: 3 BASIC CONCEPT

In the above figure, if T if the turning point and C is the centre of the system, then time lag is equal to the time taken by the system to travel the distance CT. If it is true that the major structural features of the tropical cyclones tend to rotate and maintain the same relative position with respect to the moving centre, then a possible way of determining the future direction of motion exists. But the method may not always be successful because of two factors:

a) This method is effective only at the intense stage of the cyclone when the cloud structure similarity is retained for a longer time and
b) The cloud structure turning is caused by the upper level flow is strong enough to change the mean environment flow, then the turning of the track flows the future turning. Therefore, this method can be used as an aid to the tropical cyclone track forecasting in major turning cases.

Analysis is based on observation that in general the matured cyclones as seen in satellite infrared imagery assumes elliptic shape and the front end of the major axis orients in the probable track of the cyclone. In this analysis the Central Dense Overcast (CDO) area of in a cyclone is given important consideration. By looking at the satellite image, the centre of the cyclone can be located. A cloud top temperature map is prepared wherein temperature in the major cloud features is designated with corresponding characters. Each character in the map represents certain temperature ranges in the CDO area of the cyclone. Using these CTT maps from IR data the intensification or weakening features in association with the locations of the convective zone in the CDO area of the cyclone can be determined.

4. Results and Discussions

4.1 The Bangladesh cyclone (November, 1992)

Remnants of Typhoon “Forrest” emerged in the Andaman Sea and concentrated into a depression at 1200 UTC of 15 November. Moving in a Westerly direction it intensified into cyclonic storm on 17th morning. Then moving in Northwesterly direction it intensified into a severe cyclonic storm with a core of hurricane intensity. Winds of 230 km/h and a pressure of 952 hPa were observed at the pick hour. It moved further Northwards up to 19th midday and then re-curved towards Northeast and crossed the Bangladesh- Myanmar coast in the afternoon as a cyclonic storm and weakened rapidly into a depression [5].Only two deaths took place in the country and overall damage was light.

For this cyclone, three hourly images from INSAT are available .As the cyclone was intense between 19 and 20 of November, cloud top temperature (CTT) maps of these days show similar structure of high clouds. The thermal map of 18 November 1200 UTC shows the orientation (fig-5) of the high cloud area represented by the sign ‘’.” surrounded by the letters ‘’Z” and ‘’Y” which represents the cloud with temperature less than 229°k. From the thermal map of 19 November in 15 UTC, it was found that the orientation of the structure rotated clockwise by 28°, indicating that the cloud structure started rotating at the same time between 1200 UTC and 1500 UTC of the same day.

On 1200 UTC of 19 November, the centre of the cyclone was located at latitude 17.6°N and longitude 88.0° E. During this time the cyclone moved roughly with a speed of 11 km/h. From the CTT map it is seen that the size of the CDO is about 200 km. Therefore, to travel half this distance, that is the distance CT will take about 10 hours. Thus the track of the cyclone is turning sometime between 0900 UTC to 1900 UTC of 19 November. From the thermal map of 1200 UTC of 20 November (fig) it is observed that the re-curvature of the cyclone is about 32°. Landfall time of the cyclone was evening of 21 November. If the speed of the cyclone is considered the same as the previous day then it will reach the land after 50 hours from 19 November 1200 UTC at 22.0°N and 92.3° E but actually it reached 21.0° N and 92.6° E. In this case, according to persistence the location of the landfall would be at 22.3°N and 89.7°E. The persistence error should be about 300 km. The basic cause of this error is due to the sharp turning of the cyclone. Analyzing the satellite infrared imageries through thermal maps, this error could be reduced prominently. So, this method is more effective when the turning is more and more [6].

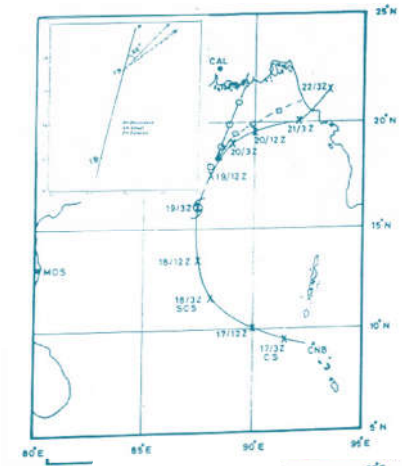

Figure: 4

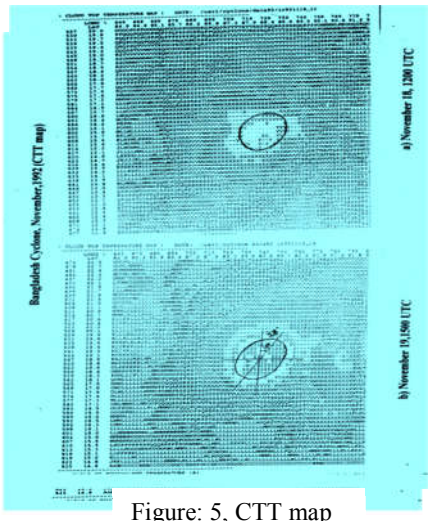

Figure: 5. CTT map

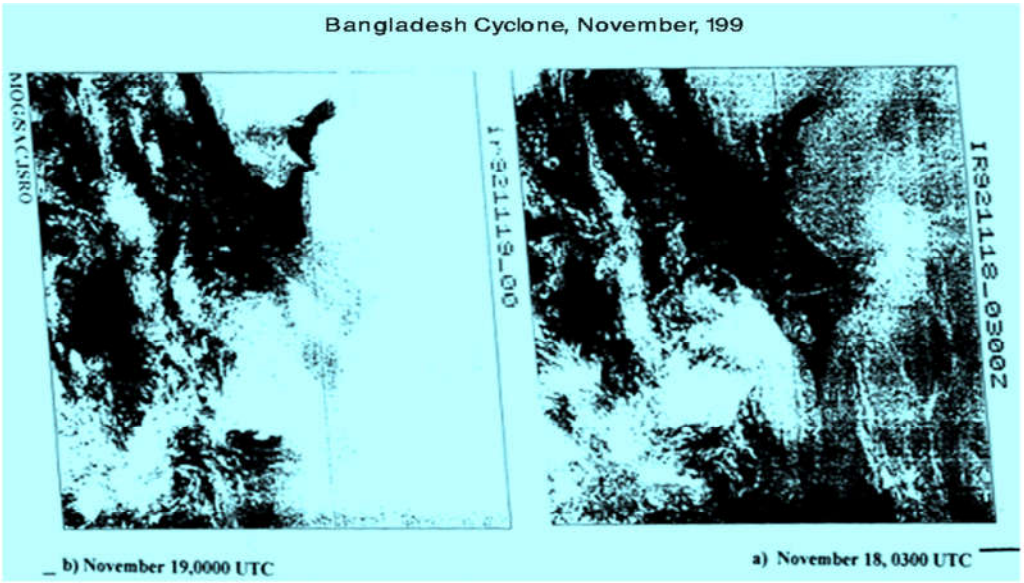

Figure: 6

4.2 The Gujarat Cyclone (June, 1998)

A low pressure area has formed over Southeast Andaman Sea and adjoining Lakshadweep on the evening of 2 June and became well marked on 4 June. It concentrated into a depression at 0900 UTC of the same day and further intensified into a deep depression at 1200 UTC. It further intensified into a cyclonic storm in the evening of 5 June and moved in a North-Northwesterly direction and at 0300 UTC of 6 , It was about 560 km Southwest of Goa. It further intensified into a severe cyclonic storm at 0900 UTC of 6 June and at 1200 UTC of

6 it lay near 13.0°N and 69.0°E and moved in a North-Northwesterly direction. On 7 June at 0300 UTC its location was 14.5°N and 68.0°E about 650 km West-Southwest of Goa.

It further intensified into a very cyclonic storm and lay at 1200 Z of 7 June near 16.0°N and 68.0°E. At 0300 Z of 8 June, it lay near 18.0°N and 68.0°E about 400 km Southwest of Veraval. Then it moved in a North - Northwesterly direction and crossed Gujarat coast near Porbandar of 9 June morning and lay as a very severe cyclonic storm about 50 km NNE of Porabandar of 9 morning. It moved in a NNE'ly and weakened into a depression and lay at 0300Z of 10 June near 26.5°N and 73.5°E about 50 km Northeast of Jodhpur. It further weakened into a low-pressure area over Punjab and adjoining parts of Himachal Pradesh [7]. The track of the cyclone is shown in figure 7.

\

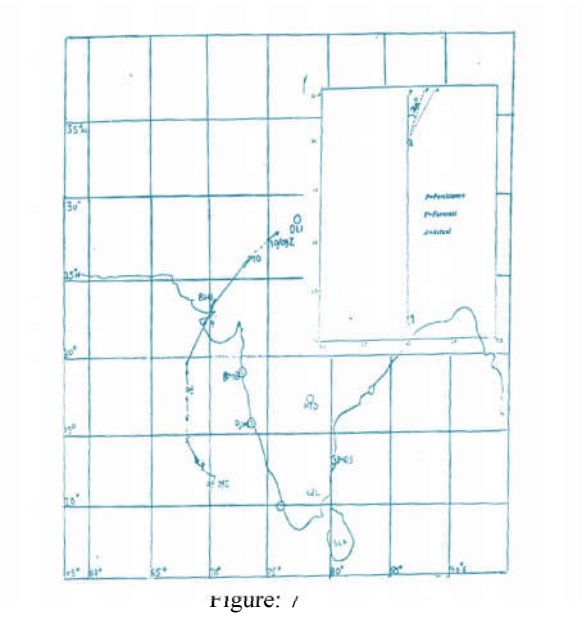

Figure: 7

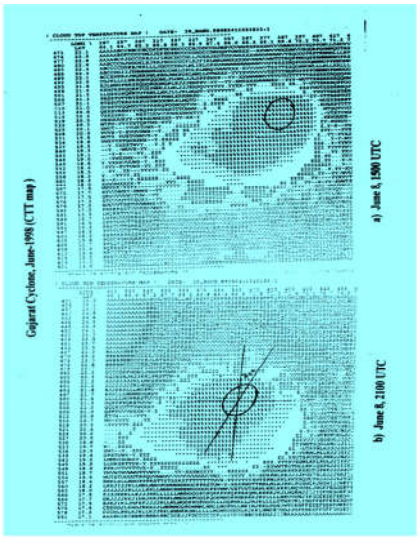

Figure: 8

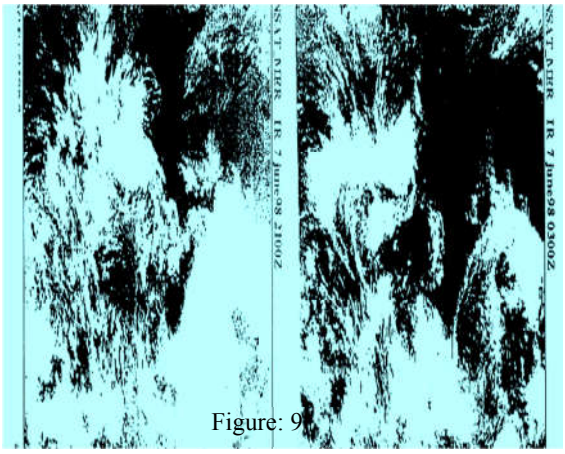

Figure: 9

For this cyclone, three hourly imageries from INSAT are available. From 6 June, cloud top temperature maps are analyzed but there was no significant turning observed in the cyclone until 8 June 1800 UTC. At 2100 UTC of 8 June, the cyclone changed its track from Northerly to Northeasterly direction and it was then in its most intense stage. It turned into clockwise direction by an angle 20°. At this stage, the cloud organization was more significant. From CTT map it was found that the high cloud above the level of 204°K started turning in clockwise direction by an angle of about 20° at 2100UTC of 8 June. On 7 June 2100 UTC the position of the cyclone was at 16.4°N and 68.0°E and after 24 hours it reached at 19.9°N and 68.0°E. By this time, the cyclone moved roughly with a speed of about 16 km/h. From CTT map, the size of the Central Dense Overcast (CDO) was about 330km.

According to persistence, the cyclone will reach the coast at 23.9°N and 68.0°E and considering its uniform speed, the landfall time can also be calculated. From satellite imageries through thermal maps, if one forecast the cyclone track, then the landfall l position would be at 22.8°N and 69.2°E. In this case the persistence forecast error would be 132 km and forecast through thermal imageries, this error should be reduced to about 88 km. A large error for persistence forecast was observed due to the re-curvature of the cyclone. In this case, forecast by satellite imageries showed a good correlation with the actual track of the cyclone.

4.3 The Orissa Super Cyclone (October, 1999)

A well marked low formed over GULF of Siam and neighborhood on 25th October. It moved on a North Northwesterly direction and rapidly intensified into a cyclonic storm lay centered at 0300 UTC of 26 October at 13.5°N and 95.0°E about 350 km Northeast of Port Blair. It further moved in Northwesterly direction and was centered at 1200 UTC of 26 October near 14.4°N and 94.0°E. Again it moved in a Northwesterly direction and intensified into a severe cyclonic storm and was centered at 0300 UTC of 27 October near 16.0°N and 92.0°E about 750 km Southeast of Paradeep. Further moving in a Northwesterly direction it reached at 17.0°N and 90.0°E at 1200 UTC of 27 October. Moving in the same direction further, it attained the intensity of very severe supper cyclonic storm concentrated at 0300 UTC of 28 October at latitude 18.0°N and longitude 89.0°E. At 0300 UTC of 29 October its location was at 19.9°N and 86.7°E about 20 km East of Paradeep. At 1200 UTC of 29, it was very close of Bangladesh. It moved in a Northeasterly direction and rapidly weakened into a

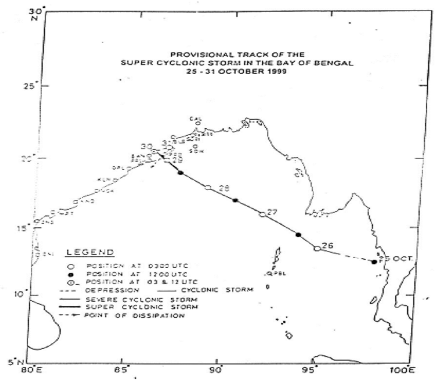

Fig.10: Track of Orissa super Cyclone, October 1999

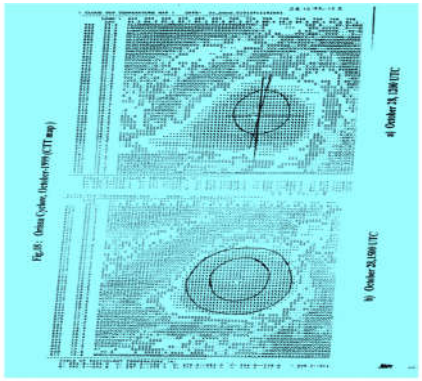

Fig.11: CTT map of Orissa super Cyclone at 1200 Z, 28 October 1999

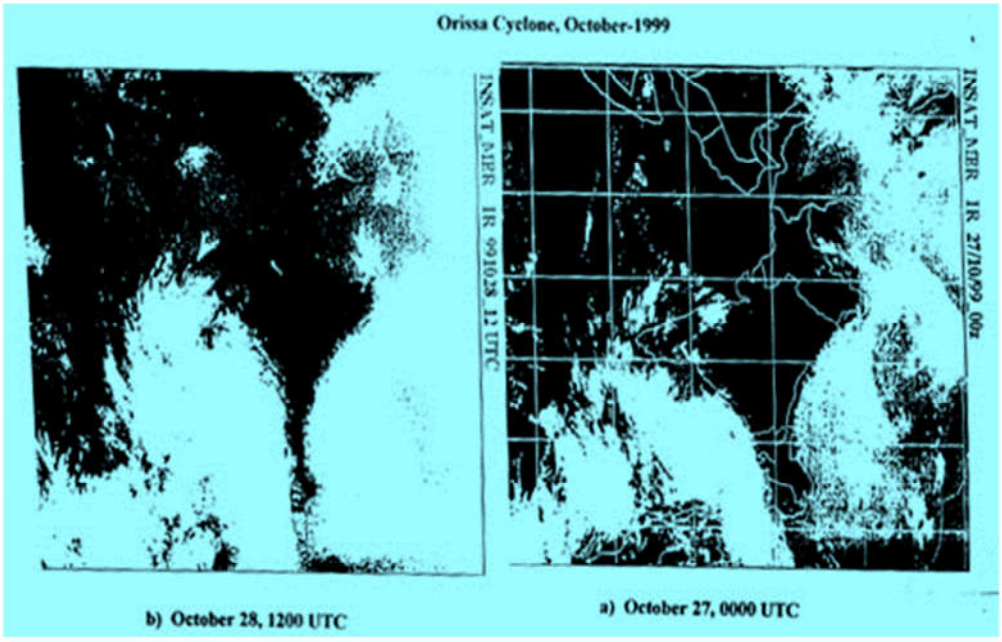

Figure:12

depression. It was the most intense tropical cyclone in the history of Orissa for last 114 years.

It was a straight moving cyclone. This cyclone gained a super cyclonic intensity on 28 November and it was in its most intense stage on that day. CTT maps were observed from 27. But there was no turning in the cloud features. For this cyclone, three hourly observations are also taken. From 27, 0300 UTC to 28 October, similar orientation of high cloud was observed. At 1200 UTC of 28 October, there was a slight clockwise turn in the track which was insignificant.

On 27 October 0300 UTC, the centre of the cyclone was 16.0°N and 92.0°E. After 24 hours, it reached at 18.0°N and 89.0°E. By this time, the cyclone moved roughly with a speed of about 9 km/h. As no prominent turning was observed up to 0300 UTC of 28 October, so it was presumed that the cyclone will move straight. In reality, it crossed the coast very close to Paradeep without changing its track.

4. Conclusions

In this paper, an attempt has been made to study the features of cloud structure observed in the cloud top temperature map derived from satellite imageries. INSAT infrared data for three cyclones formed in the Bay of Bengal and Arabian Sea during the period 1992–1999 have been analyzed. Out of these three cyclones, two were re-curving and one was straight moving in which no turning in the cloud features was observed. For 1992 cyclone, the turning is sharper than that of 1998 cyclone. Both the cyclones turned in clockwise direction. Cloud top temperature analysis is useful in predicting future cyclone track and reduced the forecast error when the cyclone is re-curve, especially, when the central cloud features has a major turning. The limitation of this method is that it is effective only when the cyclone is in its intense stage. In both the turning cases, a good correlation between the actual track and the forecast (given by using satellite imageries through CTT maps) was observed. For making this method operational, more re-curving cyclones in the North Indian Ocean approaching Bangladesh would have to be analyzed.

Acknowledgement

First of all I would like to thank the Director of CSSTE-AP and the Director of BMD for giving me opportunity to attend the course.

References

1. Rao, Bhaskar D.V, 1997: Tropical Cyclone simulation with Emanule's convective scheme. Mausam 4, pp114.
2. Narayanan, M.S. and B. M. Rao, 1981. Cloud top temperature structural charges during the life cycle of Saurashtra cyclone (1978). Mausam, 32: 1.
3. Fett, R. W., Brand, S., 1975. Tropical cyclone movement forecasts based on observations from satellites. J. of Appl. Meteorol, 14(4), 452-465.
4. P.K. Pal, B.M.Rao, C.M. Kishtawl, M.S.Narayanan G. Rajkumar, 1989: Cyclone Track Prediction using INSAT data., proc. Indian Acad. sci. 1998, pp 353-364.
5. All Indian Daily Weather Report, November 15-18, 1992
6. Cyclones and Depressions over the Indian Seas and neighborhood during 1992: Mausam 1999,pp 224
7. Cyclones and Depressions over the Indian Oceans During 1998, Mausam, July 1999.

SIMULATION OF THE STRUCTURE AND TRACK OF THE TROPICAL CYCLONE RASHMI USING NUMERICAL MODELS

Md. A. E. Akhter[1,2]*, Md. M Alam[1] and M. A. K. Mallik[3,4]

[1]*Department of Physics, Khulna University of Engineering & Technology, Bangladesh*
[2]*SAARC Meteorological Research Centre, Bangladesh*
[3]*Bangladesh Meteorological Department, Bangladesh*
[4]*Department of Physics* Physics, Jahangirnagar University, Savar, Dhaka Bangladesh
[*]*E-mail: afraabida@hotmail.com*

Abstract: Tropical cyclone (TC), one of the most devastating and deadly weather phenomena, is a result of organized intense convective activities over warm tropical oceans. In the recent years, mesoscale models are extensively used for simulation of genesis, intensification and movement of tropical cyclones. During 24-27 October 2008, a cyclonic Storm named, Rashmi was active in the Bay of Bengal part of the Indian Ocean. At 2100 UTC on 26 October 2008, the system started to cross Khulna-Barisal coast of Bangladesh near Patharghata and completed crossing the coast by 0300 UTC of 27 October 2008. The cyclonic storm crossed Bangladesh coast near 89.50E (about 50 km west of Khepupara). In the present study, two state-of-the-art mesoscale models, MM5 and WRF, have been used to simulation the structure and track of TC Rashmi. Horizontal resolution of 90 km and 30 km respectively for mother and nested domain were used in both the models. Various meteorological fields' viz. central pressure, winds, vorticity, temperature anomaly etc obtained from the simulations are verified against those observed to test their performance. The simulated tracks are also compared with that obtained from JTWC. The results indicate that WRF model has better forecast skill in terms of intensity and track prediction.

KEYWORDS: Tropical cyclone, Mesoscale models, Intensity, structure and Track.

1. INTRODUCTION

The Bay of Bengal tropical cyclone disaster is the deadliest natural hazard in the Indian sub-continent. It has a significant socio-economic impact on the countries bordering the Bay of Bengal, especially India, Bangladesh and Myanmar. Therefore, it is very important to predict these cyclones with high accuracy to save the valuable lives and wealth. Recently, there have been considerable improvements in the field of weather prediction by numerical models. The Pennsylvania State University (PSU)/National Center for Atmospheric Research (NCAR) mesoscale model MM5 has been used in a number of studies for the simulation of tropical cyclones [1]. Mohanty et al. [2] used MM5 model to simulate the Orissa super cyclone (1999). Again, WRF model has also been used in a number of studies for the simulation of tropical cyclones [3, 4]. There are a number of comparative studies on the performance of the mesoscale models for severe weather events triggered by convection. Sousounis et al. [5] made a comparative study on the performance of WRF, MM5, RUC and ETA models for heavy precipitation event and suggested that WRF model has the capability to generate physically realistic fine-scale structure which is not seen in the standard output resolution of other operational forecast models. Forecast skill of WRF model has been found better in the comparison study between WRF and ETA on the surface sensible weather forecast over Western United States [6]. On the other hand, better forecast skill of MM5 model has been demonstrated in the comparative study on the performance of MM5 and RAMS models in simulating the Bay of Bengal cyclone [7]. Again, Pattanayak et al. [8] made a comparative study on the performance of MM5 and WRF models in simulating of tropical cyclones over Indian seas. The intensity of the tropical cyclones Mala, Gunu and Sidr in terms of MSLP and maximum sustainable wind illustrates that MM5 simulates the intensity of the system fairly, whereas WRF gives reasonably good results, similar to the observations.

In the present study, MM5 version 3.7 and WRF-ARW version 3.1 are used to simulate the structure and track of TC Rashmi formed over Bay of Bengal. The performances of the models have been evaluated and compared with observations and verifying analyses. A brief description of the mesoscale models along with the numerical experiments and data used for the present study are given in section II. The synoptic situation for the above mentioned cyclone used in the present study is described in section III. The results are presented in section IV in order to evaluate the performance of the models and the conclusions are in section V.

2. MODEL DESCRIPTION AND METHODOLOGY

MM5 has been widely used for simulation/prediction of severe weather events such as tropical cyclones, heavy rainfall, thunderstorms etc. MM5 is a nonhydrostatic mesoscale model with pressure perturbation p´ three velocity components (u, v, w), temperature T and specific humidity q as the prognostic variables. Model equations in the terrain following sigma co-ordinate are used in surface flux form and solved on Arakawa B grid. Leapfrog time integration scheme with time splitting technique is used in model integration. With a number of sensitivity tests, it has demonstrated that the combination of Kain–Fritisch cumulus parameterization scheme with MRF PBL, in general, provides better result for simulation of tropical cyclones [9]. Table 1 summarizes the model configuration and various options used by MM5 in the present study.

The WRF-ARW modeling system developed by the Mesoscale and Microscale Meteorology (MMM) Division of NCAR is designed to be a flexible, state-of-the-art atmospheric simulation system which is suitable for a broad range of applications such as idealized simulations, parameterization research, data assimilation research, real-time NWP etc. Model equations are in the mass-based terrain following coordinate system and solved on Arakawa-C grid. Runge-Kutta 2nd and 3rd order time integration technique is used for model integration. The new generation of the MRF PBL scheme is introduced here as Yonsei University (YSU) PBL. It has an explicit representation of entrainment at the PBL top, which is derived [10] from large eddy simulation. Table 1 summarizes the model configuration and various options used by WRF-ARW in the present study are partly chosen from the study carried out by Pattanayak et al. [8].

Table 1 Brief description of the MM5 and WRF models

parameters	Used for MM5 V 3.7 model	Used for WRF version 3.1 model
Dynamics	Non-hydrostatic with 3-D Coriolis force	Non-hydrostatic with 3-D Coriolis force
Mother Domain	0.22°S - 37.94°N, 67.36°E-108.64°E	1.58°S–38.94°N, 66.10°E-110.02°E
Inner Domain	5.36°N -28.71°N, 81.66°E - 99.20°E	4.19°N -28.50°N, 81.25°E - 99.17°E
Resolution	90 and 30 km	90 and 30 km
Map projection	Mercator	Mercator
No of vertical levels	28	28
Horizontal grid scheme	Arakawa B grid	Arakawa C grid
Time integration scheme	Leap-frog scheme with time splitting technique	Runge-Kutta 2nd & 3rd order time splitting technique
Radiation scheme	Dudhia's shortwave/longwave simple cloud	Dudhia's shortwave /RRTM longwave
PBL scheme	MRF	YSU
Cumulus parameterization scheme	Kain Fritsch	Kain Fritsch
Microphysics	Simple ice	Ferrier

To analyze the intensity, structure and track of TC Sidr, the MM5 and WRF models were run for 96 hrs with the initial field at 13 November 2007and the models simulated data were compared with those obtained from Joint Typhoon Warning Centre (JTWC). The National Center for Environmental Prediction (NCEP) FNL reanalysis data (1° X 1° horizontal resolution) are used to provide the initial and lateral boundary conditions respectively to all the models.

3. System Description

Synoptic situation of TC Rashmi (24-27 October 2008)

A low formed over west central Bay and adjoining area on 24 October 2008 and intensified into a well-marked low over the same area at 0000 UTC of 25 October 2008. At 0600 UTC of the same day the system concentrated into a depression over the same area (positioned near lat. 16.5°N and long. 86.5°E) and started to move in a northerly direction initially. At 0300 UTC of 26 October the system intensified into a deep depression over northwest Bay and adjoining west central Bay. After that the system changed its direction of movement and moved north-northeastwards and concentrated into a cyclonic storm 'Rashmi' at 1200 UTC of the

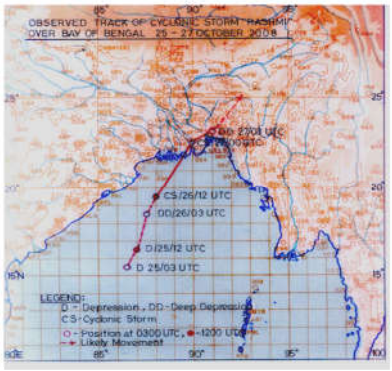

Figure 1. Track of the cyclone 'Rashmi' during 24-27 October 2008.

same day over northwest Bay and adjoining area (near lat. 20.2°N and long. 88.2°E).

By moving rapidly towards the same direction the system started to cross Khulna-Barisal coast of Bangladesh near Patharghata at 2100 UTC of the same day and completed crossing the coast by 0300 UTC of 27 October and lay over south-central part of the country as a land depression. Then the system moved towards the same direction further and became unimportant by giving precipitation. The track of the cyclone 'Rashmi' is given in Figure 1. Under its influence heavy rainfall with high winds were recorded over most parts of Bangladesh. The recorded maximum winds were at Hatiya, Patuakhali, Mongla, Barisal 45 kts (83 km/hr) each, Khulna and Dhaka 35 kts (64 km/hr) each, Bhola and Jessore 30 kts (56 km/hr) each. No causalities were reported.

4. Results and Discussion

To analyze the evolution and structure of TC Sidr, the MM5 and WRF model was run for 96 hrs with the initial field at 00 UTC of 24 October 2008. Different meteorological parameters obtained from both the models are discussed for the evolution and structure of the TC Rashmi in the following sub-section. Model simulated results are compared with available data obtained from Joint Typhoon Warning Centre (JTWC). Models output are taken for 3 hourly intervals and plotted by Grid Analysis and Display System (GrADS) software.

A Pressure Field

Figure 2a shows the comparative evolution of observed MSLP and simulated MSLP of MM5 and WRF models of TC Rashmi. It appears from the Figure 2a that MM5 model simulated and observed MSLP gradually drops with time and coincides with each other at 18 UTC of 24 October and 06 UTC of 25 October (i.e. 18 and 30 hours of simulation respectively). After that simulated MSLP decreases and finally reached the peak intensity with lowest pressure of 976 hPa just before landfall making an oscillation with higher MSLP 992 hPa and thereafter MSLP increases. The Model simulated MSLP of 976 hPa is obtained at 15 UTC of 26 October where as the observed MSLP of 989 hPa is obtained at 18 UTC of 26 October 2008.

Again, the WRF model simulated and observed MSLP gradually drops with time and attains peak intensity just before the landfall and thereafter MSLP increases. The Model simulated MSLP of 979 hPa is obtained at 03 UTC of 27 October whereas the observed MSLP 989 hPa is obtained at 18 UTC of 26 October 2008. The model simulated MSLP at the centre of the cyclone after 09 hours from the observed MSLP. It is noted that landfall occurs faster for MM5 model than that for WRF model. The variation of MM5 and WRF models simulated MSLP compared to that of observed with time shows that both the models simulated realistic temporal variation of MSLP.

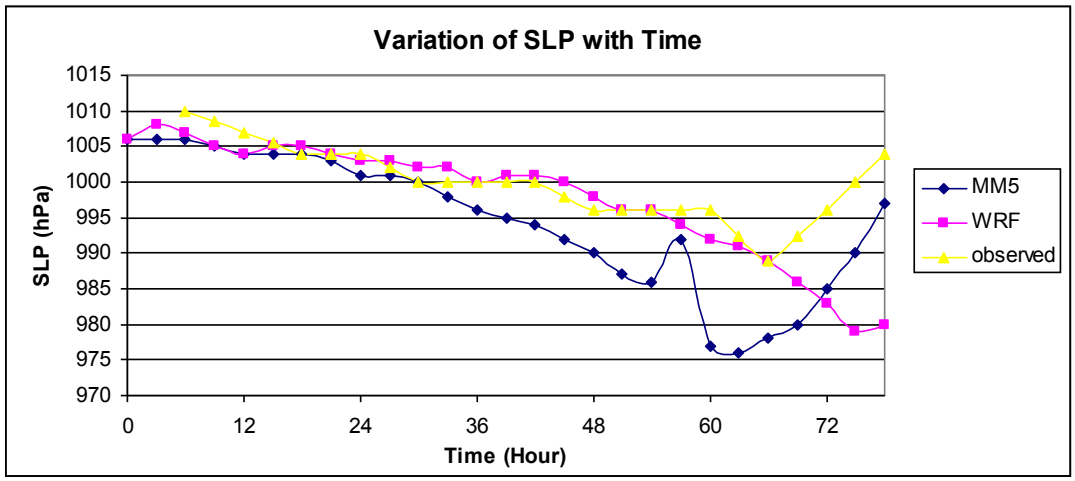

Figure 2a: Evolution of MM5 and WRF models simulated minimum central pressure and observed minimum central pressure of the eye of the TC Rashmi with time.

The distributions of SLP for the TC Rashmi obtained from MM5 model at 00 UTC on 24, 25, 26 October and at 15 UTC on 26 October 2008 (i.e. its mature stage) and obtained from WRF model at 00 UTC on 24, 25, 26 October and at 03 UTC on 27 October 2008 (i.e. its mature stage) are shown in Figures 2b and 2c respectively. The figure demonstrates that the intensity of the TC increases as the MSLP drops with time up to its peak intensity and TC changes it position with time. The isobar has circular arrangement around the TC centre with some asymmetric features in the outer periphery. The contour interval is different for different positions because of different intensity of the system.

At mature stages the contour interval is 2.5 or 3 hPa for both the models. The lowest simulated MSLP of 976 hPa and 979 hPa for MM5 and WRF models respectively are obtained at 15 UTC on 26 October 2008 and at 03 UTC on 27 October 2008 whereas the observed lowest MSLP of 989 hPa is obtained at 18 UTC on 26 October 2008. According to MM5 model, at mature stage (at 15 UTC on 26 October 2008), considering the outermost closed isobar, the system's horizontal size is estimated as 7.5° in the east-west direction and 9.0° in the north-south demonstrating a little bit spatial asymmetry in its horizontal structure. Again, according to WRF model, at mature stage, considering the outermost closed isobar, the system's horizontal size is estimated as 7.5° in the east-west direction and 6.0° in the north-south demonstrating a little bit spatial asymmetry in its horizontal structure.

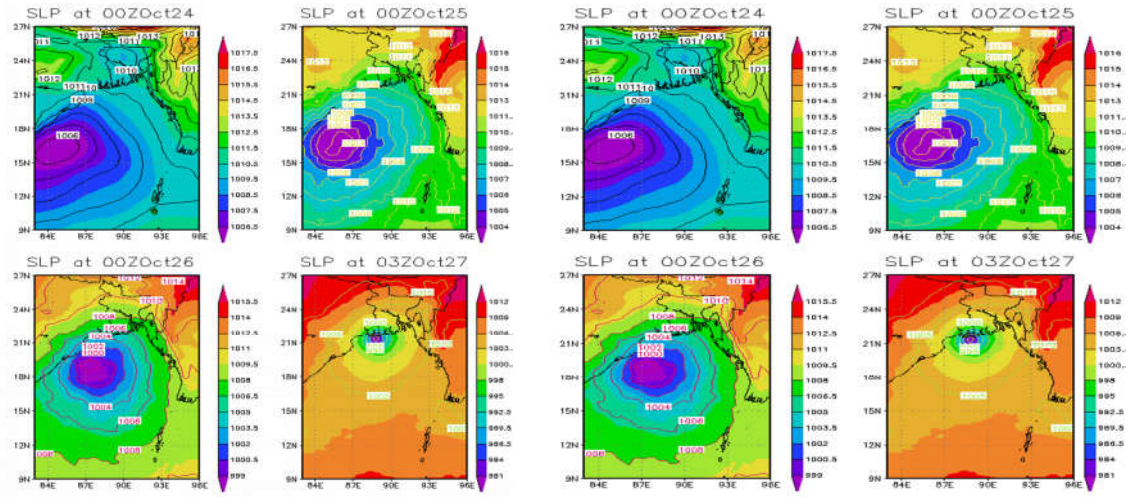

Figure 2: (b) MM5 and (c) WRF Models simulated SLP of TC Rashmi

The distribution of the sea level pressure of the TC Rashmi along east-west cross section passing through its centre (21.894°N and 90.607°E) for MM5 model and passing through its centre (21.357°N and 89.856°E) for WRF model are shown in Figure 2d and 2e respectively. The figures demonstrate the moderate pressure gradient around the centre with maximum gradient at around 80-90 km from the centre for MM5 and WRF models. Thus the radius of the TC eye is found to be below 90 km both for MM5 and WRF model according to the simulation.

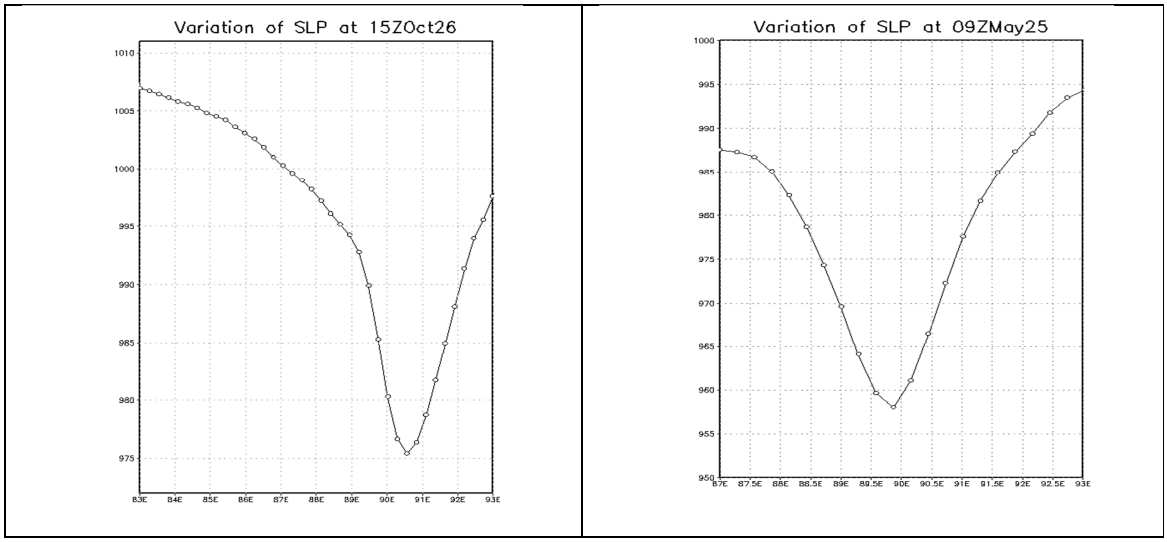

Figure 2d: East West cross sectional view of simulated SLP of TC Rashmi obtained from (d) MM5 and (e) WRF models through the centre.

B Wind Field

Figure 3a shows the temporal variations of MM5 and WRF models simulated MWS and observed winds of TC Rashmi. The model simulated MWS are obtained at the standard meteorological height of 10 m. The MM5 and WRF Models simulated MWSs are higher than the observed values through almost full forecast hours without any exception. The simulated highest MWS are obtained at 15 UTC on 26 October and at 03 UTC on 27

October whereas that for observed MWS is obtained at 18 UTC on 26 October 2008. After that both the simulated winds by MM5 and WRF and observed winds decrease with time gradually.

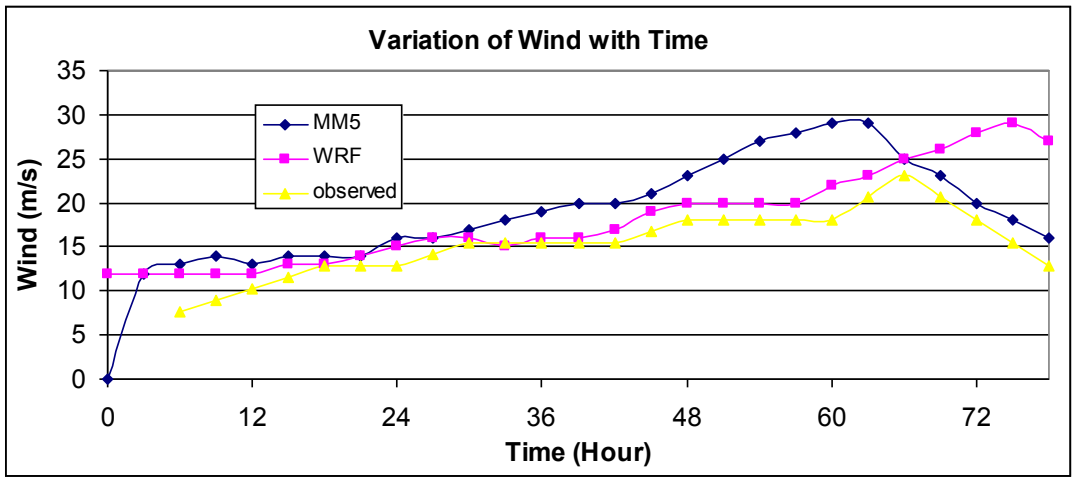

Figure 3a: Observed and MM5 and WRF Models simulated wind speed (m/s) with time of TC Rashmi.

The distribution of surface (10 m) wind of Rashmi at 00 UTC of 24, 25, 26 October and at 15 UTC on 26 October 2008 (i.e. its mature stage) for MM5 model and at 00 UTC on 24, 25, 26 October and at 03 UTC on 27 October 2008 (i.e. its mature stage) for WRF model are shown in Figures 3b and 3c respectively. The Figure 3b obtained from MM5 model shows that the wind field of the TC is highly asymmetric in the horizontal direction. At 00 UTC on 24 October 2008 (i.e. at the initial time of simulation) the TC is in the sea. The value of the wind is zero. At 00 UTC of 25 October 2008 (i.e. 24 hours of simulation), the figure shows that the pattern has an asymmetric wind distribution with strong wind bands in the front right side, rear left and front left sides far to the centre of northward moving storm. The wind flow in the core region shows a near circular feature with minimum wind speed at the centre. Similar pattern is also seen at 00 UTC on 26 October 2008 with strong wind bands at the front right side, rear and rear left sides. In this stage, TC is organized with strong wind bands around the wind flow and core region shows asymmetric feature with minimum wind speed at the centre. At 15 UTC on 26 October 2008 (i.e. at mature stage), a strong wind bands (wind speed > 27 m/s) having strongest wind exceeding 29 m/s is found around the system centre with elongation in north-south direction. It may be noted that the model has generated slight higher winds of 29m/s (56 knot) than the observed winds of around 45 knot.

Again, the Figure 3c obtained from WRF model shows that the wind field of the TC is highly asymmetric in the horizontal distribution. At 00 UTC of 24 October 2008 (i.e. at the initial time of simulation) the TC is in the sea. The figure shows that the pattern has an asymmetric wind distribution with strong wind bands in the front right side, rear left and rear right sides close to the centre of north directed moving storm. The wind flow in the core region shows a near circular feature with minimum wind speed at the centre. Similar pattern is also seen at 00 UTC of 25 October 2008 with strong wind bands at the front right side and rear and rear left sides. At 00 UTC of 26 October 2008, TC is organized with strong wind bands around and the wind flow in the core region shows asymmetric feature with minimum wind speed at the centre. At 03 UTC of 27 October 2008 (i.e. at mature stage), a strong wind bands (wind speed >27m/s) having strongest wind exceeding 29 m/s is found around the centre with elongation in east-west direction. It may be noted that the model has generated slightly higher winds of 29m/s (56 knot) than the observed winds of around 45 knot. It is also noted that, due to friction of landmass, Figures 3b and 3c show the landfall feature of surface wind distribution where the winds is much less in the front side compared to others of the cyclonic system.

Figures 3d and 3e show the distribution of the surface wind of the TC Rashmi obtained from MM5 model along east-west cross section passing through its centre (21.894°N and 90.6074°E) at 15 UTC on 26 October 2008 and obtained from WRF model along east-west cross section passing through its centre (21.894°N and 90.6074°E) at 03 UTC on27 October 2008. The figures demonstrate that a calm region is found inside the eye of the system and maximum wind was found in the eye wall. The radius of maximum wind of the TC Rashmi is found to be just lower than 100 km according to the simulation.

The horizontal distribution of vector wind field obtained from MM5 model at levels 850, 500, 300 and 200 hPa at time 15 UTC on 26 October 2008 (i.e. its mature stage) and field obtained from WRF model at levels 850, 500, 300 and 200 hPa at 03 UTC on 27 October 2008 (i.e. its mature stage) are shown in the Figures 3f and 3g.

MM5 and WRF Model derived maximum winds are tabulated in the Table 2. A well organized TC circulation with strong winds encircling the centre is found at the 850 and 500 hPa levels. It is noted that the strong wind is confined to the right of the direction of the movement of the system. At 300 hPa wind shows cyclonic circulation in the right side of the TC and weak outflow in the left side. At 200 hPa level strong outflow is evident from the central part of the TC. So, using simulated results obtained from MM5 and WRF models, Figures 3f and 3g demonstrate inflow in the lower level and outflow in the upper level.

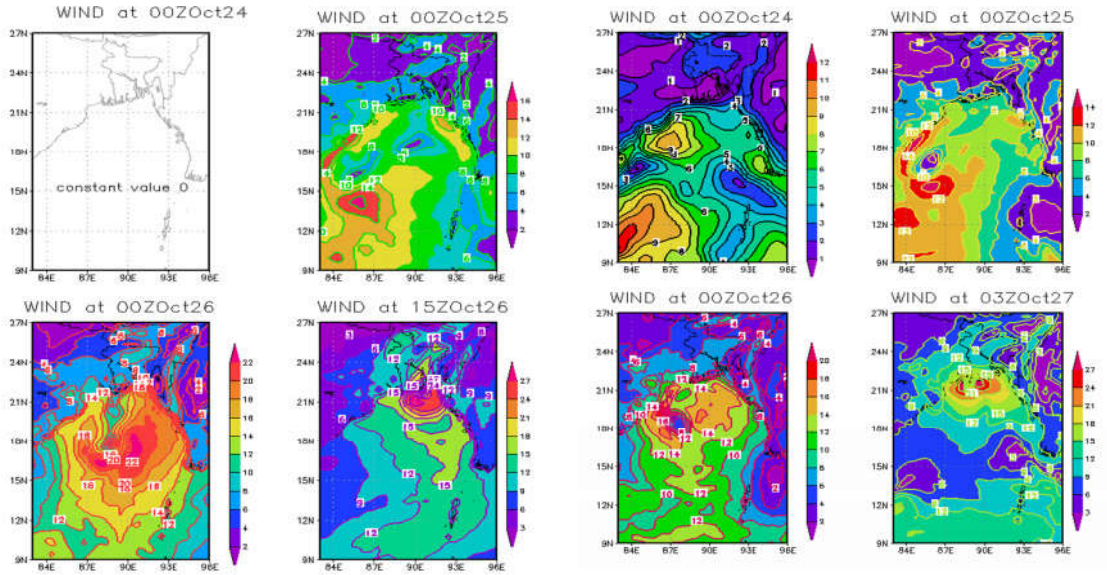

Figure 3: (b) MM5 and (c) WRF Model simulated Wind speed (m/s) of TC Rashmi at 10 m

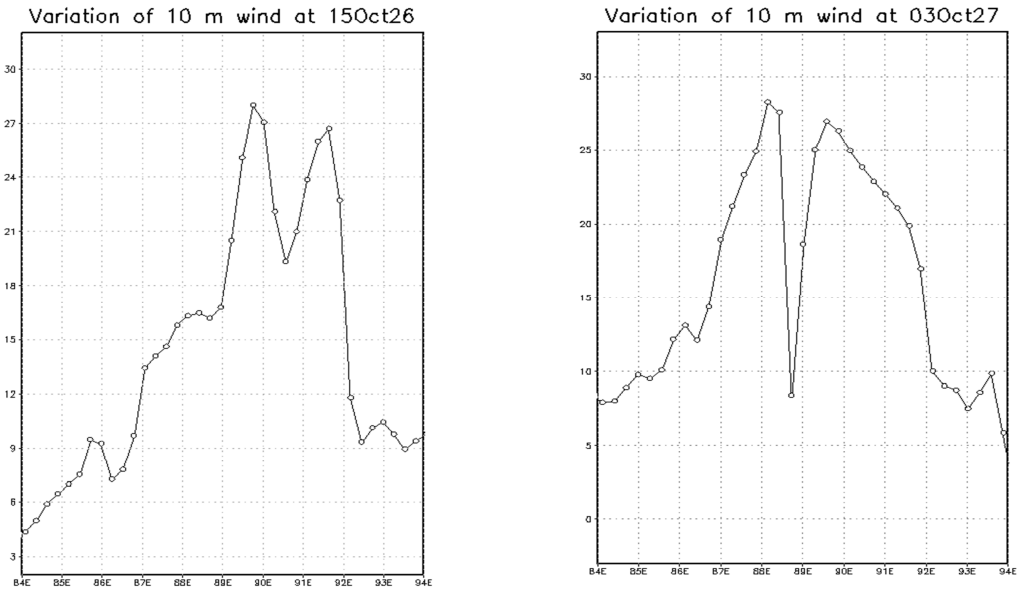

Figure 3d: East-West cross sectional view of (d) MM5 and (e) WRF models simulated wind speed (m/s) of TC Rashmi along its centres

MM5 model derived maximum winds at the mature stage (15 UTC on 26 October 2008) are about 50, 60, 50 and 50 m/s at 850, 500, 300 and 200 hPa levels respectively. Again WRF model simulated maximum winds at the mature stage (03 UTC on 27 October 2008) are about 50, 40, 40 and 40 m/s at 850, 500, 300 and 200 hPa levels respectively. So, at mature stage maximum wind (at different levels) obtained from MM5 model is higher

than or equal to those obtained from WRF model and the mature stage obtained by MM5 model is earlier than that obtained by WRF model.

Table 2: MM5 and WRF Model simulated wind speed (m/s) at different pressure levels of TC Rashmi

model	Pressure level	Wind Speed (m/s) at				
		00 UTC on 24 October	00 UTC on 25 October	00 UTC on 26 October	15 UTC on 26 October	03 UTC on 27 October
MM5	850	10	20	40	50	
	500	20	20	30	60	
	300	40	40	40	50	
	200	50	50	60	50	
WRF	850	10	20	30		50
	500	20	20	20		40
	300	50	40	50		40
	200	50	40	50		40

Figures 3h and i show the vertical profile of radial, tangential, vertical and horizontal winds of TC Rashmi obtained from MM5 model at 15 UTC of 26 October 2008 (i.e. its mature stage) and obtained from WRF model at 03 UTC of 27 October 2008 (i.e. its mature stage) respectively. Results are also given in Table 3 respectively for the models MM5 and WRF for different times mentioned in the Tables. From the tables it is clear that the value of the vertical profile of radial, tangential, vertical and horizontal wind of TC Rashmi obtained from MM5 and WRF models increases with the process of time.

From the figure it is found that vertical profile of radial wind is much more organized and it is also clearly seen that the system has strong inflow in the lower levels which bring the air to the system through the boundary level and lower level and outflow in the upper level. The maximum values of the radial component of wind at mature stage obtained from MM5 are higher than that obtained from WRF model (Tables 3).

The tangential wind flows in a northerly direction at the eastern side of the system and in a southerly direction at the western side. The strong wind with different speeds (Table 3) is confined to the different levels in lower troposphere and extended up to 200 hPa level for MM5 and up to 100 for WRF model in the right and left side of the system. The value of the tangential wind in the eastern side is higher than that of western side.

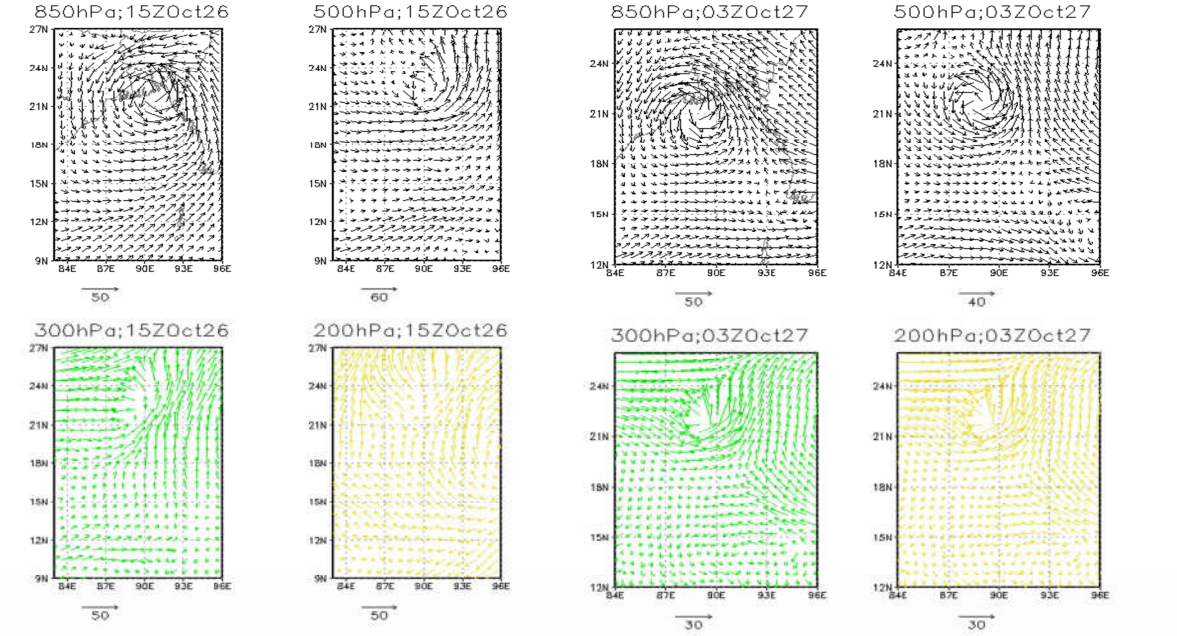

Figure 3: (f) MM5 and (g) WRF Models simulated wind vector at levels 850, 500, 300 and 200 hPa at 15 UTC on 26 October 2008.

The values of the vertical motion are different in magnitude for different times and it reveals that strong upward motion of about 120 cm/s for MM5 model exists along the eye wall (at 15 UTC on 26 October 2008) and other

parts of the system which feed moisture into the system. Again, this value is 650 cm/s for WRF model at 03 UTC on 27 October 2008. It is noted that Rashmi has very weak updraft motion within 110 cm/s around at the eye wall in the west throughout mid and upper troposphere. The downward motion is visible in the central parts of the TC and other areas in between rain bands.

The vertical profile of horizontal wind of the system at its mature stage shows the distribution of strong winds up to 200 hPa and 100 hPa for MM5 and WRF models respectively around the centre of TC. It further confirms that the maximum winds are confined to the right of the direction of the movement of the system. This value decreases with the radial distance from both side of the eye. Calm wind zone is sharp and narrow and little bit tilted to the westward and get expanded towards upper levels. This is in agreement with the previous studies of [11] TC Orissa. Cyclonic circulation is generally seen up to about 300 hPa level and anticyclonic circulation with divergence fields aloft. In case of TC Rashmi, cyclonic circulation is also seen up to about 350, 300 hPa level for MM5 and WRF model respectively and anticyclonic circulation with divergence fields aloft.

Table 3: MM5 and WRF model simulated radial wind, tangential wind, vertical velocity and horizontal wind (cm/s) of TC Rashmi

model	Component of wind	Simulated wind speed (cm/s) at				
		00 UTC on 24 October	00 UTC on 25 October	00 UTC on 26 October	15 UTC on 26 October	03 UTC on 27 October
MM5	Radial wind	400	600	1200	2500	
	Tangential wind	800	15	3000	4000	
	Vertical velocity	7	30	70	120	
	Horizontal wind	1000	1000	3000	4000	
WRF	Radial wind	400	600	1200		2000
	Tangential wind	600	1200	2000		3000
	Vertical velocity	0.10	45	650		120
	Horizontal wind	1000	1000	3000		4000

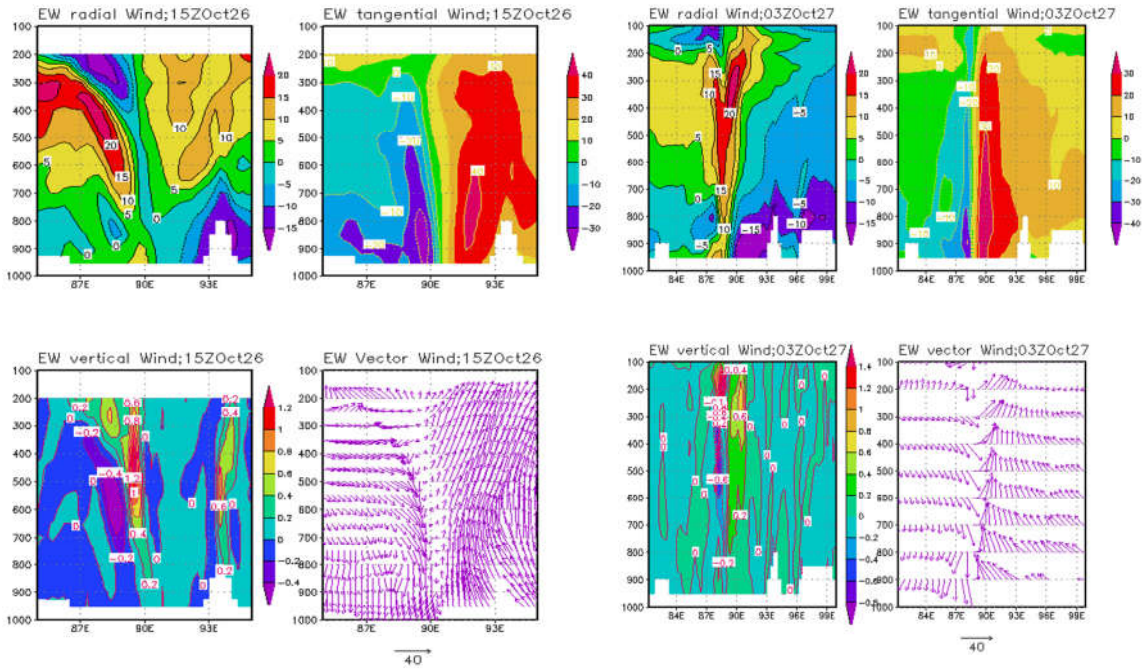

Figure 3: (h) MM5 and (i) WRF models simulated east-west cross section of vertical structure of radial wind, tangential wind, vertical velocity and horizontal wind (cm/s) of TC Rashmi along the centre

C Vorticity Field

To know the evolution, the MM5and WRF model simulated relative vorticity at 850 hPa as a function of time is shown in Figure 4a. From the figure it is observed for MM5 model that there is a gradually rise in the vorticity

value in the first 63 hours of integration of the model. Thereafter the value shows a fall. Again, it is observed for WRF model that there is a gradually rise of vorticity in the first 48 hours of simulation of the model and sustains the maximum value for 9 hours duration (48 -54 hours of forecast). Thereafter the value shows a decreasing tendency and again increases up to 72 hours of simulation. Simulated vorticity obtained from WRF model is higher that obtained from MM5 model.

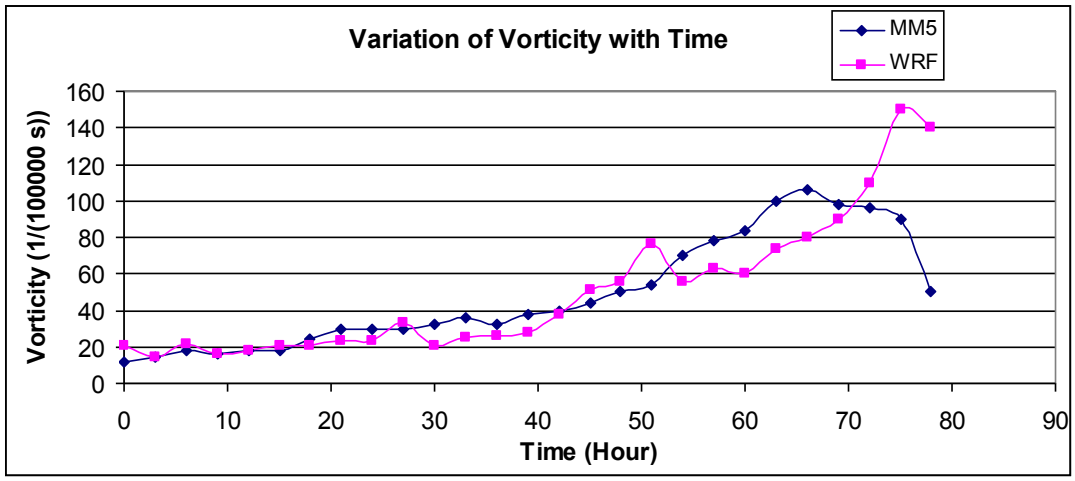

Figure 4a: Evolution of model simulated vorticity with time of TC Rashmi

The horizontal distribution of the relative vorticity obtained from MM5 at 15 UTC of 26 October 2008 (i.e. its mature stage) of TC Rashmi for 850, 500, 300 and 200 hPa levels and obtained from WRF at 03 UTC of 27 October 2008 (i.e. its mature stage) of TC Rashmi for 850, 500, 300 and 200 hPa levels are shown in the Figures 4b and 4c respectively.

It is seen from the figures that the vorticity is distributed with maximum value at the centre and these values for the levels 850, 500, 300 and 200 hPa are tabulated in Table 4 for MM5 and WRF models respectively. The values of relative vorticity are increased with the increase of time (i.e. in the development of the TC) at all levels. At 850 hPa, the distribution maintains circular pattern with some asymmetric features in the outer periphery. Negative vorticity field are situated far from the centre. This distance of the negative vorticity from the centre is increased due to development of TC (not shown). Low level relative vorticity fields confirm the strong cyclonic circulation at low levels with different time and distance in feeding the moisture into the system to sustain its intensity. At 500 and 300 hPa levels, the distribution of relative vorticity also shows a symmetric character in the horizontal distribution. The values of relative vorticity are increased with the development of TC. At 200 hPa level, the weak positive vorticity embedded with negative vorticity field is visible at 200 hPa level. Negative vorticity is found at the centre of the TC.

Table 4: MM5 and WRF Models simulated maximum vorticity ($x10^{-5}$ s^{-1}) of TC Rashmi

model	Pressure levels	Vorticity ($x10^{-5}$ s^{-1}) at				
		00 UTC on 24 October	00 UTC on 25 October	00 UTC on 26 October	15 UTC on 26 October	03 UTC on 27 October
MM5	850	12	20	50	90	
	500	10	18	35	60	
	300	6	12	25	35	
	100	2	12	10	20	
WRF	850	20	20	50		140
	500	40	20	60		90
	300	6	15	40		80
	200	15	12	35		70

It is clear from the figure that relative vorticity is more organized in the mature stage and the value of vorticity in this stage obtained from WRF model is higher than the value obtained from MM5 model.

Table 4b: MM5 and WRF Models simulated Vertical distribution of vrticity ($x10^{-5}$ s^{-1}) of TC Rashmi

model		Vorticity ($x10^{-5}$ s^{-1}) at				
		00 UTC on 24 October	00 UTC on 25 October	00 UTC on 26 October	15 UTC on 26 October	03 UTC on 27 October
MM5	Position of TC centre	16.080°N, 84.677°E	15.979°N, 85.677°E	17.731°N, 88.892°E	21.894°N, 90.607°E	
	Vertical distribution		24	40	90	
WRF	Position of TC centre	16.084°N, 84.719°E	116.799°N, 85.895°E	18.972°N, 87.293°E		21.331°N, 88.754°E
	Vertical distribution	10	20	50		140

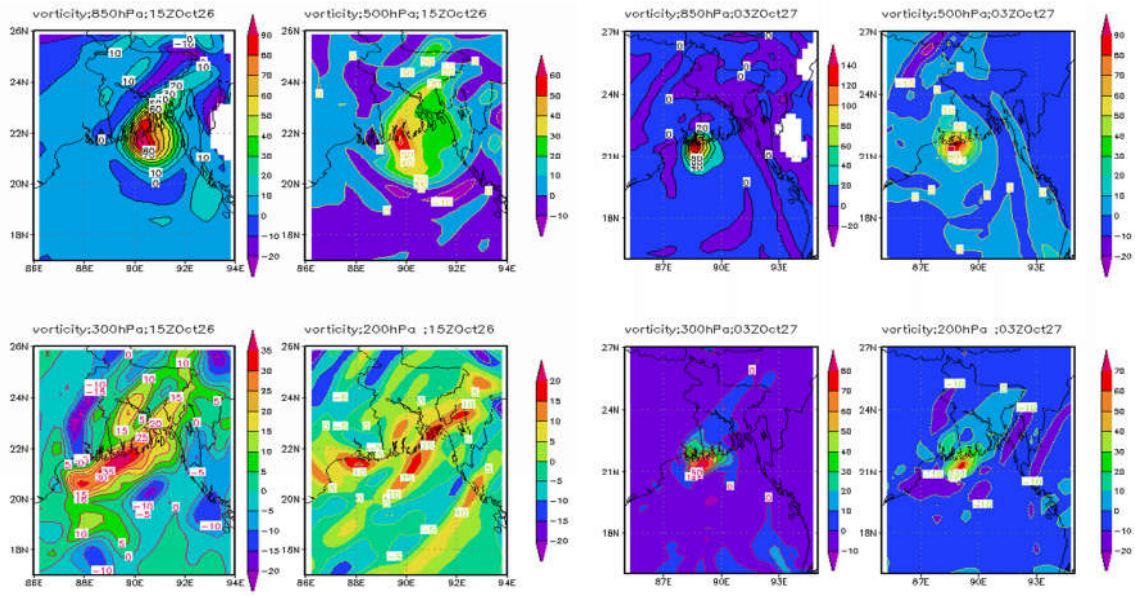

Figure 4: (b) MM5 and (c) WRF Model simulated vorticity field associated with TC Rashmi at 850, 500, 300 and 200 hPa levels

Vertical distribution of the relative vorticity obtained from MM5 model along the centre in the east-west direction is shown in Figure 4d and the values at different pressure levels are tabulated in Table 4b. Similarly, vertical distribution of the relative vorticity obtained from WRF model along the centre in the east-west direction is shown in Figure 4e and the values at different pressure levels are tabulated in Table 4b.

According to the MM5 simulated results at 00 UTC on 24 October 2008 (i.e. the initial time), the positive vorticity is spread over a horizontal distance with strong vorticity at slightly westward of the centre (16.080^{o}N 84.677°E). This pattern of distribution extends from surface to around 150 hPa level with the exception that the magnitude of the vorticity decreases with height. Similar pattern with higher positive value of vorticity is found at the centre after 24 hours of simulation at 00 UTC on 25 October 2008 along the centre (15.979°N and 85.677°E). At 00 UTC on 26 October 2008 the system has the positive vorticity along the centre up to 200 hPa level with higher value (17.731°N and 88.892°E). At 15 UTC on 26 October 2008 the system has the highest value of positive vorticity along the centre (21.894°N and 90.607°E) up to 200 hPa with low magnitude.

According to the MM5 simulated results at 00 UTC on 24 October 2008 (i.e. the initial time), the positive vorticity is spread over a horizontal distance with strong vorticity at slightly western side of the centre (16.084°N and 84.719°E). This pattern of distribution extends from surface to around 150 hPa level with the exception that the magnitude of the vorticity decreases with height. Similar pattern with higher positive values of vorticity is found at the centre after 24 hours of simulation at 00 UTC on 25 October 2008 along the centre (16.799°N and 85.895°E). At 00 UTC on 26 October 2008, the system has the positive vorticity along the centre (19.847°N and 89.634°E) up to 200 hPa level with higher value. At 03 UTC on 27 October 2008, the system has the highest value of positive vorticity along the centre (21.357°N 89.856°E) up to 100 hPa with low magnitude.

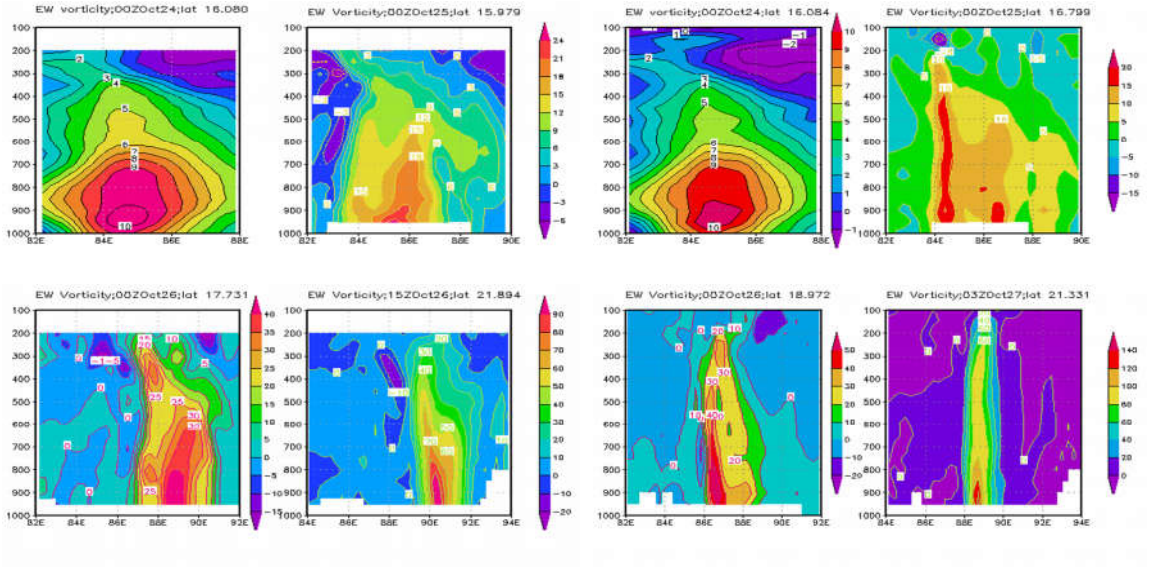

Figure 4: (d) MM5 and (e) WRF Models simulated vertical distribution of relative vorticity field in the east-west cross section of TC Rashmi

D Temperature Anomaly

The MM5 model simulated temperature anomaly at 00 UTC of 24, 25, 26 October and 15 UTC of 26 October 2008 (i.e. its mature stage) of TC Rashmi from surface to 200 hPa levels is shown in Figure 5a and the values at different pressure levels are tabulated in Table 5.

At 00 UTC of 24 October 2008, maximum temperature is 6^{o}C at around 450 hPa level. It is noted that the warm core region is largely expanded outward at 700-400 hPa level. The simulated temperature anomaly demonstrates that the warm core is visible mainly at upper troposphere. Negative temperature anomalies are also simulated at the upper and lower levels.

At 00 UTC of 25 October 2008, warm core is observed between 900-350 hPa level. It is noted that the warm core region is expanded outward at 900-350 hPa level. The highest 7^{o}C temperature anomaly is simulated around 450 hPa level at the western side of the cyclone centre. The simulated temperature anomaly demonstrates that the warm core is visible mainly at upper troposphere. Negative temperature is also observed at the upper levels.

At 00 UTC of 26 October 2008, warm core is observed at 950-200 hPa layer. It is noted that the warm core region is expanded outward at 750-250 hPa level. The greatest anomaly of 9°C is found at around 450 hPa level in the western side of the eye of the cyclone. The simulated temperature anomaly demonstrates that the warm core is visible mainly in the upper troposphere. Negative temperature anomalies at lower levels are due to contamination by heavy precipitation.

At 15 UTC of 26 October 2008, warm core is observed in 950-150 hPa layer. It is noted that the warm core region is expanded outward at 700-300 hPa level. The greatest anomaly of 9°C is simulated at around 550-650 hPa level. The simulated temperature anomaly demonstrates that the warm core is visible mainly in the upper troposphere. Negative temperature anomalies at lower levels are due to contamination by heavy precipitation. Maximum value of temperature anomaly obtained from WRF model is higher than that obtained from MM5 model.

Table 5: MM5 and WRF Model simulated temperature anomaly (°C) associated with TC Rashmi

model	Temperature anomaly (°C) at				
	00 UTC on 24 October	00 UTC on 25 October	00 UTC on 26 October	15 UTC on 26 October	03 UTC of 27 October
MM5	6	7	9	9	
WRF	9	8	12		9

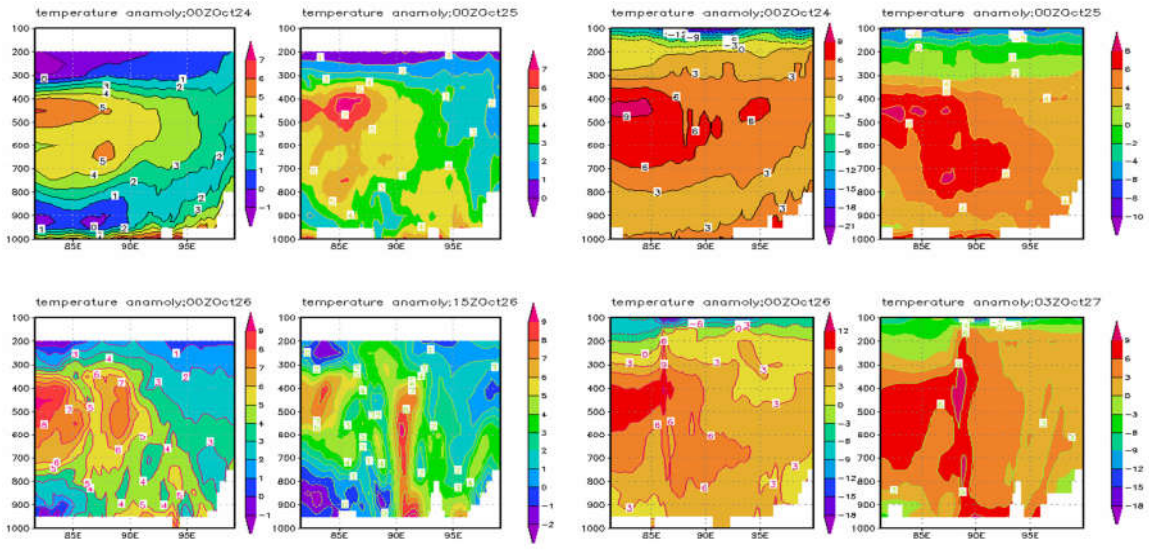

Figure 5: (a) MM5 and (b) WRF models simulated vertical distribution of temperature anomaly in the east-west direction of TC Rashmi through the centre.

Again, the WRF model simulated temperature anomaly associated with TC Rashmi at 00 UTC on 24, 25, 26 October and at 03 UTC on 27 October 2008 (i.e. its mature stage) from surface to 100 hPa level is shown in Figure 5b and the values are tabulated in Table 5. At 00 UTC on 24 October 2008, warm core with 9^{o}C is observed in 800-250 hPa layer. It is noted that the warm core region is slightly expanded outward at 800-300 hPa level. The greatest anomaly is occurred around 450 hPa level. The simulated temperature anomaly demonstrates that the warm core is visible mainly at upper troposphere. Negative temperature anomalies are also seen at the upper levels.

At 00 UTC on 25 October 2008, warm core with 8°C is observed in 850-300 hPa layer. It is noted that the warm core region is expanded outward at 700-300 hPa level. The greatest anomaly is observed around 450 hPa level. The simulated temperature anomaly demonstrates that the warm core is visible mainly at upper troposphere. At 00 UTC on 26 October 2008, a warm core with 12°C is observed in 950-150 hPa layer. It is noted that the warm core region is expanded outward at 750-250 hPa level. The greatest anomaly is observed around 500 hPa level. The simulated temperature anomaly demonstrates that the warm core is visible mainly at upper troposphere.
At 03 UTC on 27 October 2008, a warm core with 9°C is observed in 950-150 hPa layer. It is noted that the warm core region is expanded outward at 700-300 hPa level. The greatest anomaly is observed around 500 hPa level. The simulated temperature anomaly demonstrates that the warm core is visible mainly at upper troposphere.

At first the water vapour moves in the upward direction and transformed into liquid water and ice particle. The water vapour losses heat in the environment due to the transformation of liquid water and ice particle and then the temperature of the upper atmosphere increases.

E Track Pattern

MM5 and WRF models simulated track of TC Rashmi along with observed track are plotted in the Figures 6a and 6b respectively. The track forecasts of TC Rasmi for 96, 72 48 and 24 hrs are based on the initial fields of 00 UTC of 24 October , 00 UTC of 25 October, 00 UTC of 26 October and 12 UTC of 26 October respectively for MM5 model.

It is seen from Figure 6a that the simulated track obtained by running the MM5 model for 96, 72, 48 and 24 hours are parallel to observed track but it is deviated to the east side of the observed track. It may be because of initial data error. Figure shows that model is able to generate northward movement of the system very well. It reveals that tracks obtained from 24 and 48 hrs simulation of model are more close to the JTWC best track compared to tracks obtained from 72 and 96 hrs simulation of model. However, there are some errors in the positions with respect to time which shows some ahead in landfall. The track from 48 hours simulation track is better than that of any others simulation. The landfall position for 48 hrs simulation track is much closer to that of observed track than any other simulation. So, by changing initial data in simulated, track becomes close to the observed track.

It is seen from Figure 6b that the simulated track obtained by running the WRF model for 96, 72, 48 and 24 hours is parallel to observed track but it is deviated east and west side of the observed track. It may be because of initial data error. Figure shows that model was able to generate northward movement of the system very well. It reveals that tracks obtained from 24 and 48 hrs simulation of model are more close to the JTWC best track compared to tracks obtained from 72 and 96 hrs simulation of model. However, there are some errors in the positions with respect to time which shows some ahead in landfall. The track from 48 hours simulation track is better than that of any others simulation. The landfall position for 48 hrs simulation track is much closer to the track obtained from JTWC observed data than any other simulation of model. So, by changing initial data in simulated, track becomes close to the observed track.

It is seen from the Figures 6a and 6 b that simulated track obtained from MM5 and WRF model is parallel to observed track. But it is deviated eastern side of the observed track using MM5 model and eastern and western side of the observed track using WRF model. It may be because of initial data problem. Again, track obtained from MM5 and WRF model for 48 hrs simulation is the best among other simulations. By changing initial data we can improve this track.

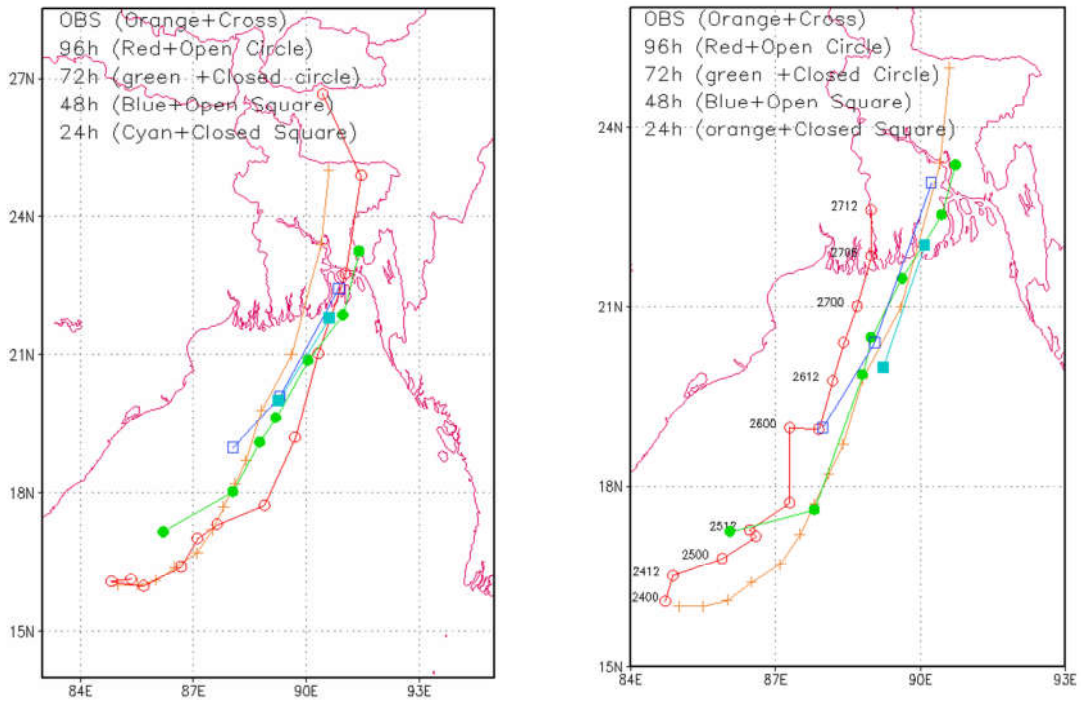

Figure 6: (a) MM5 and (b) WRF models simulated and observed tracks of TC Rashmi.

Table 6a: Landfall point and time error during cyclone Sidr (11-16 November 2007), Rashmi (24-28 October 2008) and Aila (23-27 May 2009)

Cyclone	Forecast Hours	obs/ models	initial condition date/Time (UTC)	landfall time date/Time (UTC)	landfall position		Error	
					lat°N	lon°E	Distance (km)	Time (hours)
Rashmi				27/0000	22.50	90.00		
	96	MM5	10/2400	26/1545	22.10	90.75	94e	8.25E
	72		10/2500	26/1930	22.10	91.02	122e	4.50E
	48		10/2600	26/2230	22.10	90.15	47e	1.5W
	24		10/2612	27/0115	22.10	90.60	80e	1.25D
	96	WRF	10/2400	27/0445	21.60	89.75	104w	4.75D
	72		10/2500	26/1445	22.00	90.00	56	9.25E
	48		10/2600	26/1845	21.75	89.75	88w	5.25E
	24		10/2612	26/2115	21.90	90.00	67	2.45E
D and E indicate forecast landfall time is delayed and earlier respectively compared to actual time, w and e indicate landfall position is west and east respectively of the actual landfall position.								

The landfall times and positions are tabulated in Table 6a. The error of landfall and time are also summaries in Table 6b. Mean position error for 24, 48, 72 and 96 hours are 73, 89, 68 and 73 km respectively and respective mean time errors are 1.85, 3.375, 6.375 and 6.5 hours.

Table 6b: Mean landfall position and time errors of selected tropical cyclone

Forecast Hours	Mean landfall Position Error (km)	Mean landfall Time Error (hrs)
96 hrs	99	7 (6.5)
72 hrs	89	7 (6.875)
48 hrs	68	3 (3.375)
24 hrs	73	2 (1.85)

5. CONCLUSIONS

TC Rashmi has been selected to simulate the structure, intensity, MSLP, wind (vector, radial, tangential, vertical wind), voticity, temperature anomaly and track by both of the models. Simulated parameters are compared with the data obtained from Joint Typhoon Warning Centre (JTWC).

- Both the models are able to simulate some salient features of TC such as pressure distribution, vertical motion around the centre, vertical and horizontal distribution of wind, vorticity and temperature anomaly. Some of them are very close to the observations.
- WRF model simulated SLP is better than that of MM5 model. But for both models, sharp pressure gradient in the vicinity of the centre of the TC are observed by the simulated pressure field at surface level.
- Asymmetric patterns of surface wind distribution with well organized banded structure having the maximum about 40 to 240 km far from the centre and relatively weak winds at the centre are well simulated. Well organized circulation patterns are simulated at 850 hPa level confirming that maximum winds are confined to the right of the track of the TC movement. Anticyclonic circulation patterns at 200 hPa level or lower are visible in most of the cases. Model simulated MWS is nearly equal to the observed value.
- WRF model predicts intensity better than MM5 model.
- The model has successfully simulated the strong relative vorticity at lower level spreading over the strong convective region of each cyclone. For the very strong systems the positive vorticity is found to extend up to 100 hPa level. Simulated low level vorticity fields at 850 hPa level demonstrate the size of the system with strong convective regions of each cyclone, which are in agreements with the observations.
- The warm core characteristics with maximum temperature anomaly of 6-12°C simulated in the middle and upper troposphere successfully by the models. This warm core has the vertical extends from the lower level to tropopause for strong system.
- With regard to track predictions of selected TC, models are run for 24, 48, 72 and 48 hours forecast. Simulated tracks are improved for short time forecast both modes. Performances of both models for track prediction are comparable.

Considering the above, it can be mentioned that both the models simulate the cyclonic feature well again WRF model has better forecast skill in terms of intensity and track prediction of the cyclonic storm. So, both of the models may be used as operational model by using the suitable microphysics and cumulus parameterization schemes.

REFERENCES:

1. Zhang, D. –L. and Wang, X. , Dependence of hurricane intensity and structure on vertical resolution and time-size, Adv. Atmos. Sci., 2003, **20**, 711-725.
2. Mohanty, U.C., Mandal, M. and Raman, S., Simulation of Orissa super cyclone (1999) using PSU/NCAR mesoscale model, Natural Hazards, 2003, **31**, 2, 373-390.
3. Pattanaik, D. R. and Rama Rao, Y. V. , Track prediction of very severe cyclone 'Nargis' using high resolution weather research forecasting (WRF) model, J. Earth Syst. Sci. **118**, No. 4, August 2009, pp. 309–329.

4. Rama Rao, Y. V. , Hatwar, H.R. , Ahmed, K. S. and Sudhakar, Y. , An Experiment using the High Resolution Eta and WRF Models to Forecast Heavy Precipitation over India, Pure appl. geophys. 164 (2007) 1593-1615.
5. Sousounis, P. J., Hutchinson, T. A., Marshall, S. F., A comparison of MM5, WRF, RUC, ETA performance for great plains heavy precipitation events during the spring of 2003, Preprints 20th Conference on Weather Analysis and Forecasting, Seattle, Amer. Meteor. Soc., 2004, **J24.6**.
6. Cheng, William Y. Y. and Steenburgh W. J., Evaluation of Surface Sensible Weather Forecasts by the WRF and the Eta Models over the Western United States, Weather and Forecasting, 2005, **20**, 812 – 821.
7. Patra, K. P., Santhanam, M.S., Potty, K.V.J., Tewari, M. and Rao P.L.S., Simulation of tropical cyclones using regional weather prediction models, Current Science, 2000, **79**, 1, 70-78.
8. Pattanayak S. and Mohanty, U.C. , A comparative study on performance of MM5 and WRF models in simulation of tropical cyclones over Indian seas Current Science, Vol. **95**, 923 (2008).
9. Mandal, M., Mohanty, U. C., Raman, S., A study on the impact of parameterization of physical processes on prediction of tropical cyclones over the Bay of Bengal with NCAR / PSU mesoscale model, Natural Hazards, 2004, **31**, 391-414.
10. Noh, Y., Cheon, W. –G., Hongs, and S. –Y., Improvement of the K-profile model for the planetary boundary layer based on large eddy simulation data, Bound. –Layer Meteor., 2003, **107**, 401-427.
11. Goswami, P., A.. Mandal, H.C. Upadhyasa nd F. Hourdin, 2006: Advance forecasting of cyclone track over north Indian Ocean using global circulation model, Mausam, 57 (1), 111-118

DEW DROP 02(2016) 75-79

TRENDS AND VARIABILITY OF RAINFALL OVER KHULNA DIVISION IN BANGLADESH

Md. Anisur Rahman[1*], S. M. Mostafa Kamal[2], Md. Azizur Rahman[3]

[1]*Assistant professor, Department of Mathematics, Islamic University, Kushtia-7003, Bangladesh.*
[2]*Professor, Department of Mathematics, Islamic University, Kushtia-7003, Bangladesh.*
[3]*Assistant Director, Bangladesh Meteorological Department, Agargaon, Dhaka-1207.*
**Corresponding author: anismathiu@yahoo.com*

Abstract: The expected amount of rainfall over an area is an important cause for availability of water to meet various demands for agriculture, industry, irrigation, generation of hydroelectricity and other human activities. In this study the variability and trends in monsoon and annual rainfall are analyzed for the period 1989 to 2013. To do so we estimated mean with standard deviation, cross-correlation and anomaly of monsoon rainfall. Findings reveal that, the trends of mean monsoon rainfall and annual rainfall in Chuadanga, Jessore and Satkhira have decreased, while that in Mongla has slightly increased. Of the study period, the years 1989, 1992, 1994, 2001, 2010 and 2012 are observed to have lesser rainfall. Among the five stations, the stations namely Mongla and Khulna were found to have positive anomaly and other two stations namely Chuadanga and Jessore were observed to have negative anomaly; whereas the other station namely Satkhira did not show any apparent relationship for anomaly with other stations. The estimated correlation coefficients of the annual mean rainfall between Jessore, Khulna, and Satkhira and that of between Khulna and Mongla were significant at <0.05. These results indicate lesser precipitation in future over Khulna division.

Keywords: Variability and Trend, Rainfall, Anomaly, Khulna, Bangladesh

1. INTRODUCTION

Bangladesh is mainly an agrarian country where almost one in five of its people are directly or indirectly engaged in a wide range of agricultural activities. Rainfall is the most important natural part that determines the agricultural productions in Bangladesh. The variability of rainfall and the pattern of extreme high or low precipitation are very important for the farming as well as the economy of the country. The climatic change in recent years due to global warming is a main concern, particularly for agricultural activities in Bangladesh. Over the world, the precipitation is changing due to global warming [1, 2]. The implications of these changes are particularly significant for Bangladesh where hydrological disaster is a common observable fact [3]. Hydrological changes have one of the most significant impacts on climatic change in Bangladesh. A study on climate change vulnerability based on certainty of impact noted that water resources as the greatest concern due to climate change in Bangladesh [4]. Studies in different parts of the world suggest that, global warming has changed the precipitation patterns and resulted in recurrent extreme weather events, such as floods, droughts and rainstorms [5-8]. The estimate of the probabilistic rainfall is extreme in Bangladesh during the pre-monsoon and southwest monsoon season [9, 10]. Thus, in the context of global climatic change, the study of rainfall variability and the trends of wet and dry events are; therefore, important for long-term water resources planning, agricultural development and disaster management in Bangladesh. In addition, since the variability of rainfall is high, the study of rainfall variability is of great importance at spatial and temporal scales for planning of water resources.

The distribution pattern of rainfall in Bangladesh is mostly uneven and varies considerably from year to year and region to region. In Bangladesh the meteorologists divided the year into the following four principal seasons: (i) the cold weather season- December to February; (ii) the hot weather season- March to May; (iii) the southwest monsoon season- June to September; and (iv) the post Monsoon season- October to November. The study of rainfall variability also helps in assessing drought and flood risk, relief and rehabilitation during extreme events, and finally local level contingency planning. Bangladesh is one of the most flood prone countries in the world due to its geographic position. It is notable that, severe floods that occured in the years 1974, 1984, 1987, 1988, 1998, 2004 and 2007 devastated the country. Drought in the northern part of the country is also a growing concern in the recent years. The country experienced eight droughts of severe magnitude in the years 1973, 1977, 1979, 1982, 1989, 1992, 1994-1995 and 1999 [3, 11]. Rainfall variability in

space and time is one of the most relevant characteristics of the climate of Bangladesh. Meteorological issues like variability of the arrival and withdrawal of summer monsoon, trends and patterns of rainfall during monsoon in Bangladesh are also investigated [12-14]. All these studies are carried out to show the annual and monsoon rainfall in Bangladesh. However, little attention has been paid to study the meteorological issues like rainfall variability in Khulna division –one of the most probable vulnerable regions for natural calamities in Bangladesh. To fill in this gap, this study aims to examine the annual and monsoon of rainfall variation over Khulna division for the period 1989-2013.

2. DATA AND METHODOLOGY

Five different stations located at different representative regions of Khulna division are selected purposively for this study. The stations are: Chuadanga, Jessore, Khulna, Satkhira and Mongla. The rainfall (mm) data of this area collected from Bangladesh Meteorological Department (BMD) are used in this study. The study period is January 1989 to December 2013. It is notable that, there were some missing data in some months. The missing rainfall values are computed by expectation maximization (EM) method. A full description of the EM algorithm can be found in McLach lan and Krishnan [15]. The collected data have been compiled, tabulated and analyzed by MS Excel and SPSS. Annual average and monsoon average of rainfall for different stations are anticipated to analyze the variation and to estimate trend line for the period 1989 to 2013. The monthly and yearly rainfall data have been obtained from daily rainfall data. Then, the mean and the standard deviation (SD) has been estimate from yearly rainfall data.

The excessive and deficient rainfalls, i.e., the anomaly of the rainfall in different years have been estimated. The mathematical computation of anomaly of rainfall is as follows:

Let R_{fi} be the rainfall of ith year. Then, if $R_{fi} \geq \overline{R} + \sigma$, the year is called an excess rainfall year; and if $R_{fi} \geq \overline{R} - \sigma$, the year is called the deficient year in rainfall. Let us assume that if $R_f(u,t)$ is the rainfall at station u for time t, and $R_f(t) = \left(R_f(u_1,t), R_f(u_2,t), \text{K K K } R_f(u_k,t)\right)$ at point $u_1, u_2, \text{K K K }, u_k$; then, the spatial mean and SD for time t can be represented as

$$\overline{R}_f(t) = \frac{1}{k}\sum_{i=1}^{k} R_f(u_i,t) \qquad \ldots\ldots\ldots (1)$$

$$\sigma^2(t) = \frac{1}{k}\sum_{i=1}^{k}\left[R_f(u_i,t) - R_f(t)\right]^2 \qquad \ldots\ldots\ldots (2)$$

$$Anomaly = n(u_i,t) = \frac{R_f(u_i,t) - R_f(t)}{\sigma(t)} \qquad \ldots\ldots\ldots (3)$$

Since the rainfall distribution by geographical variation is important, the cross correlationship between the stations for two data series has been estimated by using the following Pearson's correlation formula:

$$Corr\left(R_{f_1}, R_{f_2}\right) = \frac{\sum\left(R_{f_1} - \overline{R}_{f_1}\right)\left(R_{f_2} - \overline{R}_{f_2}\right)}{\sqrt{\left(R_{f_1} - \overline{R}_{f_1}\right)^2\left(R_{f_2} - \overline{R}_{f_2}\right)^2}} \qquad \ldots\ldots\ldots (4)$$

where $\overline{R}_{f_1}$ and $\overline{R}_{f_2}$ are the sample mean for the series R_{f_1} and R_{f_2}, and σ_1 and σ_2 are SDs respectively for the series R_{f_1} and R_{f_2} between different stations.

3. RESULTS AND DISCUSSION

The seasonal rainfall analysis for stations during monsoon season shows higher inter-annual variability. It may be noted that, temporal variations of the time series is higher than the spatial variation among stations. The variations of mean annual rainfall and mean monsoon rainfall in the study area for 5 stations data are analyzed and demonstrated in Figure I and Figure II. The amount of mean annual rainfall for different stations is found to be between 109 mm and 187 mm with SDs of 8 mm to 36 mm; whereas, the mean monsoon rainfall amount for different stations ranges between 215 mm and 427 mm with SDs of 20 mm to 116 mm. Overall, the mean rainfall amounts showed large variability in the study area and have been found below the average for the years 1989, 1992, 1994, 2001, 2010 and 2012 annually. Besides, the mean annual rainfall was found below the average for the years 1989, 1992, 1994, 1998, 2001, 2003, 2005, 2010, 2012 and 2013 in the monsoon period. Some years such as 1998, 2002, 2004, 2005, 2011 for annual, and 2002, 2004, 2006 and 2011 for monsoon

season showed higher mean rainfall than that of the average. The excessive and deficient of rainfall years have been shown respectively in Figure I and Figure II below.

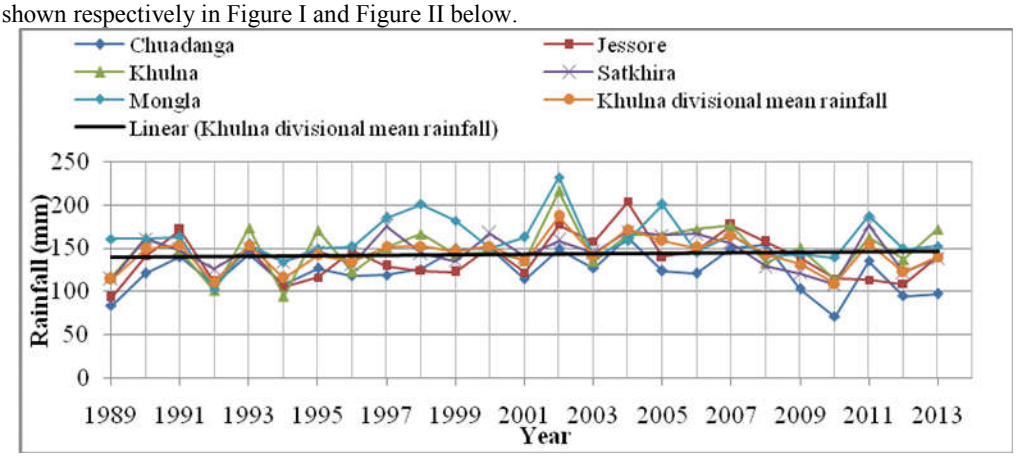

Figure I: Time series of mean annual rainfall with ± one σ at 5 stations during 1989 to 2013.

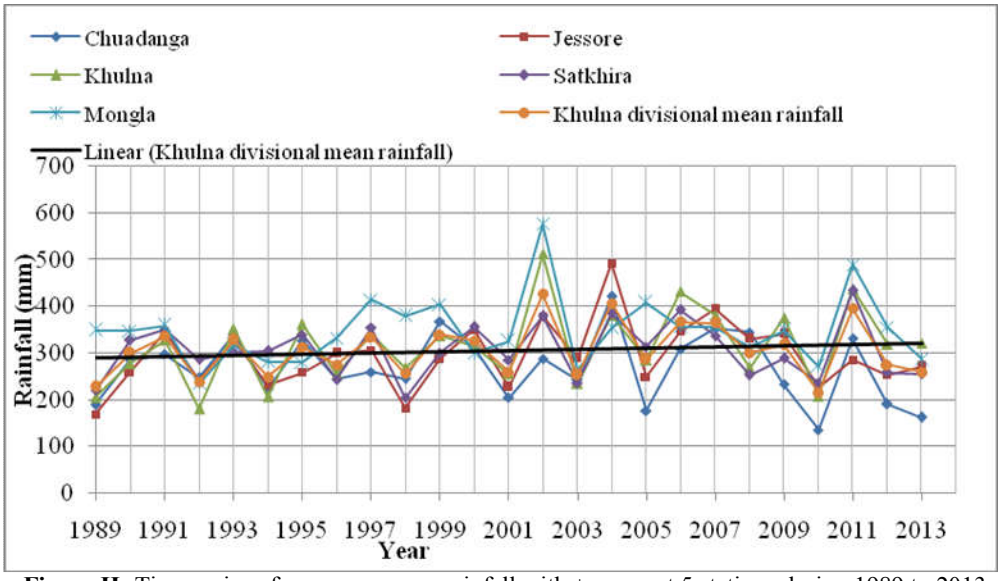

Figure II: Time series of monsoon mean rainfall with ± one σ at 5 stations during 1989 to 2013.

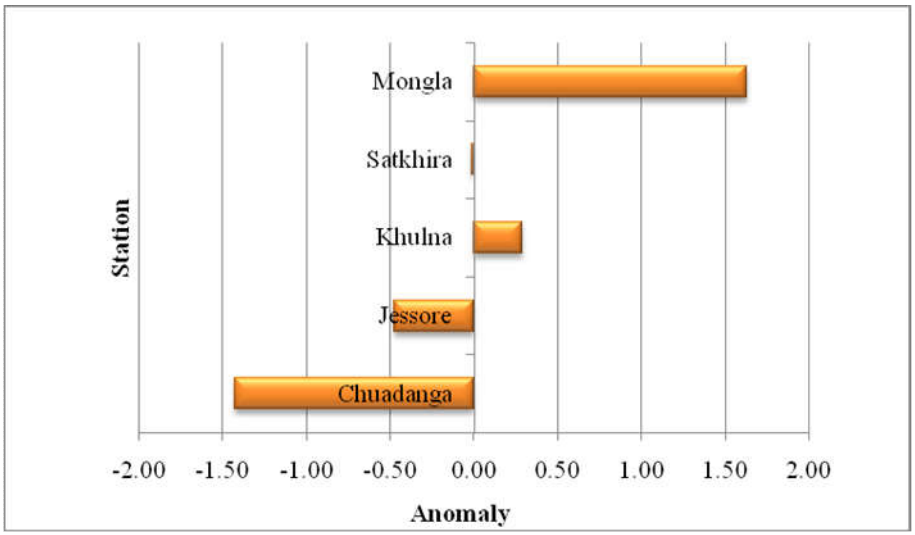

Figure III: Monsoon rainfall anomalies at study area scale for 5 rain gauge stations during 1989 to 2013.

The estimated mean rainfall anomaly using the equations 1 to 3 for monsoon period has been demonstrated in Figure III. The analysis reveals that out of 5 stations 2 have positive anomaly, while other 2 stations have negative anomaly and another one showed negligible change. The estimated anomalies for Khulna and Mongla were +0.29 and +1.63 respectively; and those for Chuadanga and Jessore were -1.43 and -0.48 respectively. The estimated correlation coefficients for different stations under Khulna division have been captured in Table 4.1(a) and 4.1(b). The correlation coefficients yielded moderate and high level of correlations in the mean annual and monsoon rainfall for the selected stations. The findings of the present study are consistent with those obtained in other parts of Bangladesh.

Table 4.1(a): Correlation among annual mean rainfall of stations of the study area

Station	Chuadanga	Jessore	Khulna	Satkhira	Mongla
Chuadanga	1.000	0.703**	0.505*	0.626**	0.347
Jessore		1.000	0.543**	0.458*	0.207
Khulna			1.000	0.620**	0.672**
Satkhira				1.000	0.480*
Mongla					1.000

Note: Level of significance *p < 0.05, **p < 0.01.

Table 4.1(b) : Correlation among monsoon mean rainfall of stations of the study area

Station	Chuadanga	Jessore	Khulna	Satkhira	Mongla
Chuadanga	1.000	0.702**	0.702**	0.594**	0.231
Jessore		1.000	1.000**	0.608**	0.248
Khulna			1.000	0.608**	0.248
Satkhira				1.000	0.494*
Mongla					1.000

Note: Level of significance *p < 0.05, **p < 0.01.

4. CONCLUSION

This study dealt with rainfall variability for some selected stations of Khulna division in Bangladesh for the period 1989-2013. The station classifications of study have been done to improve understanding about the rainfall variability across stations. We estimated the mean annual and monsoon rainfall and anomalies for monsoon period. The findings reveal wide variations of rainfall for both annual and monsoon period. The estimated correlation ratios between stations yielded moderate to high correlation for annual and monsoon period. The estimated mixed anomalies reveals decreasing of mean rainfall which implies that study region are tended towards drought. However, careful cautions are warranted to interpret these findings as the study used secondary data. Despite this limitation, the findings are appreciable and may provide valuable information for climate related studies such as water resources planning, agricultural productions and drought or flood contingency services.

ACKNOWLEDGMENT

The authors are thankful to the Bangladesh Meteorological Department (BMD) for providing rain-gauge data and reference materials for preparing the article.

REFERENCES

1. Hulme M, Osborn TJ, Johns TC. 1998: Precipitation sensitivity to global warming: comparison of observations with HADCM2 simulations. Geophysical Research Letter 25: 3379–3382.
2. Lambert F, Stott P, Allen M. 2003: Detection and attribution of changes in global terrestrial precipitation. Geophysical Research Abstract 5: 06140.
3. Shahid S, Behrawan H. 2008: Drought risk assessment in the western part of Bangladesh. Natural Hazards 46(3): 391–413.
4. Organization for Economic Co-operation and Development, Development and climate change in Bangladesh: focus on coastal flooding and the sundarbans. In Organization for Eco-nomic Co-operation and Development (OECD) Report COM/ENV/EPOC/DCD/DAC(2003)3/FINAL, Agrawala S, Ota T, Ahmed AU, 2003.
5. Briffa K R, van der Schrier G, Jones P D. 2009: Wet and dry summers in Europe since 1750: evidence of increasing drought. International Journal of Climatology 29(13): 1894–1905.

6. Schmidli J, Frei C. 2005: Trends of heavy precipitation and wet and dry spells in Switzerland during the 20th century. International Journal of Climatology 25(6): 753–771.
7. WMO, Statement on the status of global climate in 2003, WMO Publication no. 966, World Meteorological Organization: Geneva. 2003.
8. Zhang Q, Xu C-Y, Zhang Z. 2009: Observed changes of drought/wetness episodes in the Pearl River basin, China, using the standardized precipitation index and aridity index. Theoretical and Applied Climatology 98(1-2): 89–99.
9. Ahmed R. 1989: Probabilistic estimates of rainfall extremes in Bangladesh during the pre-monsoon season. Indian Geographical Journal 64: 39–53.
10. Karmakar S, Khatun A. 1995: Variability and probabilistic estimates of rainfall extremes in Bangladesh during the southwest monsoon season. Mausam 46(1): 47–56.
11. Shahid S. 2008: Spatial and temporal characteristics of droughts in the western part of Bangladesh. Hydrological Processes 22(13): 2235–2247.
12. Ahmed R, Karmakar S. 1993: Arrival and withdrawal dates of the summer monsoon in Bangladesh. International Journal of Climatology 13: 727–740.
13. Ahmed R, Kim I-K. 2003: Patterns of daily rainfall in Bangladesh during the summer monsoon season: case studies at three stations. Physical Geography 24(4): 295–318.
14. Rahman M R, Salehin M, Matsumoto J. 1997: Trends of monsoon rainfall pattern in Bangladesh. Bangladesh Journal of Water Resources 14–18: 121–138.
15. McLachlan, G.J. and T. Krishnan, The EM Algorithm and Extensions. Wiley, New York City, New York. 1997.

Climatology of southwest monsoon season in Bangladesh

Haripada Sarker[1*], Abdul Mannan Chowdhury[1] and Samarendra Karmakar[2]
[1]*Jahangirnagar University*
[2]*Bangladesh Centre for Advanced Studies*

Abstract: Attempts have been made to study the monsoon climatology of Bangladesh using the mean (normal) of 30 years data during 1981-2010. Different meteorological parameters such as mean sea level pressure, rainfall, dew-point depression, minimum temperature and maximum temperature, cloud amount, humidity and sunshine hours over Bangladesh during the onset, on-going and withdrawal phases of southwest monsoon season have been used. The study reveals that a low pressure exists over the western part of Bangladesh with one of its trough extended towards northeast. Relatively higher pressure is found over the eastern part of the country during the southwest monsoon season. The mean sea level pressure remains lower in June and July as compared to that in May and then increases. During the withdrawal phase of the southwest monsoon, the distribution pattern becomes different with low pressure shifted towards the east more and the high pressure is found to intrude from the northwest. The high pressure over Chittagong and Chittagong hill tracts is found to shift to the east and becomes more prominent during the withdrawal phase of monsoon. . The dew-point depression decreases with the onset of monsoon over Bangladesh, having ranges from 1.2 to 3.6°C in June, 1 to 3°C in July, 1 to 3.2°C in August and 1 to 3.2°C in September with the lower values in the eastern part of Bangladesh. The dew point depression increases during the withdrawal phase of monsoon with higher values over Bangladesh except the extreme southeastern part of the country. Rainfall has been found to increase with the onset of southwest monsoon over Bangladesh. Monsoon rainfall is higher in the southeastern part of the country in all the months and even in the withdrawal month of monsoon. There exists a belt of relatively low rainfall along the latitude belt of 22-25°N. The minimum temperature is lower in the eastern half and higher in the western half of the country. Before onset and after withdrawal phases of the southwest monsoon, the minimum temperature becomes lower in the northern part and higher in the southern part of Bangladesh. Higher minimum temperature prevails over Bangladesh during the southwest monsoon season due to the prevailing of more moisture in this season. The study has also revealed that there exists a belt of relatively higher maximum temperature along the latitude 22-24°N during the southwest monsoon season where the rainfall is lower during the southwest monsoon.

Key words: Climatology, southwest monsoon, mean sea level pressure, rainfall, dew-point depression, maximum and minimum temperatures.

1. Introduction

Bangladesh is situated in a peculiar location with the Himalayan range in the north and the Bay of Bengal in the south, having hills in the northeastern and southeastern parts. Meteorologically, there are four seasons in Bangladesh such as: Pre-monsoon (march-May), Southwest Monsoon (June-September), Post-monsoon (October-November) and Northeast monsoon (December-February). Of these seasons, southwest monsoon, here-in-after called monsoon only, is a long season and has great bearings on the socio-economic conditions of the people of Bangladesh as well as India-Bangladesh-.Pakistan sub-continent. About 80% of Bangladesh's rain falls during the monsoon season. The monsoons result from the contrasts between low and high air pressure areas that result from differential heating of land and water. During this season, the weather pattern involves winds blowing from the south-west direction (known as the South-West Monsoon) from the Indian Ocean onto the sub-continental. These winds are generally laden with much moisture, blowing from sea to land, and bring rains to most parts of the subcontinent [1]. Dividing against the Indian landmass, the monsoon flows in two branches, one of which strikes western India. The other travels up the Bay of Bengal and over eastern India and Bangladesh, crossing the plain to the north and northeast before being turned to the west and northwest by the foothills of the Himalayas. Variations in monsoon rainfall give evidence of climate variability over Bangladesh. Seasonal variation of rainfall is the most distinguishing feature of the densely populated monsoon rainfall regions of the world [2].

According to Dynamic Theory, during the summer months of Northern Hemisphere, the ITCZ shifts northwards pulling the SW Monsoon winds onto the land from the sea. However, the huge landmass of the Himalayas continues to restrict the low pressure zone onto the Himalayas itself. It is only when the Tibetan Plateau heats up a lot more than the Himalayas does the ITCZ abruptly and swiftly shift northwards leading to *burst of Monsoon showers* over the Indian subcontinent. According to the Jet Stream Theory, the onset of SW Monsoon over Indian subcontinent is driven by the shift of the *subtropical westerly jet* northwards from over the plains of India towards the Tibetan Plateau. This shift is due to the intense heating of the Plateau during the summer months. This shift of the *westerly jet* to the north of the Himalayas is not a slow and gradual process, as expected for most changes in weather pattern. The primary cause of these is believed to be the height of the Himalayas. As the Tibetan Plateau heats up the low pressure created over it pulls the *westerly jet* northwards. Due to lofty Himalayas, the *westerly jet* is inhibited from moving northwards. However, with continuous dropping pressure, sufficient force is created for the movement of the *westerly jet* across the Himalayas after a significant period. As such, the shift of the jet is sudden and abrupt causing the *bursting of SW Monsoon rains* onto the India-Bangladesh plains.

According to Yin, the Tibetan Plateau acts as a physical barrier [3]. At the beginning of June, the subtropical jet stream disappears completely over northern India. At this time, the jet stream shifts to the north of the Himalayas and Tibet, and takes up a position at about 40°N. Yin considers that there is a correspondence between the shifting of the jet and the slowing down of the westerlies over the whole of Eurasia. In fact, the plateau of Tibet becomes very cold in winter, and proves to be the most important factor in causing the advance of the jet far to the south in the middle of October. Thus, he opines that the abrupt onset of summer monsoon at the beginning of June is prompted by the hydro-dynamic effect of the Himalayas and not by the thermally induced low pressure centre over northwest India. In recent years it has been argued that the summer-time heating of Tibetan Plateau makes it a heat source. A warm-core anticyclone is formed over this plateau during the summer monsoon period. The formation of this anticyclone takes place in the middle part of the troposphere at 500 mb level. It is the result of a process called anticyclogenesis. However, on the southern side of this upper-air anticyclone, the direction of air flow is from east to west. In fact, these easterly winds blowing in the mid-troposphere are known as the tropical easterly jet [4]. The tropical easterly jet extends far to the south of Tibet and the jet maximum is roughly along the latitude belt (10-15°N) at around 200 hPa. These upper-air easterlies descend in the permanent high pressure area formed over the south Indian Ocean.

Karmakar and Khatun studied the variability and probabilistic estimates of rainfall in Bangladesh during the southwest monsoon season and found that the variability decreases from June to July and then starts increasing from August to September [5]. The study also reveals that the mean rainfall and the probabilistic rainfall extremes are maximum over the southeastern and northeastern parts of the country where the variability of rainfall is low and the rainfall is reliable. There exists a belt of low rainfall over the central part of Bangladesh roughly between 23°N and 24°N. Dhar and Nandagiri made a study to find out the contribution of low pressure areas (or lows) towards the rainfall of northern and central India during the monsoon months of June to September in the absence of more intense cyclonic disturbances such as depressions, deep depressions and cyclonic storms [6]. This study has shown that the occurrence of moderate to heavy rainfall mainly depends upon their frequency, life span, track followed and origin of these disturbances provided there are not inhibiting meteorological factors like 'break' monsoon situations.

In Bangladesh, no work has been done on the long-term average of different meteorological parameters during the onset, ongoing and withdrawal phases of southwest monsoon after 1990. The present study has been undertaken to study the climatology with spatial distribution of different meteorological parameters over Bangladesh.

2. Data and methodology

Daily mean sea level pressure, rainfall, maximum and minimum temperature, dew point temperature for May through October for the year 1981 to 2010 at 34 stations (Figure 2.1) of Bangladesh Meteorological Department (BMD) have been collected and utilized in the present study. From the daily temperature and dew-point temperature, daily dew-point depression has been computed at each station and the monthly average of dew-point depression has been determined for study period. Monthly mean of all other parameters have been computed. Win surfer analysis has been used for the spatial distribution of the above parameters during the onset, on-going and withdrawal phases of the southwest monsoon season in Bangladesh.

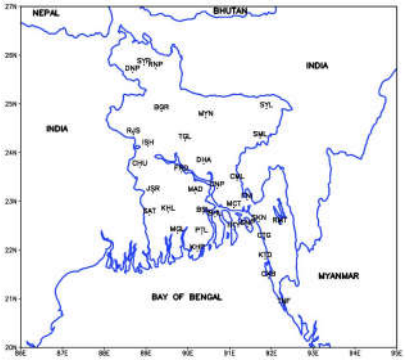

Fig. 2.1: Location of meteorological stations of BMD

Here May is taken as the onset period and October is taken as the withdrawal phase of the monsoon season.

3. Results and discussion

3.1 Mean sea level (msl) pressure over Bangladesh from May to October during 1981-2010

The distribution of mean sea level (msl) pressure over Bangladesh from May through October of 1981-2010 are shown in Figs. 3.1(.a.-.f). In May, the mean sea level pressure is found to range from 1002.8 to 1004.6 hPa over Bangladesh [Fig. 3.1 (a)]. The low pressure is found over western part of the country near Kushtia with a trough extending towards the southeast. High pressure exists over Chittagong hill tracts. Similar pattern of distribution of mean sea level pressure is found in June [Fig. 3.1(b)] with low pressure over a larger western area over Khulna, Mongla, Barisal and Madaripur. One of its troughs is extended up to Sylhet and another towards southeast. It may be mentioned that there is a small high pressure area over Satkhira-Kustia region. In this month, the pressure is decreased considerably ranging from 1000 to 1002 hPa. In July, the low pressure has shifted towards north near Pabna and adjoining area with one of its trough extended towards southeast [Fig. 3.1 (c)]. But the mean sea level pressure has remained the same ranging from 1000 hPa to 1002 hPa. The small high pressure area over Satkhira-Kustia region is found to exist. Relatively high pressure exists over Chittagong hill tracts. In August, the distribution pattern of mean sea level pressure is almost the same as that in May with low pressure over western part of Bangladesh with one of its trough passing towards southeast and another in the northeast. The pressure has been found to increase slightly over Bangladesh [Fig. 3.1 (d)]. The msl pressure of September has increased ranging from 1004.4 to 1005.6 hPa. In this month, a low pressure exists over Jessore-Khulna-Faridpur region, having a trough extended towards northeast [Fig. 3.1 (e)]. The area of high pressure over Chittagong hill tracts is reduced and shifted toward the east too. In October, the distribution of monthly mean pressure is completely different. The low pressure area is shifted over central Bangladesh with one of its troughs extended to Sylhet and another towards southeast. A high pressure is found to penetrate through the Jessore-Kushtia-Ishurdi and another high pressure is found to penetrate through Nilphamary-Kurigram. This intrusion of high pressure indicates the withdrawal of southwest monsoon over the northern part of the country.

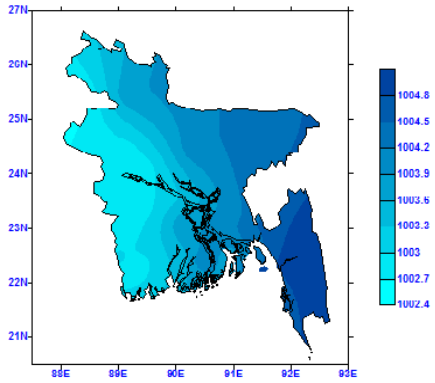

Fig.3.1 (a): Monthly normal mean sea level pressure over Bangladesh in May during 1981-2010

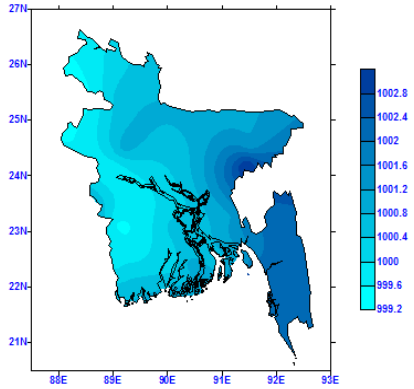

Fig.3.1 (b): Monthly normal mean sea level pressure over Bangladesh in June during 1981-2010

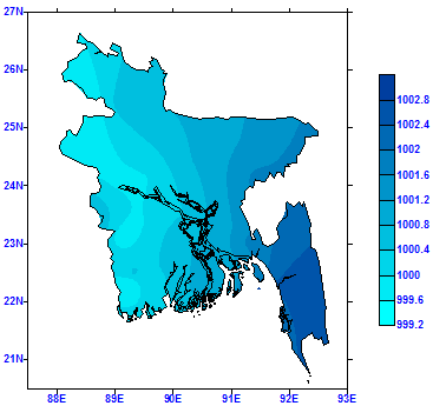

Fig.3.1 (c): Monthly normal mean sea level pressure over Bangladesh in July during 1981-2010

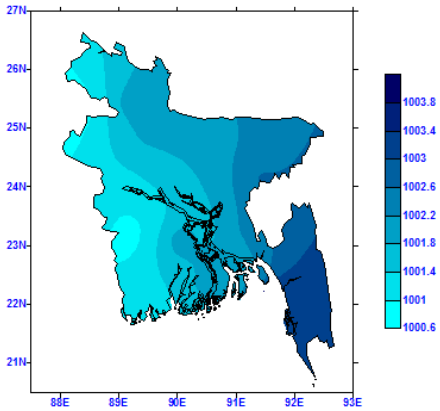

Fig.3.1 (d): Monthly normal mean sea level pressure over Bangladesh in August during 1981-2010

The high pressure over Chittagong hill tracts has become more prominent. In this month, the pressure has increased considerably over the country ranging from 1008.4 hPa (in the central part) to 1009.2 hPa in the eastern and western parts of the country [Fig. 3.1 (f)]. It may be mentioned that a trough of easterly low seems to exist over the coastal region of Bangladesh. This figure shows the characteristics of the withdrawal phase of the southwest monsoon.

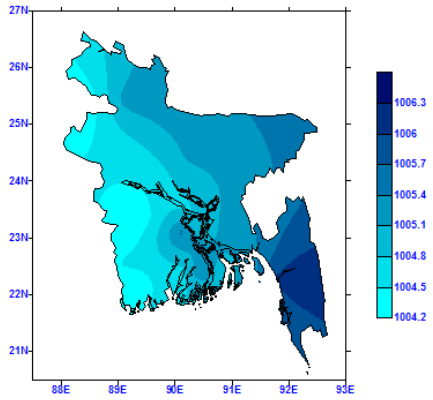

Fig.3.1 (e): Monthly normal mean sea level pressure over Bangladesh in September during 1981-2010

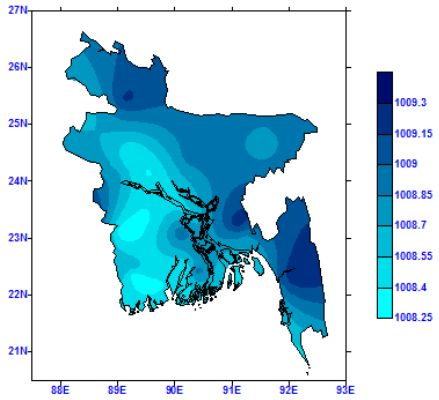

Fig.3.1 (f): Monthly normal mean sea level pressure over Bangladesh in October during 1981-2010

From the above discussion it appears that during the onset and ongoing phases of southwest monsoon, there exists a low pressure over the western part of Bangladesh with one of its trough extended towards northeast and another towards the southeast. Relatively higher pressure is found over the eastern part of the country. During the withdrawal phase of the southwest monsoon, the distribution pattern becomes different with low pressure shifted more towards the east and the high pressure is found to intrude from the north/northwest. The high pressure over Chittagong and Chittagong hill tracts has become more prominent

3.2 *Monthly mean dew-point depression over Bangladesh during May to October during 1981-2010*

The spatial distributions of monthly mean dew-point depression over Bangladesh from May through October in 1981-2010 are shown in Figs. 3.2 (a-f)). During the onset phase of monsoon in May, the dew-point depression ranges from about 1.8°C in the southern part to about 5.2°C in the western part of Bangladesh [Fig. 3.2 (a)]. The maximum dew-point depression is found in the Jessore area with an extension towards northwest, indicating the drier region and minimum over Barisal division with the lowest minimum of around 1.8°C over Bhola-Hatiya area. This area is moister than other areas of the country. The higher dew-point depression has penetrated like a ridge up to Comilla through the central part of the country. A region of relatively lower dew-point depression exists over the Mymensingh region.

In June, the dew-point ranges from 1.2°C in the south to about 3.6°C in the extreme west i.e. Jessore region with an extension towards the north [Fig. 3.2 (b)]. The minimum dew-point depression lies over the same area as in

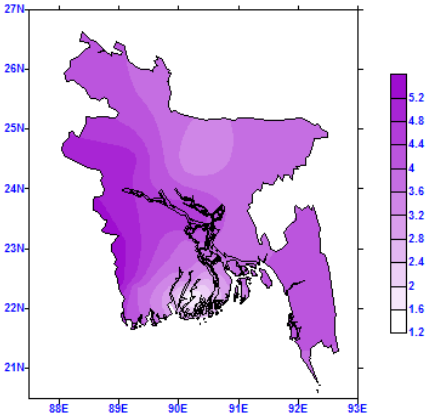

Fig.3.2(a): Normal dew-point depression in May in Bangladesh during 1981-2010

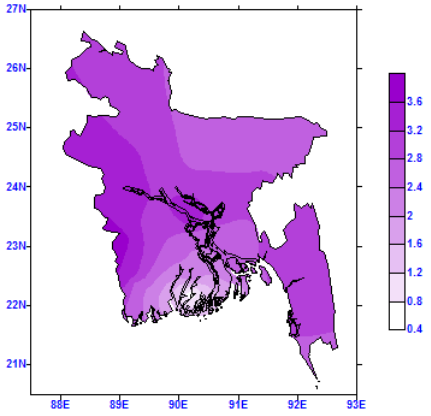

Fig.3.2(b): Normal dew-point depression in June in Bangladesh during 1981-2010

May and the dew-point depression is higher in the western part than that of the eastern part of Bangladesh. This means that the eastern part of Bangladesh is moister than the western part. This is because of the onset of southwest monsoon over the eastern part earlier than the western part. The dry zone in the west has extended to the east through central part of the country. The dew-point depression is comparatively lower in June than that in May. In July, the range of dew-point depression is from 0.4°C in the south to about 3°C in the middle of the country over the Dhaka region [Fig. 3.2 (c)], the dry zone penetrated as a narrow zone through the northwestern part of the country extending through the middle part to the eastern part of the country. The higher value is lower in July than that in June, indicating that the whole country has become moister in this month. The eastern part of Bangladesh is relatively moister than that of the western part, the southern part is extremely moist. In August, the dew-point depression is lower over the country in general ranging from 0.2°C in the extreme south to 3.2°C in the middle of Bangladesh. This indicates that August is more humid than that in the earlier months [Fig. 3.2(d)]. The figure also shows some relatively small moist zones in the extreme southeast, northeast, west and over Nilphamary-Kurigram area. In September, the dew-point depression is found to range from 1.0°C in the extreme southern part to 3.2°C near Dhaka and Mymensingh [Fig. 3.2 (e)]. The distribution of dew-point depression is more or less uniform all over Bangladesh except extreme south, Dhaka and Mymensingh; the southeastern part of the country seems to be little more moist.

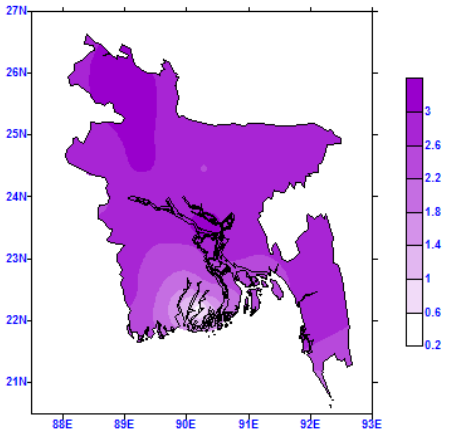

Fig.3.2(c): Normal dew-point depression in July in Bangladesh during 1981-2010

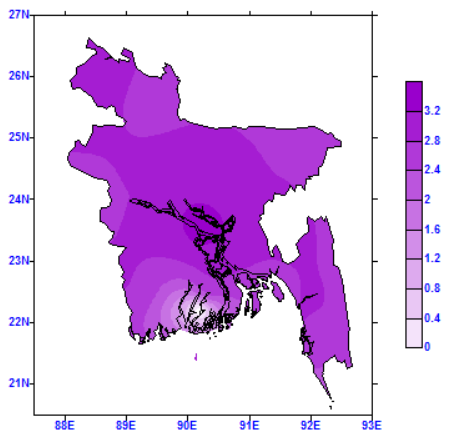

Fig.3.2(d): Normal dew-point depression in August in Bangladesh during 1981-2010

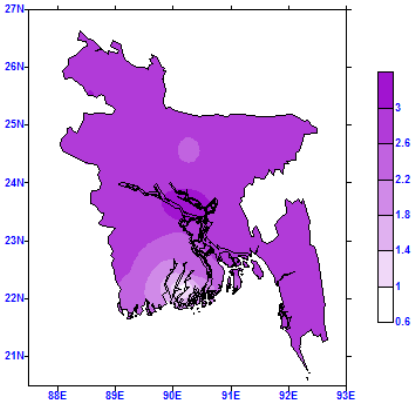

Fig.3.2(e): Normal dew-point depression in September in Bangladesh during 1981-2010

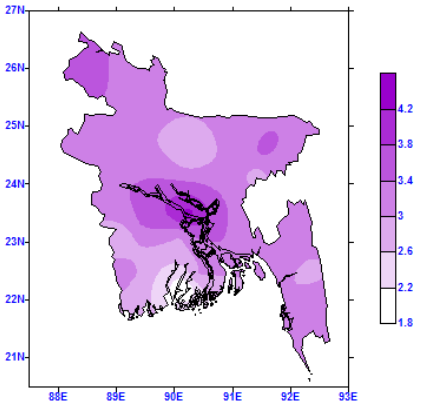

Fig.3.2(f): Normal dew-point depression in October in Bangladesh during 1981-2010

In October, the withdrawal phase of southwest monsoon, the dew-point depression ranges from 2.0°C in the southeastern part of the country to about 4.2°C in the middle part of the country. The southern part is moister, indicating that the southwest monsoon has withdrawn from the country. The distribution pattern is found to be disorganized [Fig. 3.2 (f)]. In this month, the whole country has become less humid in general because of the withdrawal of southwest monsoon from Bangladesh.

It is apparent that the dew-point depression decreases in the eastern part during the onset phase of southwest monsoon and becomes lower all over Bangladesh during the on-going phase of monsoon i.e. becomes more humid during the on-going phase. It again increases during the withdrawal phase. During the onset phase of

southwest monsoon, the dry zone retreats though the northwestern part and during the withdrawal phase of the monsoon, the dry zone penetrates through the northwestern part of Bangladesh.

3.3 Monthly mean total rainfall over Bangladesh during May to October during 1981-2010

The spatial distributions of monthly mean total rainfall over Bangladesh from May through October during 1981-2010 are shown in Figs. 3.3 (a-f)). During the onset phase of monsoon in May, the rainfall ranges from about 150 mm in the west to about 550 mm in the northeastern part of Bangladesh as shown in Fig. 3.3 (a). The maximum rainfall is found in the Sylhet area, which may be due to thunderstorm activity and some pseudo-monsoon activity. The figure also shows that there exists a belt of relatively low rainfall along the latitude 22-

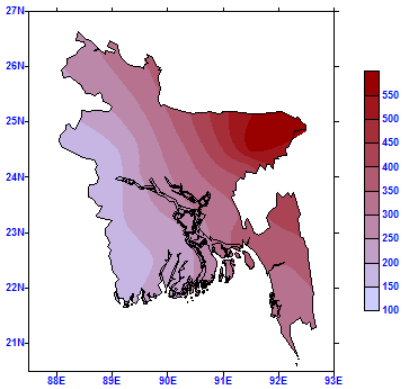

Fig. 3.3 (a) Distribution of normal rainfall in May over Bangladesh

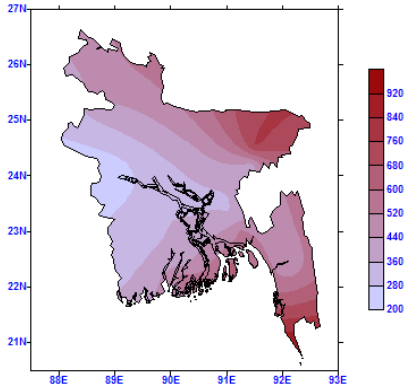

Fig. 3.3 (b) Distribution of normal rainfall in June over Bangladesh

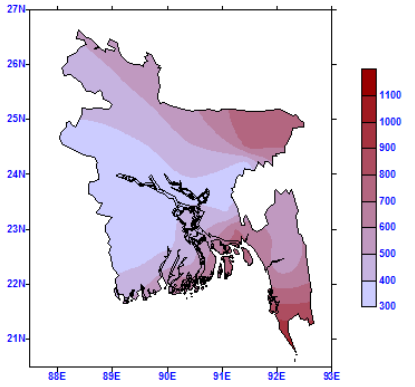

Fig. 3.3 (c) Distribution of normal rainfall in July over Bangladesh

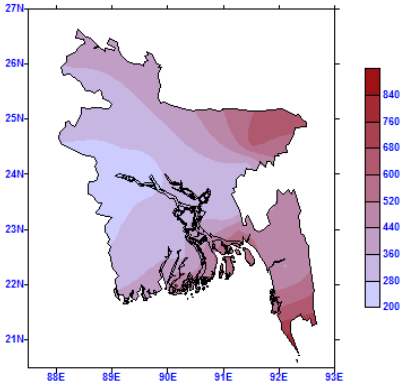

Fig. 3.3 (d) Distribution of normal rainfall in August over Bangladesh

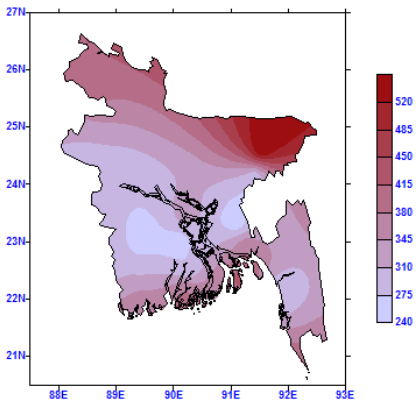

Fig. 3.3 (e) Distribution of normal rainfall in September over Bangladesh

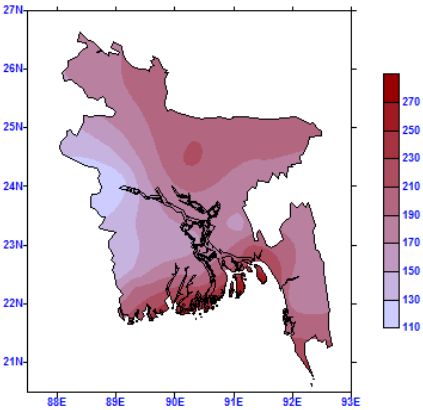

Fig. 3.3 (f) Distribution of normal rainfall in October over Bangladesh

23°N. In June, the rainfall ranges from 250 mm in the west to about 850 mm in the extreme southeast i.e. Chittagong-Cox's Bazar region with a secondary maximum rainfall of over 750 mm in the northeast i.e. Sylhet region [Fig. 3.3 (b)]. The rainfall is higher in the eastern part of Bangladesh. The rainfall is comparatively higher than that in May and this is mainly due to the onset of southwest monsoon over Bangladesh. In this month, there is also a belt of relatively lower rainfall along the latitude of 22.5-24.5°N.

In July, the rainfall ranges from 350 mm in the west to about 1000 mm in the extreme southeast with a secondary maximum rainfall area over the Sylhet region having rainfall over 750 mm [Fig. 3.3 (c)]. The minimum rainfall is over Kushtia-Jessore region. There also exists a relatively lower rainfall along the latitude belt 22.5-24.5°N. In August, the pattern of rainfall is maximum over Chittagong-Cox's Bazar with rainfall of 750 mm [Fig. 3.3 (d)]. The amount of secondary maximum rainfall of 600 mm exists over Sylhet region. The rainfall is relatively lower along the latitude belt of 23-24°N. In this month, the lowest rainfall is 250 mm in the western part of the country.

In September, the rainfall is found to decrease all over Bangladesh having the minimum rainfall of about 300 mm at the middle part of the country and maximum rainfall of 500 mm over Sylhet. The secondary maximum rainfall of 350-400 mm lies over Chittagong-Cox's Bazar region. The decrease in rainfall is because of the fact that September is the end month of southwest monsoon. The belt of relatively lower rainfall is distinct along the latitude belt of 23-24°N [Fig. 3.3 (e)]. In October, the withdrawal phase of southwest monsoon, there is no rainfall in the northern part of Bangladesh and the rainfall ranges from 120 mm in the west and about 210 mm in the extreme southeastern part of the country. The belt of relatively lower rainfall is along the latitude belt of 22.5-24.5°N [Fig. 3.3 (f)]. The belt of relatively low rainfall along the latitude belt of 23.5-24.5°N is in line with the study made by Karmakar and Khatun [5].

From the above discussion it is apparent that the maximum rainfall exists over the southeastern part of Bangladesh during the on-going phase of southwest monsoon and starts decreasing from the northwest of the country with the withdrawal of the monsoon. The belt of relatively lower rainfall is along the latitude belt of 22.5-24.5°N. The result is in line with the study made by Karmakar and Khatun [5].

3.4 Monthly mean minimum temperature over Bangladesh from May to October during 1981-2010

The spatial distributions of monthly average minimum temperature over Bangladesh from May through October during 1981-2010 are shown in Figs. 3.4 (a-f)). During the onset phase of monsoon in May, the minimum temperature ranges from about 22.8°C in the northeast to about 25.8°C in the southwest of Bangladesh as shown in Fig. 3.4 (a). The lowest minimum temperature of 22.8°C is found over Sylhet-Srimangal area and the higher minimum temperature of 26°C is found over Satkhira region. In June, the minimum temperature ranges from 24.8°C in the southeast to about 26.4°C in the extreme southwest i.e. in Khulna region [Fig. 3.4 (b)] and the distribution pattern is also different with the lower minimum temperature in the east and higher minimum temperature in the western half of the country. The minimum temperature in June is comparatively higher than that in May. The relatively lower minimum temperature in the eastern half of the country is mainly due to the onset of southwest monsoon over the eastern part first and then over the western part of Bangladesh [7]. Also the overall higher minimum temperature over the country in June is due to the less fluctuation in minimum temperature in June that that in May. In July, the minimum temperature ranges from 25°C in the southeast to about 26.2°C in the extreme southwest over the Khulna region [Fig. 3.4 (c)], having the same distribution

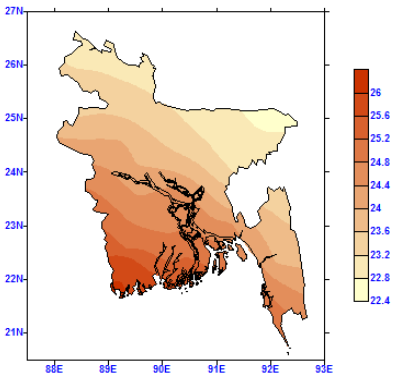

Fig.3.4(a). Distribution of normal minimum temperature in May over Bangladesh

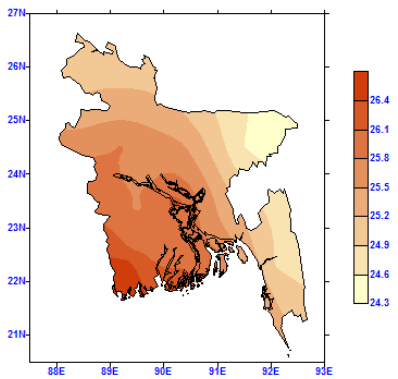

Fig.3.4 (.b). Distribution of normal minimum temperature in June over Bangladesh

pattern as in June with the relatively higher minimum temperature in the western part and lower minimum temperature in the eastern part of the country.

In August, the range of minimum temperature is from 25°C over Chittagong hill tracts to 26.4°C from Dhaka to northwest region [Fig. 3.4 (d)]. The minimum temperature is is relatively lower over the eastern part of Bangladesh and higher in the western part of the country. In September, the minimum temperature is found to decrease all over Bangladesh having the lowest minimum temperature of about 24.6°C at Sylhet-Rangamati region and highest minimum temperature of 25.8°C over Faridpur region. This is because of the fact that September is the end month of southwest monsoon [Fig. 3.4 (e)]. October is the withdrawal phase of southwest monsoon the minimum temperature has decreased considerably. The minimum temperature ranges from 22.8°C northern Bangladesh to 24.0°C in the central south part of the country [Fig. 3.4 (f)]. The distribution pattern has changed with lower minimum temperature in the north and higher minimum temperature in the south.

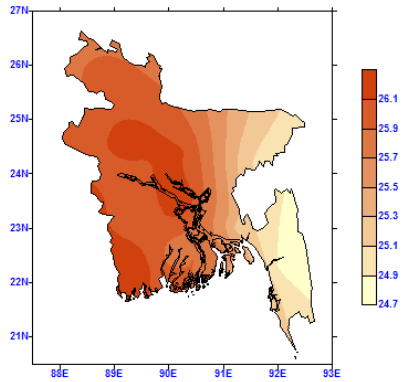

Fig.3.4(c). Distribution of normal minimum temperature in July over Bangladesh

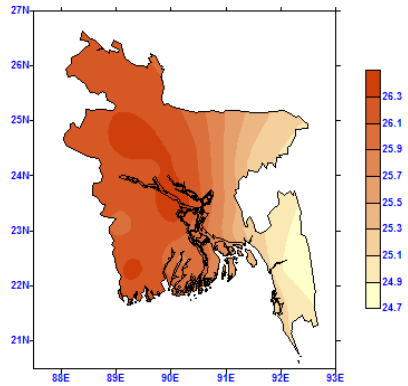

Fig.3.4 (d). Distribution of normal minimum temperature in August over Bangladesh

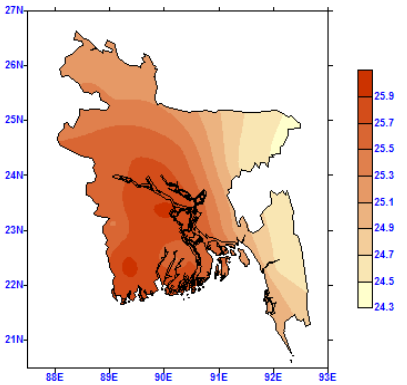

Fig.3.4(e). Distribution of normal minimum temperature in September over Bangladesh

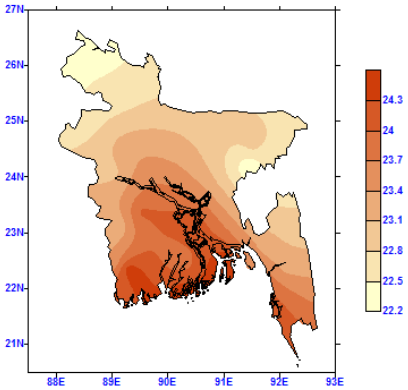

Fig.3.4(f). Distribution of normal minimum temperature in October over Bangladesh

It is apparent from the above discussion that the minimum temperature is lower in the eastern half and higher in the western half of the country during the monsoon season. Before onset and after withdrawal phases of the southwest monsoon, the distribution pattern is that the minimum temperature is lower in the northern part and higher in the southern part of Bangladesh. Higher minimum temperature prevails over Bangladesh during the southwest monsoon season due to the prevailing of more moisture in this season.

3.5 Monthly mean maximum temperature over Bangladesh from May to October during 1981-2010

The spatial distributions of monthly average maximum temperature over Bangladesh from May through October during 1981-2010 are shown in Figs. 3.5 (a-f)). In May, the maximum temperature ranges from about 31°C in the northeast to about 35.5°C in the southwest of Bangladesh as can be seen in Fig. 3.5 (a). The maximum temperature is relatively lower in the north/northeast. The highest maximum temperature is found in the Jessore area. The figure also shows that there exists a belt of relatively higher maximum temperature along the latitude 22-24°N. In June, the maximum temperature ranges from 31.4°C in the southeast and northeast to about 33.9°C in the extreme west i.e. Jessore region [Fig. 3.5 (b)]. The maximum temperature is comparatively lower in June

than that in May and this is mainly due to the onset of southwest monsoon over Bangladesh when rainfall occurs more over the country. The highest maximum temperature is found in the Jessore area. The figure also shows that there exists a belt of relatively higher maximum temperature along the latitude 22.5-24°N.

In July, the maximum temperature ranges from 30.8°C in the southeast to about 32.09°C in the extreme west [Fig. 3.5 (c)]. Highest maximum temperature is found over Rajshahi to Khulna region. The belt of relatively maximum temperature also exists along 22.5-24.5°N. In August, the maximum temperature range is 31.0°C over the southern area to 33.0°C to over Rajshahi to Khulna region [Fig. 3.5 (d)]. The belt of relatively higher maximum temperature also exists along 22.5-24°N. In September, the maximum temperature has the range of about 30.8°C at Bhola and northern part of the country and maximum of 32.5°C over Jessore-Kushtia region [Fig. 3.5 (e)]. The belt of relatively higher maximum temperature also exists over the same area. In October, the withdrawal phase of southwest monsoon of Bangladesh, maximum temperature ranges from 30.8°C in the northern part of the country to about 32.4°C in the south-western part of the country [Fig. 3.5 (f)]. It can be seen that the distribution patterns in maximum temperature are different in September and October as compared to

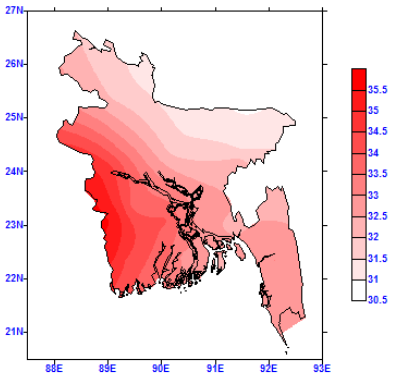

Fig.3.5.(a): Normal of maximum temperature in May in Bangladesh

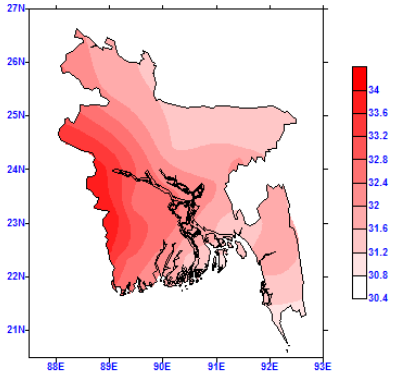

Fig.3.5.(b): Normal of maximum temperature in June in Bangladesh

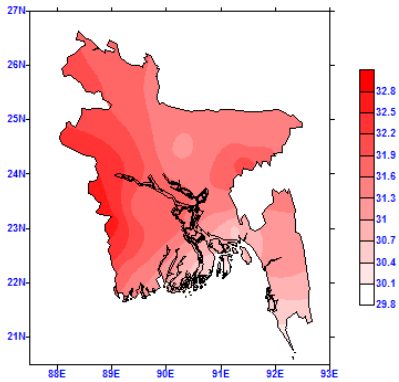

Fig.3.5.(c): Normal of maximum temperature in July in Bangladesh

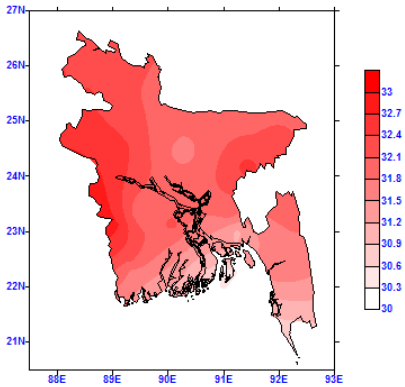

Fig.3.5.(d): Normal of maximum temperature in August in Bangladesh

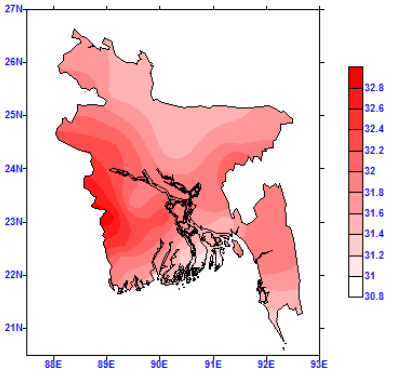

Fig.3.5.(e): Normal of maximum temperature in September in Bangladesh

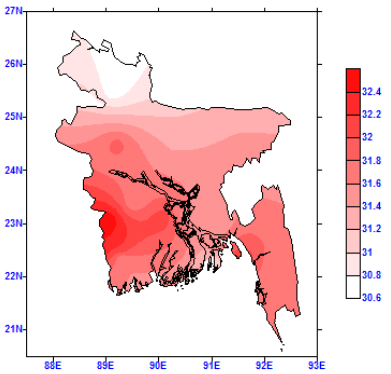

Fig.3.5.(f): Normal of maximum temperature in October in Bangladesh

those in other months. This is because of the fact that the maximum temperature becomes lower over the northern part of Bangladesh. The belt of relatively higher maximum temperature also exists over the same area in this month.

It is apparent from the above discussion that the maximum temperature is higher in the western part of Bangladesh during the onset, on-going and withdrawal phases of monsoon. Lower maximum temperature exists in the northern part of the country during the onset and withdrawal phases of the monsoon, but the maximum temperature is lower over the extreme southeastern part of Bangladesh during the on-going phase. A belt of relatively higher maximum temperature is apparent along 22-24°N.

4. Conclusions

On the basis of the present study, following conclusions can be drawn:

i. During the onset and ongoing phases of southwest monsoon in 1981-2010, a low pressure has been found over the western part of Bangladesh with one of its trough extended towards northeast and another towards the southeast. Relatively higher pressure is found over the eastern part of the country. During the withdrawal phase of the southwest monsoon, the low pressure is shifted towards the east more and the high pressure is found to intrude from the north/northwest, shifting the high pressure over the eastern part towards more east.

ii. The dew-point depression decreases in the eastern part during the onset phase of southwest monsoon and becomes lower all over Bangladesh during the on-going phase of monsoon i.e. becomes more humid during the on-going phase. It again increases during the withdrawal phase. During the onset phase of southwest monsoon, the dry zone retreats though the northwestern part and during the withdrawal phase of the monsoon, the dry zone penetrates through the northwestern part of Bangladesh.

iii. The maximum rainfall exists over the southeastern part of Bangladesh during the on-going phase of southwest monsoon and starts decreasing from the northwest of the country with the withdrawal of the monsoon. The belt of relatively lower rainfall is along the latitude belt of 22.5-24.5°N.

iv. The minimum temperature is lower in the eastern half and higher in the western half of the country. Before onset and after withdrawal phases of the southwest monsoon, the minimum temperature becomes lower in the northern part and higher in the southern part of Bangladesh. Higher minimum temperature prevails over Bangladesh during the southwest monsoon season due to the prevailing of more moisture in this season.

v. The maximum temperature is higher in the western part of Bangladesh during the onset, on-going and withdrawal phases of monsoon. Lower maximum temperature exists in the northern part of the country during the onset and withdrawal phases of the monsoon, but the maximum temperature is lower over the extreme southeastern part of Bangladesh during the on-going phase. A belt of relatively higher maximum temperature is apparent along 22-24°N.

Acknowledgement

The authors wish to thank Mr. Shah Alam, Director of Bangladesh Meteorological Department and all the officers and staff of this Department for their help and cooperation during the work in providing the relevant data.

References

1. Wiki: access on 5 September, 2015 “Monsoon in South Asia” https://en.wikipedia.org/wiki/Monsoon_of_South_Asia#Definition)
2. Kripalani, R.H., Kulkarni, A., Sabade, S.S. and Khandekar, M.L., 2003, “Indian Monsoon Variability in a Global Warming Scenario”, *Natural Hazard,* 29, pp. 189–206.
3. Yin M.T., 1949, “Synoptic-Aerologic Study of the Onset of the Summer Monsoon Over India and Burma”, Journal of the Atmospheric Sciences (Impact Factor: 3.14). 11/1949; 6, pp.393-400
4. Internet: access, 5 September 2015, “Recent Theories of the Origin of Indian Monsoon (Dynamic concept”, http://www.preservearticles.com/2011111217180/recent-theories-of-the-origin-of-indian-monsoon-dynamic-concept.html
5. Karmakar, S. and A. Khatun, 1995, “Variability and probabilistic estimates of rainfall extremes in Bangladesh during the southwest monsoon season”, *Mausam*, 46, 1, pp. 47-56.
6. Dhar, O.N. and S. Nandagiri, 1999, “Role of low pressure areas in the absence of tropical disturbances during monsoon months in India”, Int’l J. Climatology, 19, 19, pp. 1153-1159.
7. Ahmed R., Karmakar S., 1993, Arrival and withdrawal dates of the summer monsoon in Bangladesh, Int’l J. Climatology, Volume 13, Issue 7, November 1993, Pages 727–740.

Author Instructions

Paper title (14 Bold)

First Author[1*], Second Author[2] and Third Author[3] (12 Bold)

[1]*Department, College/ University Name, State, City, Country Name (10 Italic)*
[2]*Department, College/ University Name, State, City, Country Name (10 Italic)*
[3]*Department, College/ University Name, State, City, Country Name (10 Italic)*
*Corresponding author: e-mail address *(10 Italic)*

Abstract (12Bold) : The abstract should summarize the content of the paper. Try to keep the abstract below 200 words. Do not make references in the abstract. Your manuscript should be printed on A4 paper. The paper must not exceed 10 (ten) pages on A4 format, including text, tables, figures and references. Margins should be set as: Left, Right and Top: 2.5 cm; Bottom: 2.5 cm. Use a Times New Roman font with 10 pt. All text must single spaced. It is imperative that the margins and style described below be adhered to carefully. This will enable us to keep uniformity in the final printed copies of the Journal. Please keep in mind that the manuscript you prepare will be photographed and printed as it is received. Readability of copy is of paramount importance. (10 point)

Keywords (12Bold): Up to five *(10 point)*

1. INTRODUCTION (12 Bold)

The introduction of the paper should explain the nature of the problem, previous work, purpose, and the contribution of the paper. The contents of each section may be provided to understand easily about the paper. (10 point)

The main text should start on a new page. All pages should be numbered. The paper must be divided into sections such as **1.INTRODUCTION**, **2.EXPERIMENTAL SET UP & METHODOLOGY 3.RESULTS AND DISCUSSION**, **4.CONCLUSIONS** with numbers, upper case and bold. The sub sections should be numbered as 2.1, 2.2, 2.3, etc. (if any). Title of Acknowledgement and References should be bold and lower case with first one upper case letters but no number is required. (10 point)

Manuscript with original figures (the Text in MSWORD 2007 or above with Times New Roman font and 10 font size and the Figures in post script files should be sent to the Member secretary through the e-mail address: mallikak76@yahoo.com.

EXPERIMENTAL SET UP & METHODOLOGY (12 Bold)

This section should provide all information regarding sample data preparation, measurements techniques and experimental details as well (10 point).

2. RESULTS AND DISCUSSION (12 Bold)

Experimental Results and their elaborate discussion should be provided in this section. Results should be significant and concise (10 point).

Equations

All equations are numbered and referred to in the text only by a number enclosed in a round bracket (i.e., (1) reads as "equation 1"). Equations must be typed with Microsoft equation editor. Ensure that any miscellaneous numbering system you use in your paper cannot be confused with a reference [1] or an equation (1) designation. (10 point)

Figures and Tables

The number of figures should be kept to the minimum. Each figure must be placed in proper place in the text, be numbered and have a caption. Axes of figures must be labeled properly. All figures/images should be given in EPS/JPEG/PSD format. Each table should have a number and a self-explanatory title and must be mentioned in the text. Figure and table number should be like **Fig. 1.** Consecutive four days value of SI and LI and **Table 1.** Non-favorable thermodynamic parameters for pre-monsoon thunderstorms in Bangladesh
Figure captions appear below the figure, are flush left, and are in lower case letters. When referring to a figure in the body of the text, the abbreviation "Fig. 1" is used. Figures should be numbered in the order they appear in the text. (10 point)

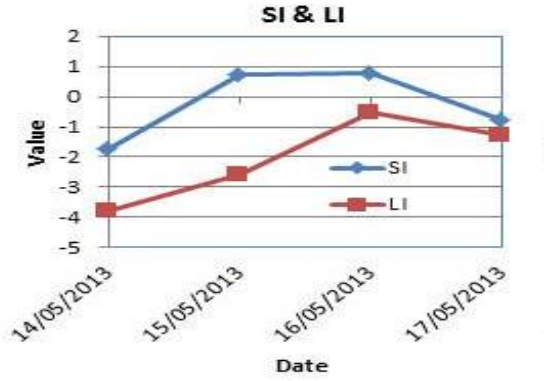

fig.1: Consecutive four days value of SI and LI

Table captions appear centered above the table in upper and lower case letters. When referring to a table in the text, no abbreviation is used and "Table" is capitalized. (10 point)

Table-1: Non-favorable thermodynamic parameters for pre-monsoon thunderstorms in Bangladesh

Not Favorable Case Study							
Place of Occurrence	**Wind speed (km/h)**	**CAPE**	**CINE**	**SI**	**LI**	**TTI**	**Comments**
Sylhet (01.05.13)	52	0	0	15.15	19.48	17.20	Not favorable
Khepupara	100	166.92	-39.09	0.81	-0.50	40.40	Not favorable
Dhaka (22.03.14)	78	881.64	-172.97	1.97	-3.36	46.8	Not favorable

Units

Use either SI (MKS) or CGS as primary units. (SI units are strongly encouraged.)

3. CONCLUSION (12 Bold)

A conclusion section must be included and should indicate clearly the advantages, limitations, and possible applications of the paper. Although a conclusion may review the main points of the paper, do not reproduce the abstract as the conclusion. A conclusion might elaborate on the importance of the work or suggest applications and extensions. (10 point)

ACKNOWLEDGEMENTS (12 Bold)

An acknowledgement section may be presented after the conclusion, if desired. (10 point)

REFERENCES (12 Bold)

All reference referred to text, table and figures of a manuscript must be combined in a single list, numbered consecutively in their order of first appearance and arranged in the some order at the end of the text material. They should be cited in text by Arabic numerals in square brackets at appropriate place of sentence, for example [1,3], [4-6] etc. The references cited should limited to the absolute minimum and the list to be submitted in a separate sheet containing names of all authors (et al. is not allowed). They should be as complete as possible and be presented as follows:

Authors are requested to follow the following examples: (10 point)

1. J. Karmakar, S., 2001: Climatology of thunderstorm days over Bangladesh during the pre- monsoon season. Bangladesh. *J. Sci. and Tech.,* **3 (1)**, 103-112. [**Journal**]
2. Lutgents Tarbuck, seventh edition, chapter 10, pages 135 – 157).[**Book**]
3. R. K. Ahrenkiel, in *Gallium Arsenide and Related Compounds 1993: Proceedings of the 20th International Symposium on Gallium Arsenide and Related Compounds*, Freiburg, Germany, 29 August–2 September 1993, edited by H. S. Rupprecht and G. Weimann (Institute of Physics, London, 1994), p. 685–690 [**Proceeding**]
4. S. L. Goldschmidt, Ph.D. thesis, University of California, Los Angeles, 1985[**Thesis**]

ISSN 2414-6056

DEW-DROP

Contents

Vol. 2, No.1, March 2016

Articles: